Chemoreceptor co-expression in *Drosophila melanogaster* olfactory neurons

Darya Task[1†], Chun-Chieh Lin[1,2‡], Alina Vulpe[3§], Ali Afify[1], Sydney Ballou[3], Maria Brbic[4], Philipp Schlegel[5], Joshua Raji[1], Gregory Jefferis[5,6], Hongjie Li[7#], Karen Menuz[3], Christopher J Potter[1]*

[1]The Solomon H. Snyder Department of Neuroscience, Center for Sensory Biology, Johns Hopkins University School of Medicine, Baltimore, United States; [2]Mortimer B. Zuckermann Mind Brain Behavior Institute, Columbia University, New York, United States; [3]Physiology & Neurobiology Department, University of Connecticut, Mansfield, United States; [4]Department of Computer Science, Stanford University, Stanford, United States; [5]Drosophila Connectomics Group, Department of Zoology, University of Cambridge, Cambridge, United Kingdom; [6]Neurobiology Division, MRC Laboratory of Molecular Biology, Cambridge, United Kingdom; [7]Department of Biology, Howard Hughes Medical Institute, Stanford University, Stanford, United States

*For correspondence: cpotter@jhmi.edu

Present address: [†]Department of Biology, Johns Hopkins University, Baltimore, United States; [‡]The Department of Pathology and Laboratory Medicine, Geisel School of Medicine, Dartmouth-Hitchcock Medical Center, Lebanon, United States; [§]Department of Neuroscience, Yale University, New Haven, United States; [#]Huffington Center on Aging, Department of Molecular and Human Genetics, Baylor College of Medicine, Houston, United States

Abstract *Drosophila melanogaster* olfactory neurons have long been thought to express only one chemosensory receptor gene family. There are two main olfactory receptor gene families in *Drosophila*, the odorant receptors (ORs) and the ionotropic receptors (IRs). The dozens of odorant-binding receptors in each family require at least one co-receptor gene in order to function: *Orco* for ORs, and *Ir25a*, *Ir8a*, and *Ir76b* for IRs. Using a new genetic knock-in strategy, we targeted the four co-receptors representing the main chemosensory families in *D. melanogaster* (*Orco, Ir8a, Ir76b, Ir25a*). Co-receptor knock-in expression patterns were verified as accurate representations of endogenous expression. We find extensive overlap in expression among the different co-receptors. As defined by innervation into antennal lobe glomeruli, *Ir25a* is broadly expressed in 88% of all olfactory sensory neuron classes and is co-expressed in 82% of Orco+ neuron classes, including all neuron classes in the maxillary palp. *Orco, Ir8a*, and *Ir76b* expression patterns are also more expansive than previously assumed. Single sensillum recordings from Orco-expressing *Ir25a* mutant antennal and palpal neurons identify changes in olfactory responses. We also find co-expression of *Orco* and *Ir25a* in *Drosophila sechellia* and *Anopheles coluzzii* olfactory neurons. These results suggest that co-expression of chemosensory receptors is common in insect olfactory neurons. Together, our data present the first comprehensive map of chemosensory co-receptor expression and reveal their unexpected widespread co-expression in the fly olfactory system.

Editor's evaluation

A combination of methods, including a new method for tagging genes, demonstrates that the chemosensory co-receptors of *Drosophila melanogaster* (Orco, IR8a, IR25a, IR76b) are expressed widely and highly overlapping. These findings challenge a long-standing dogma in the field and suggest that different types of receptors, that is, olfactory and ionotropic receptors, can be co-expressed in the same chemosensory neuron. Moreover, optogenetics and single sensillum recordings provide evidence that IR25a co-receptor might modulate the activity of typical Orco-dependent

olfactory sensory neurons. The authors also provide evidence that this co-expression is conserved by examining two other fly species.

Introduction

The sense of smell is crucial for many animal behaviors, from conspecific recognition and mate choice (*Dweck et al., 2015*; *Stengl, 2010*), to location of a food source (*Auer et al., 2020*; *Hansson and Stensmyr, 2011*), to avoidance of predators (*Ebrahim et al., 2015*; *Kondoh et al., 2016*; *Papes et al., 2010*) and environmental dangers (*Mansourian et al., 2016*; *Stensmyr et al., 2012*). Peripheral sensory organs detect odors in the environment using a variety of chemosensory receptors (*Carey and Carlson, 2011*; *Su et al., 2009*). The molecular repertoire of chemosensory receptors expressed by the animal, and the particular receptor expressed by any individual olfactory neuron, define the rules by which an animal interfaces with its odor environment. Investigating this initial step in odor detection is critical to understanding how odor signals first enter the brain to guide behaviors.

The olfactory system of the vinegar fly, *Drosophila melanogaster*, is one of the most extensively studied and well understood (*Depetris-Chauvin et al., 2015*). *D. melanogaster* is an attractive model for studying olfaction due to its genetic tractability, numerically simpler nervous system (compared to mammals), complex olfactory-driven behaviors, and similar organizational principles to vertebrate olfactory systems (*Ache and Young, 2005*; *Wilson, 2013*). Over 60 years of research have elucidated many of the anatomical, molecular, and genetic principles underpinning fly olfactory behaviors (*Gomez-Diaz et al., 2018*; *Harris, 1972*; *Pask and Ray, 2016*; *Siddiqi, 1987*; *Stocker, 2001*; *Venkatesh and Naresh Singh, 1984*; *Vosshall and Stocker, 2007*; *Yan et al., 2020*). Recent advances in electron microscopy and connectomics are revealing higher brain circuits involved in the processing of olfactory information (*Bates et al., 2020*; *Berck et al., 2016*; *Frechter et al., 2019*; *Horne et al., 2018*; *Marin et al., 2020*; *Zheng et al., 2018*); such endeavors will aid the full mapping of neuronal circuits from sensory inputs to behavioral outputs.

The fly uses two olfactory appendages to detect odorants: the antennae and maxillary palps (*Figure 1A*; *Stocker, 1994*). Each of these is covered by sensory hairs called sensilla, and each sensillum houses between one and four olfactory sensory neurons (OSNs) (*Figure 1B*; *de Bruyne et al., 2001*; *Venkatesh and Naresh Singh, 1984*). The dendrites of these neurons are found within the sensillar lymph, and they express chemosensory receptors from three gene families: *odorant receptors* (*ORs*), *ionotropic receptors* (*IRs*), and *gustatory receptors* (*GRs*) (*Figure 1C*, left; *Benton et al., 2009*; *Clyne et al., 1999*; *Gao and Chess, 1999*; *Jones et al., 2007*; *Kwon et al., 2007*; *Vosshall et al., 1999*; *Vosshall et al., 2000*). These receptors bind odorant molecules that enter the sensilla from the environment, leading to the activation of the OSNs, which then send this olfactory information to the fly brain (*Figure 1D*), to the first olfactory processing center – the antennal lobes (ALs) (*Figure 1E*; reviewed in *Depetris-Chauvin et al., 2015*; *Gomez-Diaz et al., 2018*; *Pask and Ray, 2016*). The standard view regarding the organization of the olfactory system in *D. melanogaster* is that olfactory neurons express receptors from only one of the chemosensory gene families (either *ORs*, *IRs*, or *GRs*), and all neurons expressing the same receptor (which can be considered an OSN class) project their axons to one specific region in the AL called a glomerulus (*Figure 1C*, right; *Couto et al., 2005*; *Fishilevich and Vosshall, 2005*; *Gao et al., 2000*; *Laissue et al., 1999*; *Pinto et al., 1988*; *Vosshall et al., 2000*). This pattern of projections creates a map in which the OR+ (*Figure 1E*, teal), IR+ (*Figure 1E*, purple), and GR+ (*Figure 1E*, dark blue) domains are segregated from each other in the AL. The OR+ domains innervate 38 anterior glomeruli, while the IR+ (19 glomeruli) and GR+ (1 glomerulus) domains occupy more posterior portions of the AL. One exception is the Or35a+ OSN class, which expresses an *IR* (*Ir76b*) in addition to the *OR* and *Orco*, and innervates the VC3 glomerulus (*Figure 1E*, striped glomerulus; *Benton et al., 2009*; *Couto et al., 2005*; *Fishilevich and Vosshall, 2005*). Different OSN classes send their information to different glomeruli, and the specific combination of OSN classes and glomeruli that are activated by a given smell (usually a blend of different odorants) constitutes an olfactory 'code' that the fly brain translates into an appropriate behavior (*Grabe and Sachse, 2018*; *Haverkamp et al., 2018*; *Seki et al., 2017*).

The receptors within each chemosensory gene family form heteromeric ion channels (receptor complexes) (*Abuin et al., 2011*; *Butterwick et al., 2018*; *Sato et al., 2008*). The *ORs* require a single co-receptor, *Orco*, to function (*Figure 1C*, middle row; *Benton et al., 2006*; *Larsson et al., 2004*;
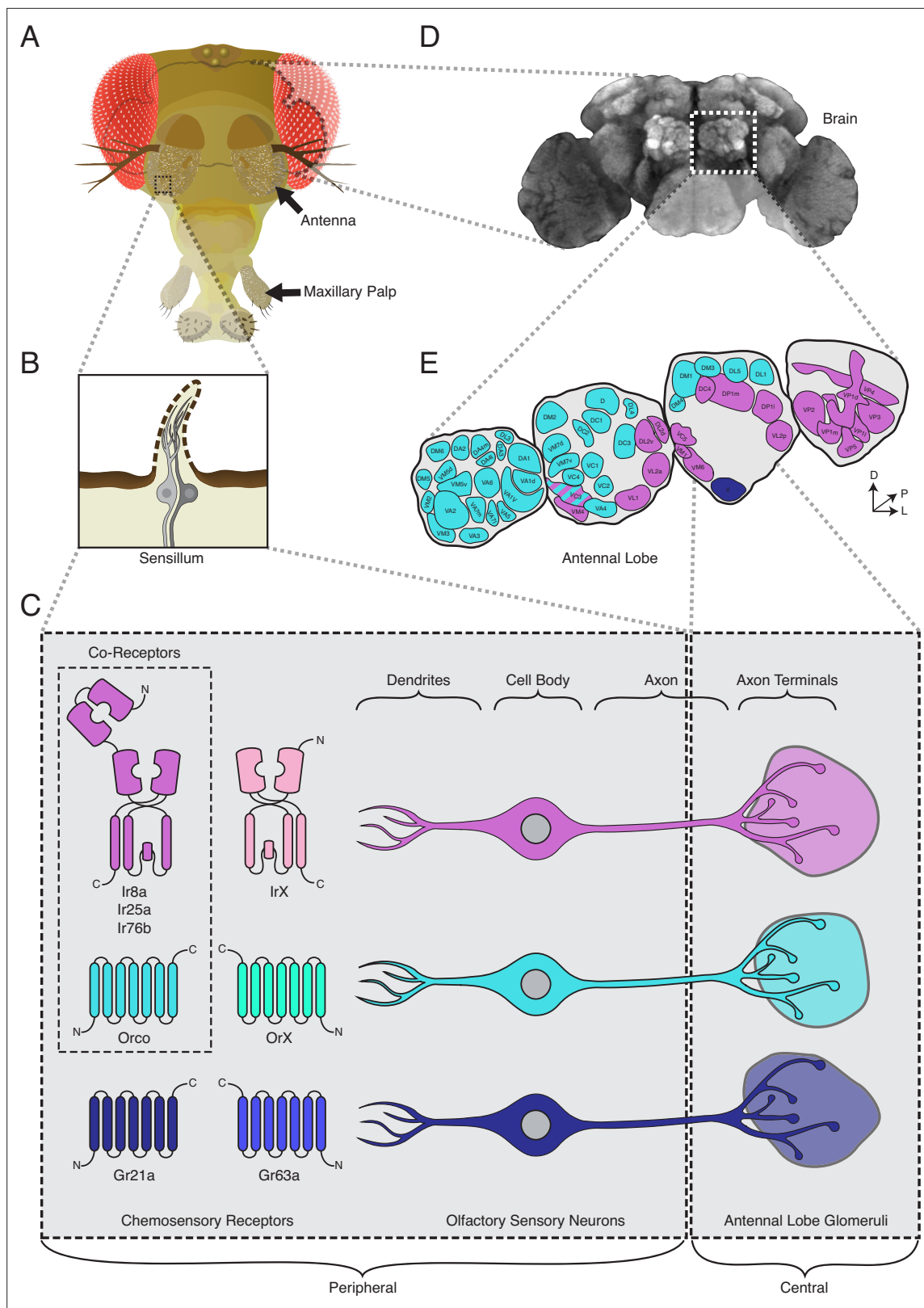
Figure 1. The standard view of olfactory receptor expression in *Drosophila melanogaster*. (**A**) The adult fly head (left) has two olfactory organs: the antennae and the maxillary palps (arrows). Olfactory neurons from these organs project to the fly brain (**D**), to the first center involved in processing of olfactory information, the antennal lobes (**E**). (**B**) The olfactory organs are covered by sensory hairs called sensilla (left). Each sensillum contains between one and four olfactory sensory neurons (two example neurons are shown in gray). The dendrites of these neurons extend into the sensilla, and the axons

Figure 1 continued

target discrete regions of the antennal lobes called glomeruli (**E**). Neuronal compartments (dendrites, cell body, axon, axon terminals) are labeled in (**C**). (**C**) Left: in the periphery, each olfactory sensory neuron is traditionally thought to express chemosensory receptors from only one of three gene families on its dendrites: ionotropic receptors (IRs, pink and purple), odorant receptors (ORs, teal and green), or gustatory receptors (GRs, light and dark blue). IRs and ORs require obligate co-receptors (dotted box outline) to form functional ion channels. All ORs utilize a single co-receptor, Orco (teal), while IRs can utilize one (or a combination) of three possible co-receptors (purple): Ir8a, Ir25a, or Ir76b. The two GRs form a functional carbon dioxide detecting channel expressed in only one class of neurons. All other olfactory neurons express one of the four co-receptors. Right: olfactory sensory neurons expressing ORs, IRs, and GRs are thought to project to mutually exclusive glomeruli in the antennal lobe (AL) of the central brain, forming the olfactory map shown in (**E**). (**D**) Fly brain stained with anti-brp synaptic marker (nc82), with left AL outlined by the dotted white box. (**E**) AL map with glomeruli color-coded by the chemosensory receptors (ORs, IRs, or GRs) expressed in the olfactory sensory neurons projecting to them. Only one glomerulus (VC3, striped) receives inputs from neurons expressing chemoreceptors from multiple gene families (ORs and IRs). Compass: D = dorsal, L = lateral, P = posterior.

Vosshall and Hansson, 2011). The ligand-binding *OrX* confers odorant specificity upon the receptor complex, while the co-receptor *Orco* is necessary for trafficking of the *OrX* to the dendritic membrane and formation of a functional ion channel (*Benton et al., 2006*; *Larsson et al., 2004*). Likewise, the ligand-binding *IrXs* require one or more *IR* co-receptors: *Ir8a*, *Ir25a*, and/or *Ir76b* (*Figure 1C*, top row). The *IR* co-receptors (IrCos) are similarly required for trafficking and ion channel function (*Abuin et al., 2011*; *Abuin et al., 2019*; *Ai et al., 2013*; *Vulpe and Menuz, 2021*). The *GR* gene family generally encodes receptors involved in taste, which are typically expressed outside the olfactory system (such as in the labella or the legs) (*Dunipace et al., 2001*; *Park and Kwon, 2011*; *Scott, 2018*; *Scott et al., 2001*); however, *Gr21a* and *Gr63a* are expressed in one antennal OSN neuron class and form a complex sensitive to carbon dioxide (*Figure 1C*, bottom row; *Jones et al., 2007*; *Kwon et al., 2007*).

The majority of receptors have been mapped to their corresponding OSNs, sensilla, and glomeruli in the fly brain (*Bhalerao et al., 2003*; *Couto et al., 2005*; *Fishilevich and Vosshall, 2005*; *Frank et al., 2017*; *Grabe et al., 2016*; *Hallem and Carlson, 2006*; *Hallem et al., 2004*; *Knecht et al., 2017*; *Marin et al., 2020*; *Ray et al., 2008*; *Silbering et al., 2011*). This detailed map has allowed for exquisite investigations into the developmental, molecular, electrophysiological, and circuit/computational bases of olfactory neurobiology. This work has relied on transgenic lines to identify and manipulate OSN classes (*Ai et al., 2013*; *Brand and Perrimon, 1993*; *Couto et al., 2005*; *Fishilevich and Vosshall, 2005*; *Kwon et al., 2007*; *Lai and Lee, 2006*; *Larsson et al., 2004*; *Menuz et al., 2014*; *Potter et al., 2010*; *Silbering et al., 2011*). These transgenic lines use regions of DNA upstream of the chemosensory genes that are assumed to reflect the enhancers and promoters driving expression of these genes. While a powerful tool, transgenic lines may not contain all of the necessary regulatory elements to faithfully recapitulate the expression patterns of the endogenous genes. In addition, the genomic insertional location of the transgene might affect expression patterns (positional effects). Some transgenic lines label a subset of the cells of a given olfactory class, while others label additional cells: for example, the transgenic *Ir25a-Gal4* line is known to label only a portion of cells expressing Ir25a protein (as revealed by antibody staining) (*Abuin et al., 2011*); conversely, *Or67d-Gal4* transgenes incorrectly label two glomeruli, whereas a *Gal4* knock-in at the *Or67d* genetic locus labels a single glomerulus (*Couto et al., 2005*; *Fishilevich and Vosshall, 2005*; *Kurtovic et al., 2007*). While knock-ins provide a faithful method to capture a gene's expression pattern, generating these lines has traditionally been cumbersome.

In this paper, we implement an efficient knock-in strategy to target the four main chemosensory co-receptor genes in *D. melanogaster* (Orco, Ir8a, Ir76b, Ir25a). We find broad co-expression of these co-receptor genes in various combinations in olfactory neurons, challenging the current view of segregated olfactory families in the fly. In particular, *Ir25a* is expressed in the majority of olfactory neurons, including most Orco+ OSNs. In addition, the *Ir8a* and *Ir25a* knock-in lines help to distinguish two new OSN classes in the sacculus that target previously unidentified glomerular subdivisions in the posterior AL. Recordings in *Ir25a* mutant sensilla in Orco+ neurons reveal subtle changes in odor responses, suggesting that multiple chemoreceptor gene families could be involved in the signaling or development of a given OSN class. We further extend our findings of co-receptor co-expression to two additional insect species, *Drosophila sechellia* and *Anopheles coluzzii*. These data invite a re-examination of odor coding in *D. melanogaster* and other insects. We present a comprehensive model of co-receptor expression in *D. melanogaster*, which will inform future investigations of combinatorial chemosensory processing.

Table 1. Summary of HACK knock-in efficiency (related to *Figure 2*).

There are two ways to generate knock-ins via the HACK technique: by direct injection or by genetic cross (see *Figure 2—figure supplement 1* and Materials and methods for details) (*Lin and Potter, 2016a*). All four co-receptor genes were targeted using the direct injection approach; additionally, the crossing approach was tested with *Orco* and *Ir25a*. Knock-in efficiency, as measured by the number of flies having the mCherry+ marker divided by the total number of potentially HACKed flies, was high for all genes tested and both approaches. Efficiency appears to depend on the genetic locus, as has been previously demonstrated (*Lin and Potter, 2016b*). To further estimate the effort required to generate a HACK knock-in, we calculated the percentage of founder flies producing knock-in lines; this gives an indication of the number of independent crosses needed to successfully create a knock-in line. Two to five individual G_0 starting crosses were sufficient to produce a knock-in. For each gene, a sample of individual knock-in lines was tested via PCR genotyping, sequencing, and by crossing to a reporter line to confirm brain expression (knock-ins sampled). For all knock-ins generated via the direct injection method, every fly tested represented a correctly targeted knock-in. However, for the cross method, some lines had the mCherry+ marker and yet did not drive GFP expression in the brain when crossed to a reporter line (labeled here as false positives). See also *Table 1—source data 1* and *Figure 2—figure supplement 1*.

Gene	Approach	mCherry+	mCherry-	Total	Efficiency (%)	Founders producing knock-in (#/total)	Knock-ins sampled	False positives	Confirmed	Correct (%)
Orco	Direct injection	180	365	545	33	43% (3/7)	30	0	30	100
Ir8a	Direct injection	53	609	662	8	20% (4/20)	5	0	5	100
Ir76b	Direct injection	79	184	263	30	100% (2/2)	10	0	10	100
Ir25a	Direct injection	82	268	350	23	40% (2/5)	6	0	6	100
Orco	Cross	37	96	133	28	100% (3/3)	2	1	1	50
Ir25a	Cross	30	95	125	24	100% (2/2)	30	5	25	83

The online version of this article includes the following source data for table 1:

Source data 1. HACK knock-in screen.

Results

Generation and validation of co-receptor knock-in lines

We previously developed the HACK technique for CRISPR/Cas9-mediated in vivo gene conversion of binary expression system components, such as the conversion of transgenic *Gal4* to *QF2* (*Brand and Perrimon, 1993*; *Jinek et al., 2012*; *Lin and Potter, 2016a*; *Lin and Potter, 2016b*; *Potter et al., 2010*; *Riabinina et al., 2015*; *Xie et al., 2018*). Here, we adapt this strategy for the efficient generation of targeted knock-ins (see *Table 1* and *Table 1—source data 1* for details). We chose to target the four chemosensory co-receptor genes to examine unmapped patterns of co-receptor expression in *D. melanogaster*. We inserted a *T2A-QF2* cassette and mCherry selection marker before the stop codon of the four genes of interest (*Figure 2A*, *Figure 2—figure supplement 1*). By introducing the T2A ribosomal skipping peptide, the knock-in will produce the full-length protein of the gene being targeted as well as a functional QF2 transcription factor (*Figure 2A*, protein products). This approach should capture the endogenous expression pattern of the gene under the control of the gene's native regulatory elements while retaining the gene's normal function (*Baena-Lopez et al., 2013*; *Bosch et al., 2020*; *Chen et al., 2020*; *Diao et al., 2015*; *Diao and White, 2012*; *Du et al., 2018*; *Gnerer et al., 2015*; *Gratz et al., 2014*; *Kanca et al., 2019*; *Lee et al., 2018*; *Li-Kroeger et al., 2018*; *Lin and Potter, 2016a*; *Vilain et al., 2014*; *Xue et al., 2014*). We found that *T2A-QF2* knock-ins were functional with some exceptions (see *Figure 2—figure supplement 2* and *Figure 2—source data 1*). For example, *Orco-T2A-QF2* knock-in physiology was normal, while a homozygous *Ir25a-T2A-QF2* knock-in exhibited a mutant phenotype. This suggests that the addition of the T2A peptide onto the C-terminus of Ir25a might interfere with its co-receptor function.

We examined the expression of the co-receptor knock-in lines in the adult olfactory organs by crossing each line to the same *10XQUAS-6XGFP* reporter (*Figure 2B–I*). *Orco-T2A-QF2*-driven GFP expression was detected in the adult antennae and maxillary palps (*Figure 2B*), as previously described (*Larsson et al., 2004*). We validated the *Orco-T2A-QF2* knock-in line with whole-mount antibody staining of maxillary palps (*Figure 2C*) and found a high degree of correspondence between anti-Orco antibody staining and knock-in driven GFP in palpal olfactory neurons (quantified in *Table 2*; see also *Figure 2—figure supplement 3A–D* for PCR and sequencing validation of all knock-in lines).
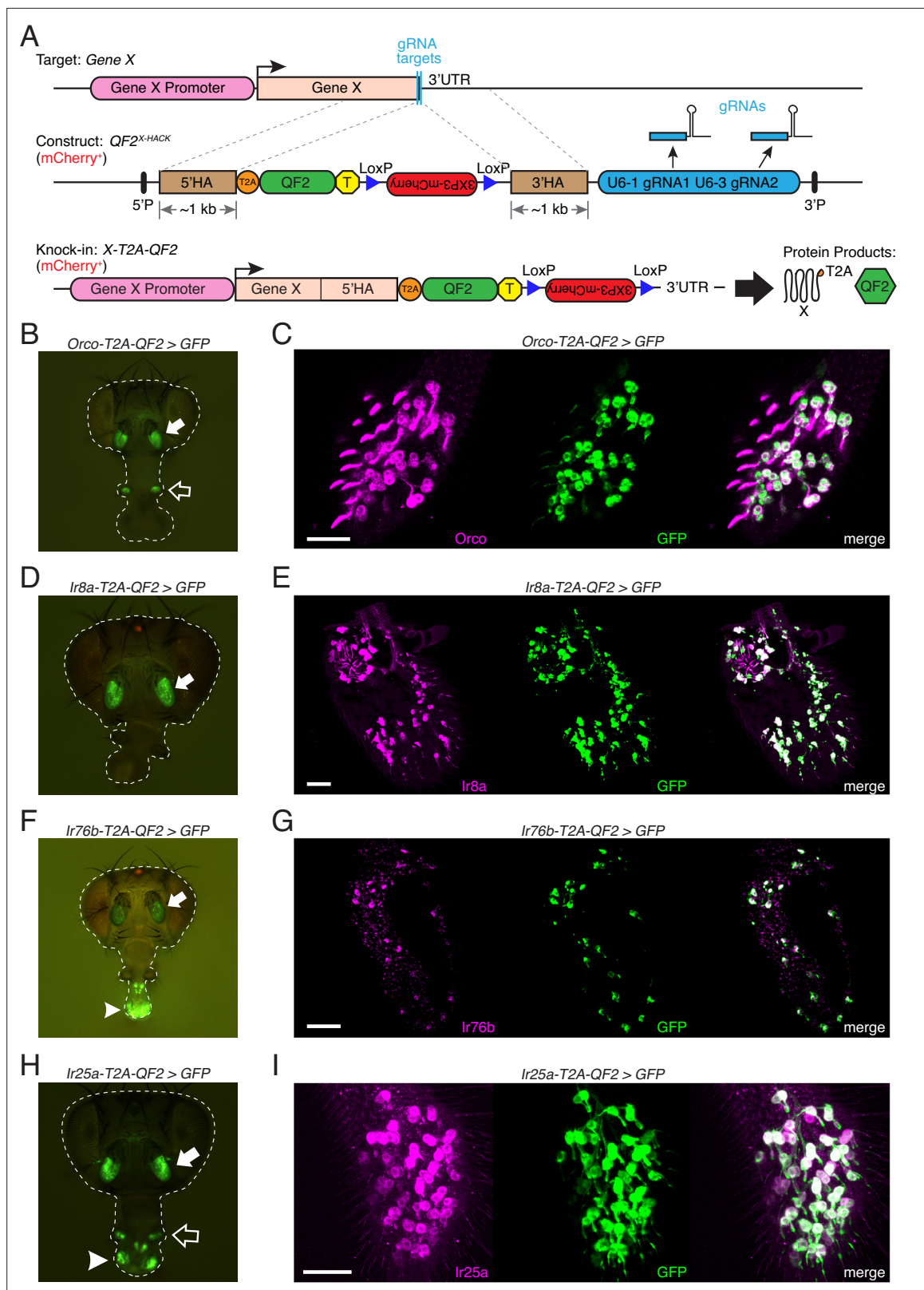
Figure 2. Generation and validation of chemosensory co-receptor knock-in lines. (**A**) Schematic of HACK knock-in approach. Top: two double-stranded breaks are induced on either side of the target gene stop codon with gRNAs (blue) expressed from the *QF2*$^{X-HACK}$ construct (middle) in the presence of Cas9. The construct includes *T2A-QF2* and a floxed *3XP3-mCherry* marker. The knock-in introduces a transcriptional stop (yellow T) after QF2. Bottom: the knock-in produces two protein products (right) from the targeted mRNA: target X and the *QF2* transcription factor (***Diao and White, 2012***). The

Figure 2 continued on next page

Figure 2 continued

X-T2A-QF2 knock-in can be crossed to a reporter (e.g., *QUAS-GFP*) to examine the endogenous expression pattern of the target gene. (**B**) *Orco-T2A-QF2* driving *QUAS-GFP* in adult fly head. GFP expression is found in the antennae (filled arrow) and maxillary palps (hollow arrow), as previously reported (***Larsson et al., 2004***). (**C**) Whole-mount anti-Orco antibody staining in *Orco-T2A-QF2>GFP* maxillary palps reveals a high degree of overlap of Orco+ and GFP+ cells. N = 3. (**D**) *Ir8a-T2A-QF2* drives GFP in the antennae (arrow), as previously reported (***Abuin et al., 2011***). (**E**) Anti-Ir8a antibody staining of *Ir8a-T2A-QF2>GFP* antennal cryosections shows high correspondence between Ir8a+ and GFP+ cells. N = 7. (**F**) *Ir76b-T2A-QF2* drives GFP expression in the antennae (filled arrow) and labella (hollow arrow), reflecting *Ir76b*'s role in olfaction and gustation, respectively (***Benton et al., 2009***; ***Zhang et al., 2013***). (**G**) In situs on *Ir76b-T2A-QF2>GFP* antennal cryosections to validate that the knock-in faithfully recapitulates the endogenous expression pattern. N = 3. (**H**) *Ir25a-T2A-QF2* drives GFP in the antennae (filled arrow) and labella (hollow arrow), which has been reported previously (***Benton et al., 2009***; ***Croset et al., 2010***). Expression in the maxillary palps (arrowhead) has not been previously reported. (**I**) Whole-mount maxillary palp staining with an anti-Ir25a antibody in *Ir25a-T2A-QF2>GFP* flies. The knock-in and Ir25a antibody co-labeled the majority of olfactory neurons in the palps. N = 5. Scale bars = 25 µm. In (**D**) and (**F**), the *3XP3-mCherry* knock-in marker can be weakly detected in the eyes and ocelli (red spot) of both *Ir8a-T2A-QF2* and *Ir76b-T2A-QF2*. See also *Figure 2—figure supplements 1–4*, *Tables 1 and 2*, *Table 1—source data 1*, *Figure 2—source data 1*, and Materials and methods.

The online version of this article includes the following source data and figure supplement(s) for figure 2:

Source data 1. Single sensillum recordings (SSRs) of knock-in lines.

Figure supplement 1. HACK crossing schematics, marker expression, and approach comparison.

Figure supplement 2. *T2A-QF2* HACK knock-in effects on target gene function.

Figure supplement 3. Additional validation of co-receptor knock-in lines.

Figure supplement 4. Knock-in expression in the larva.

We confirmed the specificity of the anti-Orco antibody by staining *Orco²* mutant palps and found no labeling of olfactory neurons (*Figure 2—figure supplement 3E*).

Unlike *Orco*, *Ir8a* expression has previously been localized only to the antenna, to olfactory neurons found in coeloconic sensilla and in the sacculus (*Abuin et al., 2011*). As expected, the knock-in line drove GFP expression only in the antenna (*Figure 2D*). To validate the *Ir8a-T2A-QF2* knock-in line, we performed antibody staining on antennal cryosections and found the majority of cells to be double labeled (*Figure 2E*, *Table 2*). There was no anti-Ir8a staining in control *Ir8a¹* mutant antennae (*Figure 2—figure supplement 3F*).

The *Ir76b* gene has previously been implicated in both olfaction and gustation and has been shown to be expressed in adult fly antennae, labella (mouthparts), legs, and wings (*Abuin et al., 2011*; *Chen and Amrein, 2017*; *Croset et al., 2010*; *Ganguly et al., 2017*; *Hussain et al., 2016*; *Sánchez-Alcañiz et al., 2018*; *Zhang et al., 2013*). We examined the *Ir76b-T2A-QF2* knock-in line and found a similar pattern of expression in the periphery, with GFP expression in the antennae and labella (*Figure 2F*). Because an anti-Ir76b antibody has not previously been tested in fly antennae, we performed in situ on *Ir76b-T2A-QF2>GFP* antennal cryosections to validate knock-in expression (*Figure 2G*) and confirmed the specificity of the probe in *Ir76b¹* mutant antennae (*Figure 2—figure supplement 3G*).

Of the four *D. melanogaster* co-receptor genes, *Ir25a* has been implicated in the broadest array of cellular and sensory functions, from olfaction (*Abuin et al., 2011*; *Benton et al., 2009*; *Silbering et al., 2011*) and gustation (*Chen and Amrein, 2017*; *Chen and Dahanukar, 2017*; *Jaeger et al., 2018*), to thermo- and hygro-sensation (*Budelli et al., 2019*; *Enjin et al., 2016*; *Knecht et al., 2017*; *Knecht et al., 2016*), to circadian rhythm modulation (*Chen et al., 2015*). In the adult olfactory system, *Ir25a* expression has previously been reported in three types of structures in the antenna: coeloconic sensilla, the arista, and the sacculus (*Abuin et al., 2011*; *Benton et al., 2009*). We examined the *Ir25a-T2A-QF2* knock-in line and found GFP expression in the adult antennae, labella, and maxillary palps (*Figure 2H*). This was surprising because no IR expression has previously been reported in fly palps. To verify Ir25a protein expression in the maxillary palps, we performed whole-mount anti-Ir25a antibody staining in *Ir25a-T2A-QF2>GFP* flies. We found broad *Ir25a* expression in palpal olfactory neurons (*Figure 2I*) and a high degree of overlap between knock-in driven GFP expression and antibody staining (*Table 2*). As expected, there was no anti-Ir25a staining in *Ir25a²* mutant palps (*Figure 2—figure supplement 3H*).

We also examined co-receptor knock-in expression in *D. melanogaster* larvae. As in the adult stage, larval GFP expression was broadest in the *Ir25a-T2A-QF2* and *Ir76b-T2A-QF2* knock-in lines, with GFP labeling of neurons in the head and throughout the body wall (*Figure 2—figure supplement 4*). The *Orco-T2A-QF2* knock-in line labeled only the olfactory dorsal organs in the larva, while

Table 2. Validation of *T2A-QF2* knock-in expression in the antennae and maxillary palps (related to *Figure 2*).
To verify that the knock-in lines recapitulate the endogenous expression patterns of the target genes, antennae or maxillary palps of flies containing the knock-ins driving GFP expression were co-stained with the corresponding antibody (Ab) (anti-Orco, anti-Ir8a, or anti-Ir25a). The overlap of Ab+ and GFP+ cells was examined, and a high correspondence between antibody staining and knock-in driven GFP was found. WM: whole-mount; cryo: cryosection. See also *Figure 2—figure supplement 3*.

Knock-in	Sample	Antibody (Ab)	Ab+ cells	GFP+ cells	Double-labeled cells	Total cells
Orco	Palp 1 (WM)	Anti-Orco	125	127	125	127
Orco	Palp 2 (WM)	Anti-Orco	112	111	108	115
Orco	Palp 6 (WM)	Anti-Orco	125	126	123	128
		Total across samples:	362	364	356	370
			Proportion of Ab+ cells that are GFP+:	Proportion of GFP+ cells that are Ab+:	Proportion of all cells that are double labeled:	
			0.98	0.98	0.96	
Ir8a	Antenna 1 (cryo)	Anti-Ir8a	20	21	20	21
Ir8a	Antenna 2 (cryo)	Anti-Ir8a	24	24	24	24
Ir8a	Antenna 6 (cryo)	Anti-Ir8a	40	43	40	43
Ir8a	Antenna 7 (cryo)	Anti-Ir8a	12	13	12	13
Ir8a	Antenna 8 (cryo)	Anti-Ir8a	16	16	16	16
Ir8a	Antenna 9 (cryo)	Anti-Ir8a	42	42	41	43
Ir8a	Antenna 10 (cryo)	Anti-Ir8a	41	40	40	41
		Total across samples:	195	199	193	201
			Proportion of Ab+ cells that are GFP+:	Proportion of GFP+ cells that are Ab+:	Proportion of all cells that are double labeled:	
			0.99	0.97	0.96	
Ir25a	Palp 1 (WM)	Anti-Ir25a	107	105	104	108
Ir25a	Palp 2 (WM)	Anti-Ir25a	86	85	85	86
Ir25a	Palp 3 (WM)	Anti-Ir25a	111	111	110	112
Ir25a	Palp 4 (WM)	Anti-Ir25a	94	94	94	94
Ir25a	Palp 5 (WM)	Anti-Ir25a	83	83	81	85
		Total across samples:	481	478	474	485
			Proportion of Ab+ cells that are GFP+:	Proportion of GFP+ cells that are Ab+:	Proportion of all cells that are double labeled:	
			0.99	0.99	0.98	

the *Ir8a-T2A-QF2* knock-in line did not have obvious expression in the larval stage (*Figure 2—figure supplement 4*). All subsequent analyses focused on the adult olfactory system.

Expanded expression of olfactory co-receptors

We next examined the innervation patterns of the four co-receptor knock-in lines in the adult central nervous system: the brain and ventral nerve cord (VNC) (*Figure 3*). Only two of the four lines (*Ir25a* and *Ir76b*) showed innervation in the VNC, consistent with the role of these genes in gustation in addition to olfaction (*Figure 3—figure supplement 1A*). In the brain, we compared the expression of each knock-in line (*Figure 3A–D*, green) to the corresponding transgenic *Gal4* line (*Figure 3A–D*, orange) to examine the differences in expression to what has previously been reported. Reporter-alone controls for these experiments are shown in *Figure 3—figure supplement 1B*. All four knock-in lines innervated the ALs, and the *Ir25a-T2A-QF2* and *Ir76b-T2A-QF2* lines additionally labeled the subesophageal zone (SEZ), corresponding to gustatory axons from the labella (*Figure 3C and D*, arrowheads; *Hussain et al., 2016*; *Zhang et al., 2013*). The co-labeling experiments revealed that all four knock-ins label more glomeruli than previously reported (see *Figure 3—source data 1* for AL
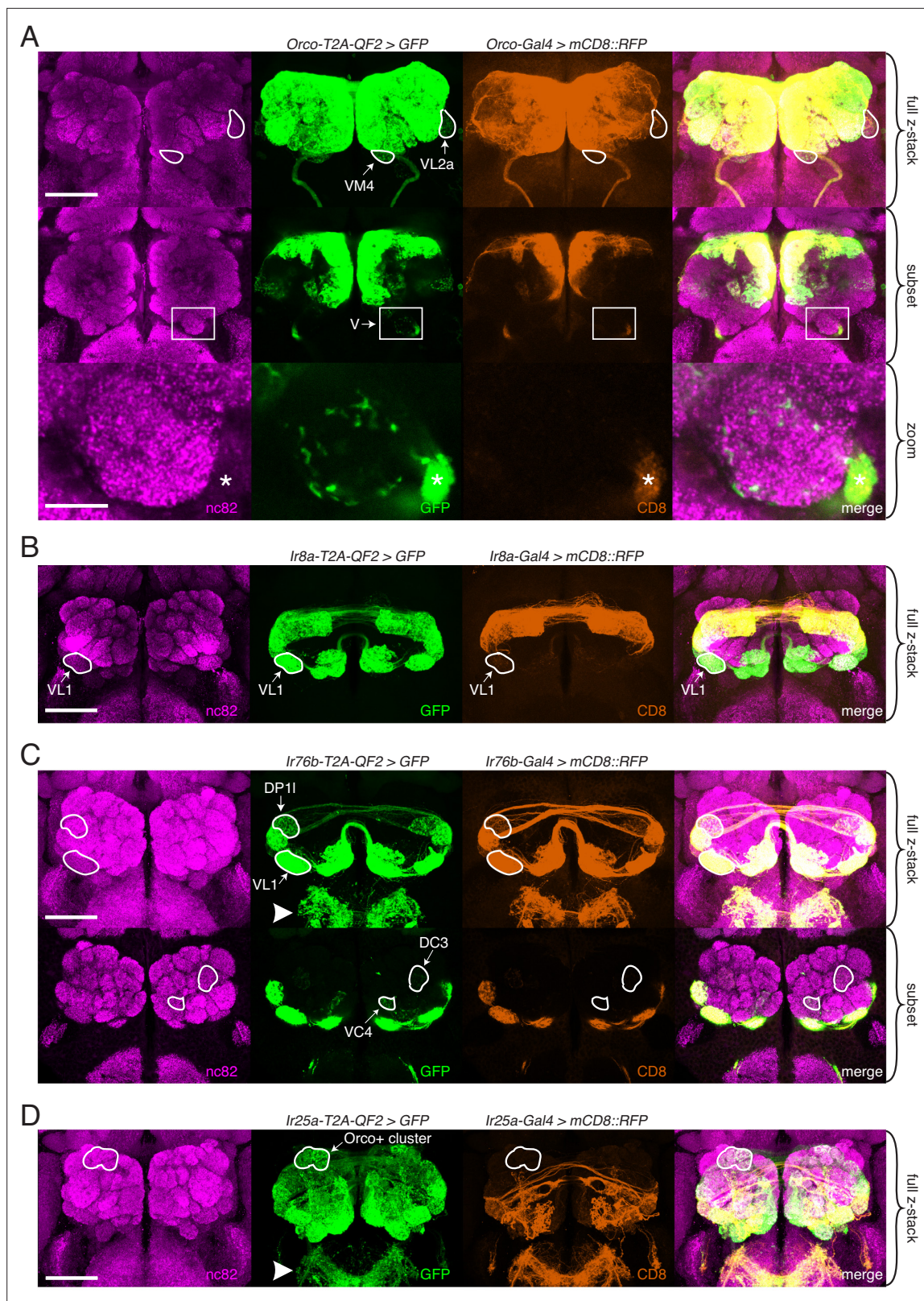
Figure 3. Expanded expression of olfactory co-receptors. (**A–D**) Comparing knock-in innervation patterns of the antennal lobe (AL) with what has previously been reported for each co-receptor. Co-labeling experiments with each co-receptor knock-in line driving *QUAS-GFP* (green) and the corresponding transgenic co-receptor *Gal4* line driving *UAS-mCD8::RFP* (anti-CD8, orange). The nc82 antibody labels synapses (magenta) and is used as a brain counterstain in these and all subsequent brain images. (**A**) The *Orco-T2A-QF2* knock-in labels more glomeruli than the *Orco-Gal4* line. Top:

Figure 3 continued on next page

Figure 3 continued

maximum intensity projection of full z-stack showing two additional glomeruli labeled by the knock-in, VM4 (Ir8a+/Ir76b+/Ir25a+) and VL2a (Ir8a+). Middle: subset of z-stack with a box around the V glomerulus. Bottom: zoom of boxed region showing sparse innervation of the V glomerulus (Gr21a+/Gr63a+) by the knock-in but not the *Gal4* line. Asterisk indicates antennal nerve that is outside the V glomerulus. In the sub z-stack and zoom panel, gain has been increased in the GFP channel to visualize weak labeling more clearly. (**B**) The *Ir8a-T2A-QF2* knock-in also drives GFP expression in more glomeruli than previously reported, including the outlined VL1 glomerulus (Ir25a+). (**C**) In the brain, *Ir76b-T2A-QF2>GFP* olfactory neurons innervate the ALs, while gustatory neurons from the labella innervate the subesophageal zone (SEZ, arrowhead). Top: both the *Ir76b* knock-in and transgenic *Gal4* line label more glomeruli than previously reported, including VL1 (Ir25a+) and DP1l (Ir8a+). Bottom: the *Ir76b-T2A-QF2* knock-in labels several Orco+ glomeruli, such as DC3 and VC4 (outlined). In the subset, gain has been increased in the GFP channel to visualize weakly labeled glomeruli more clearly. (**D**) The *Ir25a-T2A-QF2* knock-in drives GFP expression broadly in the antennal lobes and SEZ (arrowhead). Ir25a+ neurons innervate many Orco+ glomeruli, such as those outlined. The transgenic *Ir25a-Gal4* line labels a subset of the knock-in expression pattern. N = 3–10 for co-labeling experiments, N = 5–15 for additional analyses of the knock-in lines alone. Scale bars = 25 µm, except zoom panel scale bar = 10 µm. See also *Figure 3—figure supplements 1 and 2*, *Table 3*, and *Figure 3—source data 1* and *Figure 3—source data 2*.

The online version of this article includes the following source data and figure supplement(s) for figure 3:

Source data 1. Knock-in antennal lobe analyses.

Source data 2. Examples of new glomerular expression in knock-in lines.

Figure supplement 1. Knock-in expression in the adult ventral nerve cord (VNC) and reporter expression in the brain.

Figure supplement 2. Transgenic co-receptor *Gal4* lines do not fully recapitulate knock-in expression.

analyses, *Figure 3—source data 2* for traced examples of newly identified glomeruli in each knock-in line, and *Table 3* for a summary of glomerular expression across all knock-in lines). Some glomeruli were not labeled consistently in all flies, which we define as variable expression (found in <50% of brains examined).

Orco-T2A-QF2 labels seven 'non-canonical' glomeruli consistently, and one sporadically. These include VM4 and VL2a, which correspond to Ir76b+ and Ir8a+ OSN populations, respectively (*Figure 3A*, outlines). We also found that the *Orco* knock-in sparsely but consistently labels the V glomerulus, which is innervated by Gr21a+/Gr63a+ neurons (*Figure 3A*, box and zoom panel). *Orco-T2A-QF2* also labels one Ir25a+ glomerulus consistently (VL1), three additional Ir8a+ glomeruli consistently (DL2d, DL2v, DP1l), and one variably (DC4). Surprisingly, when we crossed the transgenic *Orco-Gal4* line (*Larsson et al., 2004*) to a stronger reporter (*Shearin et al., 2014*), we found that several of these additional glomeruli were weakly labeled by the transgenic line (*Figure 3—figure supplement 2A*). This suggests that there are OSN populations in which *Orco* is expressed either at low levels or in few cells, which might be why this expression was previously missed. We found this to be the case with the *IrCo* knock-ins, as well (described below).

There has been some inconsistency in the literature as to which glomeruli are innervated by Ir8a-expressing OSNs. For example, *Silbering et al., 2011* note that their *Ir8a-Gal4* line labels approximately 10 glomeruli, 6 of which are identified (DL2, DP1l, VL2a, VL2p, DP1m, DC4). An *Ir8a-Gal4* line generated by *Ai et al., 2013* also labels about 10 glomeruli, only 2 of which are identified (DC4 and DP1m) and which correspond to 2 glomeruli in *Silbering et al., 2011*. Finally, *Min et al., 2013* identify three additional glomeruli innervated by an *Ir8a-Gal4* line (VM1, VM4, and VC5) but not reported in the other two papers. DL2 was later subdivided into two glomeruli (*Prieto-Godino et al., 2017*), bringing the total number of identified Ir8a+ glomeruli to 10. However, we found that *Ir8a-T2A-QF2* consistently labels twice as many glomeruli as previously reported. These additional glomeruli include an Ir25a+ glomerulus (VL1, *Figure 3B*), numerous Orco+ glomeruli (such as VA3 and VA5), and an Orco+/Ir76b+ glomerulus (VC3) (see *Figure 3—source data 1* for a full list of new glomeruli and *Figure 3—source data 2* for outlined examples). Some of these additional glomeruli are weakly labeled by an *Ir8a-Gal4* line (*Figure 3—figure supplement 2B*), but this innervation is only apparent when examined with a strong reporter.

Of the four chemosensory co-receptor genes, the previously reported expression of *Ir76b* is the narrowest, with only four identified glomeruli (VM1, VM4, VC3, VC5) (*Silbering et al., 2011*). The *Ir76b-T2A-QF2* knock-in labels more than three times this number, including several Orco+ glomeruli (such as DC3 and VC4), most Ir8a+ glomeruli (including DP1l), and one additional Ir25a+ glomerulus (VL1) (*Figure 3C*). As with *Orco* and *Ir8a*, some but not all of these glomeruli can be identified by crossing the transgenic *Ir76b-Gal4* line to a strong reporter (*Figure 3—figure supplement 2C*). However, the *Ir76b-Gal4* line labels additional glomeruli not seen in the knock-in (*Figure 3—figure*

Table 3. Summary of expression patterns for all knock-in lines (related to *Figures 3–5*).

Summarized here are all of the olfactory sensory neuron (OSN) classes innervating the 58 antennal lobe glomeruli[†]; their corresponding sensilla and tuning receptors; the previously reported (original) co-receptors they express; and whether or not each of the co-receptor knock-in lines labels those glomeruli. Variable indicates that the glomerulus was labeled in <50% of brains examined in the given knock-in line. Sensilla or glomeruli that have been renamed or reclassified have their former nomenclature listed in parentheses. Question marks indicate expression that has been reported but not functionally validated. * See also *Figure 3—source data 1* and *Figure 3—source data 2*.

Glomerulus[†]	Sensillum	Tuning receptor(s)	Original co-receptor(s)	Orco-T2A-QF2	Ir8a-T2A-QF2	Ir76b-T2A-QF2	Ir25a-T2A-QF2	References
D	Ab9A	Or69aA, Or69aB	Orco	Yes	Variable	No	No	*Couto et al., 2005*; *Fishilevich and Vosshall, 2005*
DA1	At1A	Or67d	Orco	Yes	No	Variable	Yes	*Couto et al., 2005*; *Fishilevich and Vosshall, 2005*; *Kurtovic et al., 2007*
DA2	Ab4B	Or56a, Or33a	Orco	Yes	No	No	Yes	*Couto et al., 2005*; *Fishilevich and Vosshall, 2005*
DA3	Ai2B (At2B)	Or23a	Orco	Yes	No	No	Yes	*Couto et al., 2005*; *Fishilevich and Vosshall, 2005*; *Lin and Potter, 2015*
DA4l	Ai3C (At3C)	Or43a	Orco	Yes	No	No	Yes	*Couto et al., 2005*; *Fishilevich and Vosshall, 2005*; *Lin and Potter, 2015*
DA4m	Ai3B (At3B)	Or2a	Orco	Yes	No	No	Yes	*Couto et al., 2005*; *Lin and Potter, 2015*
DC1	Ai3A (At3A)	Or19a, Or19b	Orco	Yes	No	No	Yes	*Couto et al., 2005*; *Fishilevich and Vosshall, 2005*; *Lin and Potter, 2015*
DC2	Ai1A (Ab6A)	Or13a	Orco	Yes	No	No	Yes	*Couto et al., 2005*; *Fishilevich and Vosshall, 2005*; *Lin and Potter, 2015*
DC3	Ai2A (At2A)	Or83c	Orco	Yes	No	Yes	Variable	*Couto et al., 2005*; *Fishilevich and Vosshall, 2005*; *Lin and Potter, 2015*
DL1	Ab1D	Or10a, Gr10a	Orco	Yes	Yes	Yes	Yes	*Couto et al., 2005*; *Fishilevich and Vosshall, 2005*
DL3	At4B	Or65a, Or65b, Or65c	Orco	Yes	No	No	Yes	*Couto et al., 2005*; *Fishilevich and Vosshall, 2005*
DL4	Ab10B	Or49a, Or85f	Orco	Yes	No	No	Yes	*Couto et al., 2005*; *Fishilevich and Vosshall, 2005*
DL5	Ab4A	Or7a	Orco	Yes	No	No	Variable	*Couto et al., 2005*
DM1	Ab1A	Or42b	Orco	Yes	No	No	Yes	*Couto et al., 2005*; *Fishilevich and Vosshall, 2005*
DM2	Ab3A	Or22a, Or22b	Orco	Yes	No	No	Yes	*Couto et al., 2005*; *Fishilevich and Vosshall, 2005*
DM3	Ab5B	Or47a, Or33b	Orco	Yes	No	No	No	*Couto et al., 2005*; *Fishilevich and Vosshall, 2005*
DM4	Ab2A	Or59b	Orco	Yes	No	No	Yes	*Couto et al., 2005*
DM5	Ab2B	Or85a, Or33b	Orco	Yes	No	No	No	*Couto et al., 2005*; *Fishilevich and Vosshall, 2005*
DM6	Ab10A	Or67a	Orco	Yes	No	No	Yes	*Couto et al., 2005*
VA1d	At4C	Or88a	Orco	Yes	No	No	Yes	*Couto et al., 2005*; *Fishilevich and Vosshall, 2005*
VA1v	At4A	Or47b	Orco	Yes	No	No	Yes	*Couto et al., 2005*; *Fishilevich and Vosshall, 2005*
VA2	Ab1B	Or92a	Orco	Yes	No	No	Yes	*Couto et al., 2005*; *Fishilevich and Vosshall, 2005*
VA3	Ab9B	Or67b	Orco	Yes	Yes	Yes	Yes	*Couto et al., 2005*; *Fishilevich and Vosshall, 2005*
VA4	Pb3B	Or85d	Orco	Yes	No	No	Yes	*Couto et al., 2005*
VA5	Ai1B (Ab6B)	Or49b	Orco	Yes	Yes	Yes	Yes	*Couto et al., 2005*; *Lin and Potter, 2015*

Table 3 continued on next page

Table 3 continued

Glomerulus[†]	Sensillum	Tuning receptor(s)	Original co-receptor(s)	Orco-T2A-QF2	Ir8a-T2A-QF2	Ir76b-T2A-QF2	Ir25a-T2A-QF2	References
VA6	Ab5A	Or82a	Orco	Yes	Yes	Yes	Yes	*Couto et al., 2005*; *Fishilevich and Vosshall, 2005*
VA7l	Pb2B	Or46a	Orco	Yes	No	No	Yes	*Couto et al., 2005*; *Fishilevich and Vosshall, 2005*
VA7m	UNK	UNK	Orco	Yes	No	Variable	Yes	*Couto et al., 2005*
VC1	Pb2A	Or33c, Or85e	Orco	Yes	No	No	Yes	*Couto et al., 2005*; *Fishilevich and Vosshall, 2005*
VC2	Pb1B	Or71a	Orco	Yes	No	No	Yes	*Couto et al., 2005*; *Fishilevich and Vosshall, 2005*
VC4	Ab7B	Or67c	Orco	Yes	No	Yes	Yes	*Couto et al., 2005*
VM2	Ab8A	Or43b	Orco	Yes	No	No	No	*Couto et al., 2005*
VM3	Ab8B	Or9a	Orco	Yes	No	No	No	*Couto et al., 2005*
VM5d	Ab3B	Or85b?, Or98b?	Orco	Yes	Variable	No	Yes	*Couto et al., 2005*
VM5v	Ab7A	Or98a	Orco	Yes	Yes	No	Yes	*Couto et al., 2005*; *Fishilevich and Vosshall, 2005*
VM7d	Pb1A	Or42a	Orco	Yes	No	No	Yes	*Couto et al., 2005*; *Endo et al., 2007*; *Fishilevich and Vosshall, 2005*
VM7v (1)	Pb3A	Or59c	Orco	Yes	No	No	Yes	*Couto et al., 2005*; *Endo et al., 2007*
VC3	Ac3B	Or35a	Orco, Ir76b	Yes	Yes	Yes	Yes	*Couto et al., 2005*; *Fishilevich and Vosshall, 2005*; *Silbering et al., 2011*
V	Ab1C	Gr21a, Gr63a	N/A	Yes	No	No	Yes	*Couto et al., 2005*; *Jones et al., 2007*; *Kwon et al., 2007*
DC4	Sacculus, chamber III	Ir64a	Ir8a	Variable	Yes	No	Yes	*Ai et al., 2013*; *Ai et al., 2010*; *Silbering et al., 2011*
DL2d	Ac3A	Ir75b	Ir8a	Yes	Yes	No	Yes	*Prieto-Godino et al., 2017*; *Silbering et al., 2011*
DL2v	Ac3A	Ir75c	Ir8a	Yes	Yes	No	Yes	*Prieto-Godino et al., 2017*; *Silbering et al., 2011*
DP1l	Ac2	Ir75a	Ir8a	Yes	Yes	Yes	Yes	*Silbering et al., 2011*
DP1m	Sacculus, chamber III	Ir64a	Ir8a	No	Yes	Yes	Yes	*Ai et al., 2013*; *Ai et al., 2010*; *Silbering et al., 2011*
VL2a	Ac4	Ir84a	Ir8a	Yes	Yes	Yes	Yes	*Silbering et al., 2011*
VL2p	Ac1	Ir31a	Ir8a	No	Yes	Yes	Yes	*Silbering et al., 2011*
VC5	Ac2	Ir41a	Ir8a, Ir25a, Ir76b	No	Yes	Yes	Yes	*Hussain et al., 2016*; *Min et al., 2013*; *Silbering et al., 2011*
VM1	Ac1	Ir92a	Ir8a, Ir25a, Ir76b	No	Yes	Yes	Yes	*Min et al., 2013*; *Silbering et al., 2011*
VM4	Ac4	Ir76a	Ir8a, Ir25a, Ir76b	Yes	Yes	Yes	Yes	*Benton et al., 2009*; *Min et al., 2013*; *Silbering et al., 2011*
VL1	Ac1, Ac2, Ac4	Ir75d	Ir25a	Yes	Yes	Yes	Yes	*Silbering et al., 2011*
VM6v (VM6)	Ac1	Rh50, Amt	Ir25a	No	Yes (weak)	No	Yes	*Chai et al., 2019*; *Li et al., 2016*; *Schlegel et al., 2021*; *Vulpe et al., 2021*, this paper
VM6m (new)	Sacculus, chamber III	Rh50, Amt	N/A (this paper)	No	Yes (weak)	No	Yes	*Chai et al., 2019*; *Li et al., 2016*; *Schlegel et al., 2021*; *Vulpe et al., 2021*, this paper
VM6l* (new)	Sacculus, chamber III	Rh50, Amt	N/A (this paper)	No	Yes (strong)	No	Yes	*Chai et al., 2019*; *Li et al., 2016*; *Schlegel et al., 2021*; *Vulpe et al., 2021*, this paper

Table 3 continued on next page

Table 3 continued

Glomerulus†	Sensillum	Tuning receptor(s)	Original co-receptor(s)	Orco-T2A-QF2	Ir8a-T2A-QF2	Ir76b-T2A-QF2	Ir25a-T2A-QF2	References
VP1d	Sacculus, chamber II	Ir40a, Ir93a	Ir25a	No	No	No	Yes	*Enjin et al., 2016*; *Frank et al., 2017*; *Knecht et al., 2017*; *Knecht et al., 2016*; *Marin et al., 2020*; *Silbering et al., 2011*
VP1l	Sacculus, chamber I	Ir21a, Ir93a	Ir25a	No	No	No	Yes	*Frank et al., 2017*; *Knecht et al., 2017*; *Knecht et al., 2016*; *Marin et al., 2020*; *Silbering et al., 2011*
VP1m	Sacculus, chamber I	Ir68a, Ir93a	Ir25a	No	No	No	Yes	*Frank et al., 2017*; *Knecht et al., 2017*; *Knecht et al., 2016*; *Marin et al., 2020*; *Silbering et al., 2011*
VP2	Arista	Gr28b.d, Ir93a	Ir25a	No	No	No	Yes	*Enjin et al., 2016*; *Frank et al., 2017*; *Marin et al., 2020*; *Miwa et al., 2018*; *Ni et al., 2013*
VP3	Arista	Ir21a, Ir93a	Ir25a	No	No	No	Yes	*Budelli et al., 2019*; *Enjin et al., 2016*; *Frank et al., 2017*; *Silbering et al., 2011*
VP4	Sacculus, chambers I + II	Ir40a, Ir93a	Ir25a	No	No	No	Yes	*Enjin et al., 2016*; *Frank et al., 2017*; *Knecht et al., 2017*; *Knecht et al., 2016*; *Marin et al., 2020*; *Silbering et al., 2011*
VP5	Sacculus, chamber II	Ir68a, Ir93a	Ir25a	No	No	No	Yes	*Frank et al., 2017*; *Knecht et al., 2017*; *Marin et al., 2020*

*VM6l was initially named VC6 in version 1 of our pre-print (**Task et al., 2020**) but was reclassified using additional data from EM reconstructions in the antennal lobe (AL) and immunohistochemical experiments in the periphery (see Figure 5).

†The VM6 subdivisions (VM6v, VM6m, VM6l) are separated in this table for clarity but counted together as one glomerulus in accordance with **Schlegel et al., 2021**.

supplement 2C, Orco+ cluster). In total, the *Ir76b-T2A-QF2* knock-in labels 15 glomeruli consistently and two variably (*Figure 3—source data 1* and *Figure 3—source data 2*).

Ir25a-T2A-QF2 innervation of the AL was the most expanded compared to what has previously been reported. In addition to the novel expression we identified in the palps (*Figure 2H*), we found that the *Ir25a* knock-in innervates many Orco+ glomeruli receiving inputs from the antennae (*Figure 3D*). The extensive, dense innervation of the AL by Ir25a+ processes made identification of individual glomeruli difficult and necessitated further experiments to fully characterize this expression pattern (described in greater detail below). While it was previously reported that the transgenic *Ir25a-Gal4* line labels only a subset of Ir25a+ neurons (compared to anti-Ir25a antibody staining), it was assumed that neurons not captured by the transgenic line would reside in coeloconic sensilla, the arista, or sacculus (the original locations for all IR+ OSNs) (*Abuin et al., 2011*). When we crossed *Ir25a-Gal4* to a strong reporter, we found labeling of a few Orco+ glomeruli (*Figure 3—figure supplement 2D*), but this was a small fraction of those labeled by the knock-in. To further examine *Ir25a* expression and the potential co-expression of multiple co-receptors in greater detail, we employed a combination of approaches, including single-nucleus RNAseq (snRNAseq), immunohistochemistry, and optogenetics.

Confirmation of co-receptor co-expression

The innervation of the same glomeruli by multiple co-receptor knock-in lines challenges the previous view of segregated chemosensory receptor expression in *D. melanogaster* and suggests two possible explanations: either the same olfactory neurons express multiple co-receptors (co-expression) or different populations of olfactory neurons expressing different receptors converge upon the same glomeruli (co-convergence). These scenarios are not necessarily mutually exclusive. To examine these possibilities in a comprehensive, unbiased way, we analyzed snRNAseq data from adult fly antennae (*McLaughlin et al., 2021*). *Figure 4A* shows the expression levels of the four co-receptor genes in 20 transcriptomic clusters (tSNE plots [*Van der Maaten and Hinton, 2008*], top row), which were mapped to 24 glomerular targets in the brain (AL maps, bottom row). The proportion of cells in each cluster expressing the given co-receptor gene is indicated by the opacity of the glomerular fill color, normalized to maximum expression for that gene (see Materials and methods and *Figure 4—source data 1* for details on expression normalization). The OSN classes to which these clusters map include Orco+ neurons (*Figure 4A*, right column, teal), Ir25a+ neurons (*Figure 4A*, right column, purple), Ir8a+ neurons (*Figure 4A*, right column, pink), and GR+neurons (*Figure 4A*, right column, dark blue).
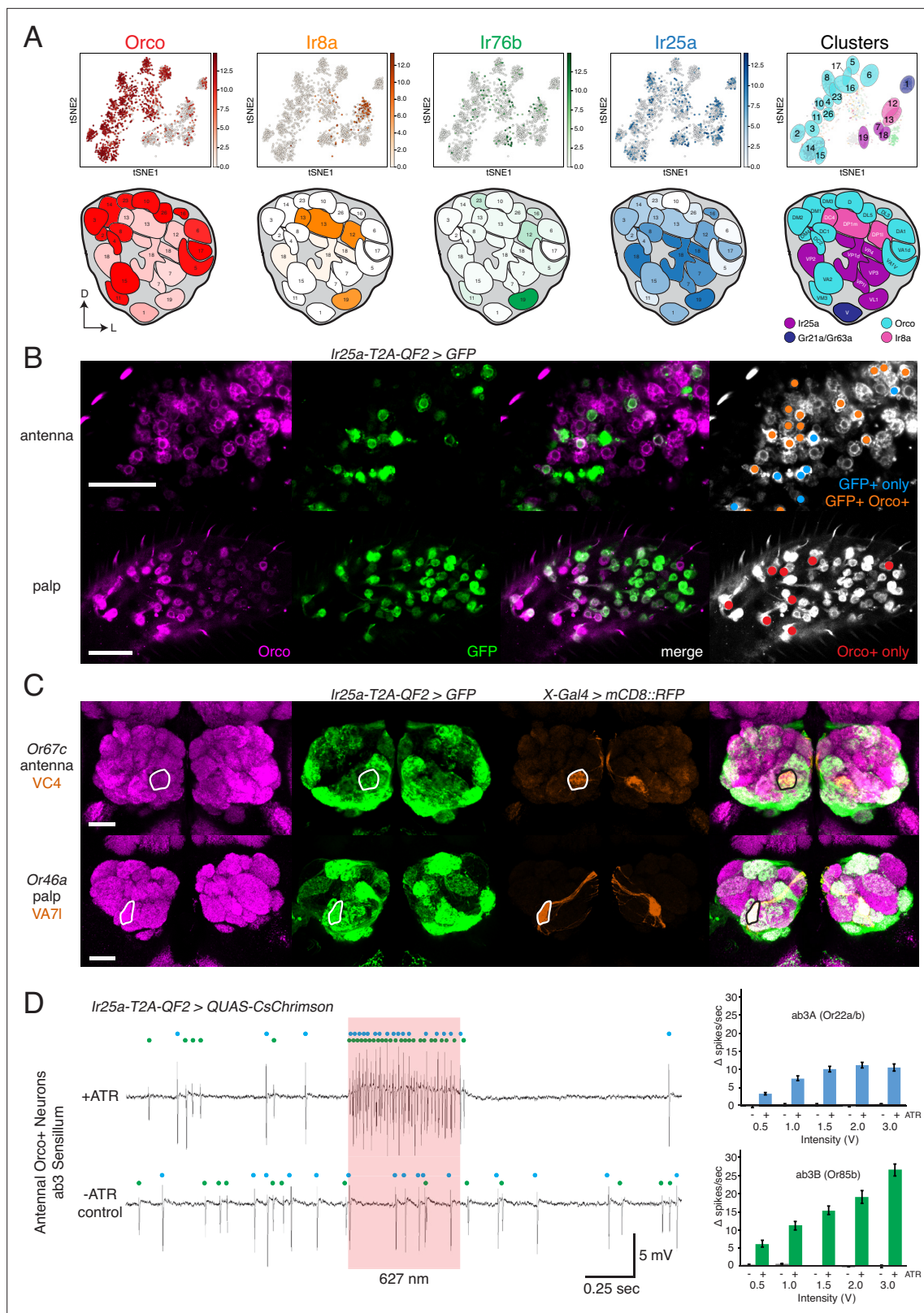
Figure 4. Confirmation of co-receptor co-expression. (**A**) snRNAseq of adult fly antennae (*McLaughlin et al., 2021*) confirms expanded expression of olfactory co-receptors. Top: tSNE plots show expression of each co-receptor in 20 decoded olfactory sensory neuron (OSN) clusters. Bottom: clusters were mapped to 24 glomeruli. Opacity of fill in each glomerulus indicates the proportion of cells in that cluster expressing the given co-receptor, normalized to total expression for that co-receptor gene (see *Figure 4—source data 1*). Right column: clusters color-coded according to original

Figure 4 continued on next page

Figure 4 continued

chemoreceptor gene family. Compass: D = dorsal; L = lateral. (**B**) Anti-Orco antibody staining in antennal cryosections (top) and whole-mount palps (bottom) confirms co-expression of Orco and Ir25a in the periphery (genotype: *Ir25a-T2A-QF2>GFP*). Right panels show cells pseudo-colored gray with specific single- or double-labeled cells indicated by colored cell markers (GFP+ only in blue, GFP+Orco+ in orange, Orco+ only in red). (**C**) Co-labeling experiments with various transgenic *Gal4* lines driving mCD8::RFP (orange) and the *Ir25a-T2A-QF2* knock-in driving GFP (green). *Ir25a-T2A-QF2* labels glomeruli innervated by both antennal (top) and palpal (bottom) OSNs. (**D**) Verification of *Ir25a* expression in antennal ab3 sensilla using optogenetics. Single sensillum recordings (SSR) from ab3 Orco+ neurons in *Ir25a-T2A-QF2>QUAS-CsChrimson* flies. Representative traces from ab3 using 1.5 V of 627 nm LED light (red box) to activate *CsChrimson*. Bottom trace is control animal, which has the same genotype as the experimental animal but was not fed the required all-trans retinal cofactor (-ATR). Spikes from the ab3A and ab3B neurons are indicated by blue and green dots, respectively. Right: quantification of neuronal activity in response to light at various LED intensities (N = 7–12). These optogenetic experiments support *Ir25a* expression in both ab3A neurons (*Or22a/b*, top; corresponding to DM2 glomerulus) and ab3B neurons (*Or85b*, bottom; corresponding to VM5d glomerulus). Scale bars = 25 µm. See also *Figure 4—figure supplement 1*, *Table 3*, *Figure 4—source data 1*, *Figure 4—source data 2*, and *Figure 4—source data 3*.

The online version of this article includes the following source data and figure supplement(s) for figure 4:

Source data 1. snRNAseq co-receptor expression in adult olfactory sensory neurons (OSNs).

Source data 2. Individual glomerular analyses.

Source data 3. Optogenetic validation of *Ir25a* expression.

Figure supplement 1. Optogenetic experiments to examine *Ir25a* expression in Orco+ neurons.

They also include example OSNs from all sensillar types (basiconic, intermediate, trichoid, coeloconic) as well as from the arista and sacculus. The snRNAseq analyses confirmed expanded expression of all four co-receptor genes into OSN classes not traditionally assigned to them. For example, *Orco* and *Ir25a* are expressed in cluster 1, which maps to the V glomerulus (Gr21a+/Gr63a+). Similarly, *Ir8a* and *Ir76b* are expressed in cluster 19 (VL1 glomerulus, Ir25a+), and *Ir25a* is expressed in multiple Orco+ clusters (such as 15/VA2, 16/DL3, and 8/DC1).

The snRNAseq analyses confirm transcript co-expression in olfactory neurons in the periphery. To demonstrate protein co-expression in OSNs, we performed anti-Orco antibody staining on *Ir25a-T2A-QF2>GFP* antennae and palps (**Figure 4B**). In the antennae, we found examples of Orco+ GFP+ double-labeled cells, as well as many cells that were either GFP+ or Orco+ (**Figure 4B**, top-right panel). Interestingly, in the palps the vast majority of cells were double labeled. We found a small population of palpal neurons that were only Orco+, and no neurons that were only GFP+ (**Figure 4B**, bottom-right panel). These results are consistent with our anti-Ir25a staining experiments in the palps (**Figure 2I**), which showed that most of the ~120 palpal OSNs express Ir25a protein.

The snRNAseq data from the antennae and peripheral immunohistochemical experiments in the palps helped to identify some of the novel OSN populations expressing *Ir25a*. We extended these analyses with co-labeling experiments in which we combined transgenic *OrX-*, *IrX-*, or *GrX-Gal4* lines labeling individual glomeruli with the *Ir25a* knock-in to verify the glomerular identity of Ir25a+ axonal targets in the AL. Two examples are shown in **Figure 4C** (one antennal and one palpal OSN population), and the full list of OSN classes checked can be found in **Figure 4—source data 2**.

For some OSN classes not included in the snRNAseq dataset for which co-labeling experiments yielded ambiguous results, we employed an optogenetic approach. We used the *Ir25a-T2A-QF2* knock-in to drive expression of *QUAS-CsChrimson*, a red-shifted channelrhodopsin (**Klapoetke et al., 2014**), and performed single sensillum recordings (SSR) from sensilla previously known to house only Orco+ neurons. If these neurons do express *Ir25a*, then stimulation with red light should induce neuronal firing. We recorded from ab3 sensilla, which have two olfactory neurons (A and B; indicated with blue and green dots, respectively, in **Figure 4D**). Ab3A neurons innervate DM2 and ab3B neurons innervate VM5d. Both neurons responded to pulses of 627 nm light at various intensities in a dose-dependent manner, confirming *Ir25a* expression in these neurons. No light-induced responses were found in control flies, which had the same genotype as experimental flies but were not fed all-trans retinal (-ATR), a necessary co-factor for channelrhodopsin function (see Materials and methods). We used similar optogenetic experiments to examine *Ir25a* expression in OSN classes innervating DM4 (ab2A, Or59b+) and DM5 (ab2B, Or85a/Or33b+) (**Figure 4—figure supplement 1A and B**), as well as D (ab9A, Or69aA/aB+) and VA3 (ab9B, Or67b+) (**Figure 4—figure supplement 1C and D**). These experiments indicated that *Ir25a* is expressed in ab2A (DM4) and ab9B (VA3) neurons, but not ab2B (DM5) or ab9A (D) neurons (see also **Figure 4—source data 2** and **Figure 4—source data 3**). Results of these experiments are summarized in **Table 3**.

Identification of new OSN classes

The co-receptor knock-ins allowed us to analyze the olfactory neuron innervation patterns for all AL glomeruli. Interestingly, the *Ir8a-T2A-QF2* and *Ir25a-T2A-QF2* knock-ins strongly labeled a previously uncharacterized posterior region of the AL. By performing a co-labeling experiment with *Ir41a-Gal4*, which labels the VC5 glomerulus, we narrowed down the anatomical location of this region and ruled out VC5 as the target of these axons (*Figure 5A*). While both knock-ins clearly labeled VC5, they also labeled a region lateral and slightly posterior to it (*Figure 5A*, outline). We performed additional co-labeling experiments with *Ir8a-T2A-QF2* and various *Gal4* lines labeling all known posterior glomeruli to confirm that this AL region did not match the innervation regions for other previously described OSN populations (*Figure 5—figure supplement 1*). We recognized that this novel innervation pattern appeared similar to a portion of the recently identified Rh50+ ammonia-sensing olfactory neurons (*Vulpe et al., 2021*). Co-labeling experiments with *Rh50-Gal4* and *Ir8a-T2A-QF2* confirmed that they indeed partially overlapped (*Figure 5B*). We determined that these Rh50+ olfactory neurons mapped to a portion of the VM6 glomerulus, with the strongly Ir8a+ region innervating the 'horn' of this glomerulus. The difference in innervation patterns between Ir8a+ and Rh50+ neurons in this AL region suggested at least two different subdivisions or OSN populations within this VM6 glomerulus. In fact, in between the main body of VM6 and the Ir8a+ horn there appeared to be a third region (*Figure 5B*, horn outlined in white, other two regions outlined in blue). We designated these subdivisions VM6l, VM6m, and VM6v (for lateral, medial, and ventral). We coordinated the naming of this glomerulus with recent connectomics analyses of the entire fly AL (*Schlegel et al., 2021*). In this connectomics study, dendrites of olfactory projection neurons were found to innervate the entire region described here as VM6l, VM6m, and VM6v. No projection neurons were identified to innervate only a subdomain. As such, the new VM6 nomenclature reflects this unique subdivision of a glomerulus by OSNs but not second-order projection neurons.

We sought to determine the identity of the olfactory neurons that might be innervating these three VM6 subdivisions. Rh50+ neurons can be found in two regions of the antenna: ac1 coeloconic sensilla and the sacculus (*Figure 5C*; *Vulpe et al., 2021*). The shape of the VM6v subdomain most closely matches the glomerulus described as VM6 by previous groups (e.g., *Couto et al., 2005*; *Endo et al., 2007*), which had been suggested to be innervated by coeloconic sensilla (*Chai et al., 2019*; *Li et al., 2016*). In addition, antibody staining had previously shown that Rh50+ ac1 neurons broadly co-express Ir25a but generally not Ir8a (*Vulpe et al., 2021*). This suggested that the other VM6 subdomains might be innervated by the Rh50+ sacculus olfactory neurons. Antibody staining in *Rh50-Gal4>GFP* antennae confirmed co-expression with both Ir25a protein (broad overlap) and Ir8a protein (narrow overlap) in the third chamber of the sacculus (*Figure 5D*; quantified in *Table 4*). Most sacculus neurons appear to be Ir25a+, and in contrast to the *Ir8a* knock-in, the three VM6 subdivisions are all strongly innervated by the *Ir25a* knock-in (*Figure 5A*). Two previously described OSN populations in the third chamber of the sacculus had been characterized to express *Ir8a* along with *Ir64a* and innervate the DP1m and DC4 glomeruli (*Ai et al., 2013*; *Ai et al., 2010*). To demonstrate that the Rh50+ Ir8a+ sacculus neurons represented a distinct olfactory neuron population, we performed immunohisto-chemistry experiments in *Rh50-Gal4>GFP* antennae with an anti-Ir64a antibody (*Figure 5E*, top), and in *Ir64a-Gal4>GFP* antennae with an anti-Ir8a antibody (*Figure 5E*, bottom). These experiments confirmed a new, distinct population of Ir8a+ Ir64a- cells in the sacculus.

The VM6l olfactory projections are difficult to identify in the hemibrain connectome (*Scheffer et al., 2020*) due to the medial truncation of the AL in that dataset (see *Schlegel et al., 2021* for additional details). Here, we used FlyWire (*Dorkenwald et al., 2020*), a recent segmentation of a full adult fly brain (FAFB) (*Zheng et al., 2018*), to reconstruct the VM6 OSN projections in both left and right ALs. Synapse-based hierarchical clustering (syNBLAST) (*Buhmann et al., 2021*) of the VM6 OSNs demonstrated the anatomical segregation into three distinct subpopulations: VM6l, VM6m, and VM6v (*Figure 5F*). This subdivision was subsequently confirmed in a reanalysis of the VM6 glomerulus in the hemibrain dataset (*Schlegel et al., 2021*). Olfactory neurons innervating VM6l were strongly Ir8a+, while olfactory neurons innervating VM6m and VM6v were weakly and sparsely Ir8a+ (see *Figure 3—source data 2*, page 3). This pattern may be due to *Ir8a* expression in only one or a few cells.

Based on the EM reconstructions, genetic AL analyses, and peripheral staining experiments, we propose a model of the anatomical locations and molecular identities of the olfactory neurons inner-vating the VM6 subdivisions (*Figure 5F*). All VM6 subdivisions broadly express *Rh50* and *Ir25a*; the
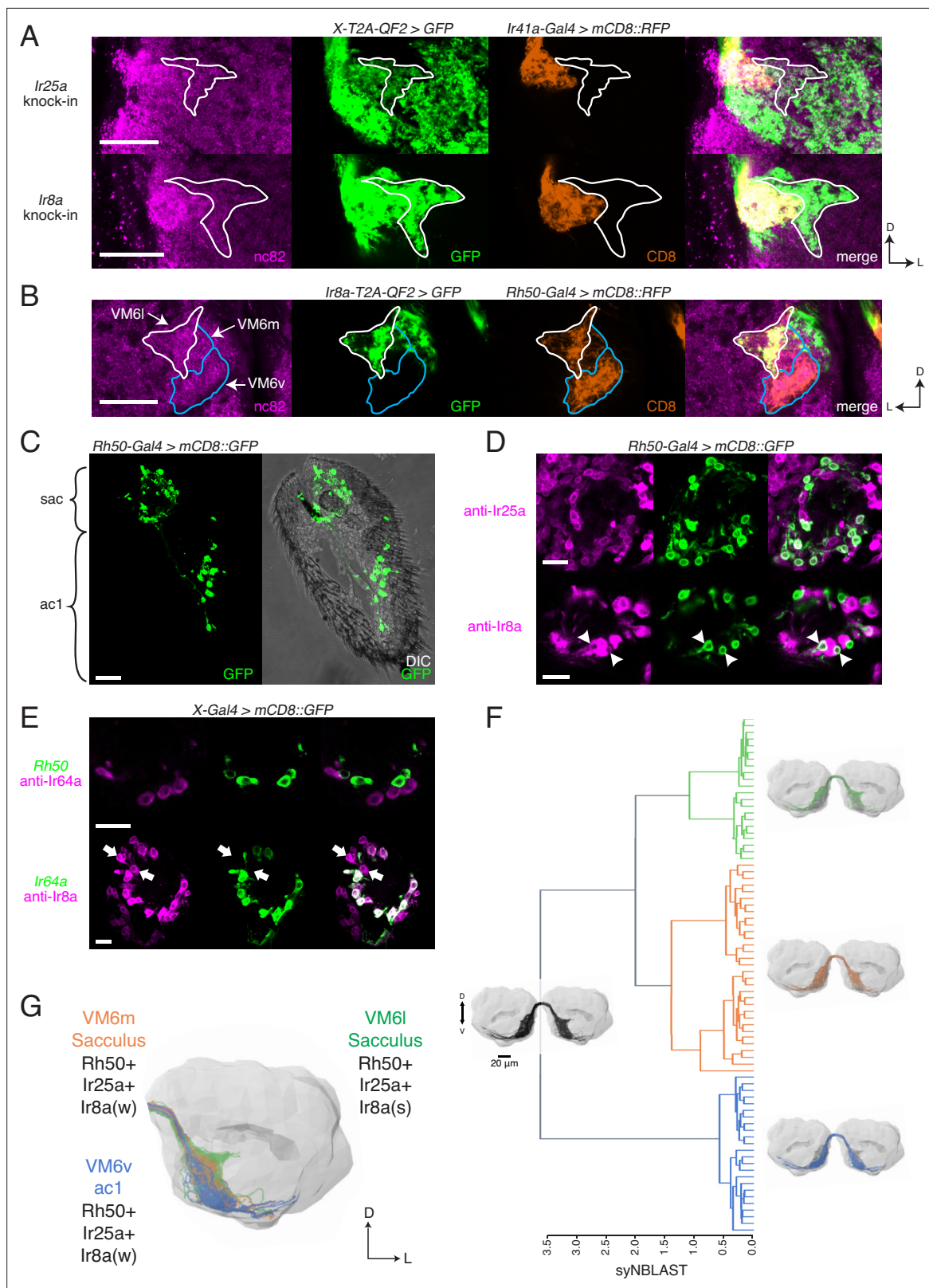
Figure 5. Identification of new olfactory sensory neuron (OSN) classes. (**A**) Co-labeling experiments with *Ir41a-Gal4* show that both *Ir25a-T2A-QF2* and *Ir8a-T2A-QF2* label the VC5 glomerulus (orange), and also a previously unidentified antennal lobe (AL) region (outline). (**B**) The new innervation pattern corresponds to the 'horn' (white outline) of the VM6 glomerulus labeled by Rh50+ neurons (orange). One portion of VM6 is strongly Ir8a+ (VM6l), while two other portions show little to no Ir8a expression (VM6m and VM6v, blue outlines). (**C**) *Rh50-Gal4>GFP* labels neurons in the sacculus (sac)

Figure 5 continued on next page

Figure 5 continued

and antennal coeloconic ac1 sensilla. (**D**) In the sacculus, all Rh50+ neurons appear to be Ir25a+ (top), and a subset are Ir8a+ (bottom, arrowheads). (**E**) Top: Rh50+ neurons in the sacculus do not overlap with Ir64a+ neurons. Bottom: there are two distinct populations of Ir8a+ neurons in the sacculus – those that are Ir64a+ and those that are Ir64a- (arrows). The latter likely correspond to Rh50+ neurons. (**F**) EM reconstructions of VM6 OSNs in a full brain volume (**Dorkenwald et al., 2020**) reveal three distinct subpopulations. (**G**) Model of OSN innervation of the VM6 region. VM6 can be subdivided into three OSN populations based on anatomical location in the periphery and chemoreceptor expression: VM6v (blue) OSNs originate in ac1, strongly (s) express Rh50 and Ir25a, and weakly (w) or infrequently express Ir8a; VM6m (orange) neurons originate in the sacculus and have a similar chemoreceptor expression profile to VM6v; VM6l (green) OSNs originate in the sacculus but strongly express Ir8a in addition to Rh50 and Ir25a. Compass: D = dorsal, L = lateral. Scale bars: 20 μm in (**A–C**) and (**F**), 10 μm in (**D, E**). N = 9–11 for (**C–E**). See also *Figure 5—figure supplement 1* and *Tables 3 and 4*.

The online version of this article includes the following figure supplement(s) for figure 5:

Figure supplement 1. The new glomerular region labeled by the *Ir8a* knock-in does not correspond to previously identified posterior glomeruli.

VM6v OSNs are housed in ac1 sensilla and express *Ir8a* either weakly or only in a small subset of neurons; both the VM6m and VM6l OSNs are found in the sacculus and can be distinguished by their levels or extent of *Ir8a* expression, with VM6l neurons being strongly Ir8a+. Because all three VM6 subdivisions share the same downstream projection neurons, this AL region has been classified as a single glomerulus (*Schlegel et al., 2021*). We maintain this convention here, for a total of 58 AL glomeruli. It is possible that this number may need to be re-evaluated in the future, and the three VM6 subdivisions reconsidered as bona fide separate glomeruli (bringing the OSN glomerular total to 60). Such a separation might be warranted if it is found that these OSN populations express different tuning receptors, and those receptors respond to different odorants.

Table 3 summarizes the chemosensory receptor expression patterns for all four co-receptor knock-in lines across all OSNs, sensillar types, and glomeruli. For clarity, this summary considers the newly identified OSN populations described here separately. We find that *Orco-T2A-QF2* consistently labels 45 total glomeruli out of 58 (7 more than previously reported); *Ir8a-T2A-QF2* consistently labels 18 glomeruli (8 more than previously identified); *Ir76b-T2A-QF2* consistently labels 15 glomeruli (11 more than previously identified); and *Ir25a-T2A-QF2* consistently labels 51 glomeruli (39 more than previously identified).

Table 4. Co-expression of Rh50 and Ir8a in the sacculus (related to *Figure 5*).
Antennal cryosections of *Rh50-Gal4>GFP* flies were stained with an anti-Ir8a antibody, and the overlap of Ir8a+ and GFP+ cells was quantified in the sacculus. 22% of Ir8a+ cells expressed Rh50, 35% of Rh50+ cells expressed Ir8a, and 16% of all cells were double labeled. N = 11.

Genotype	Sample	Ir8a+ cells	GFP+ cells	Double-labeled cells	Total cells
Rh50-Gal4>GFP	20210226 a1	18	9	2	25
Rh50-Gal4>GFP	20210226 a2	22	15	4	33
Rh50-Gal4>GFP	20210226 a3	41	22	7	56
Rh50-Gal4>GFP	20210226 a4	41	14	5	50
Rh50-Gal4>GFP	20210129 a1	26	20	9	37
Rh50-Gal4>GFP	20210129 a2	32	24	7	49
Rh50-Gal4>GFP	20210129 a3	29	19	7	41
Rh50-Gal4>GFP	20210216 a1	26	21	8	39
Rh50-Gal4>GFP	20210216 a2	30	18	7	41
Rh50-Gal4>GFP	20210216 a3	34	23	8	49
Rh50-Gal4>GFP	20210216 a4	34	23	9	48
	Total across samples:	333	208	73	468
		Proportion of Ir8a+ cells that are GFP+:	Proportion of GFP+ cells that are Ir8a+:	Proportion of all cells that are double labeled:	
		0.22	0.35	0.16	

Co-receptor contributions to olfactory neuron physiology

How might the broad, combinatorial co-expression of various chemosensory families affect olfactory neuron function? To begin to address this question, we examined olfactory responses in neuronal populations co-expressing just two of the four chemosensory receptor families (*Orco* and *Ir25a*). We chose to test eight OSN classes previously assigned to the Orco+ domain that we found to have strong or intermediate *Ir25a* expression – two in the antennae and six in the maxillary palps. The two antennal OSN classes are found in the same ab3 sensillum (ab3A, Or22a/b+, DM2 glomerulus; and ab3B, Or85b+, VM5d glomerulus). The six palpal OSN classes represent the entire known olfactory neuron population of the maxillary palps (pb1A, Or42a+, VM7d; pb1B, Or71a+, VC2; pb2A, Or33c/Or85e+, VC1; pb2B, Or46a+, VA7l; pb3A, Or59c+, VM7v; pb3B, Or85d+, VA4). In both the antennae and the palps, we compared the olfactory responses of OSNs to a panel of 13 odorants in three genotypes: *wildtype*, *Ir25a^2* mutant, and *Orco^2* mutant flies. This panel included odorants typically detected by *ORs*, such as esters and aromatics, and odorants typically detected by *IRs*, such as acids and amines (*Silbering et al., 2011*). In the previously accepted view of olfaction in *D. melanogaster*, Orco+ neurons express only Orco/OrX receptors, and all olfactory responses in the neurons can be attributed to these receptors. Thus, in an *Ir25a^2* mutant background, there should be no difference in olfactory responses from *wildtype* if either (a) *Ir25a* is not expressed in these neurons or (b) *Ir25a* is expressed, but is not playing a functional role in these neurons. In an *Orco^2* mutant background, there would be no trafficking of Orco/OrX receptors to the dendritic membrane, and no formation of functional ion channels (*Benton et al., 2006*; *Larsson et al., 2004*). Thus, in the traditional view of insect olfaction, *Orco^2* mutant neurons should have no odor-evoked activity. However, in the new co-receptor co-expression model of olfaction, if *Ir25a* is contributing to olfactory responses in Orco+ neurons, then mutating this co-receptor might affect the response profiles of these neurons. Similarly, *Orco^2* mutant neurons that co-express *Ir25a* might retain some odor-evoked activity.

We first examined olfactory responses in palp basiconic sensilla. In the palps, three types of basiconic sensilla (pb1, pb2, and pb3) contain two neurons each (A and B) (*Figure 6A*), for a total of six OSN classes (*Couto et al., 2005*; *de Bruyne et al., 1999*; *Fishilevich and Vosshall, 2005*; *Goldman et al., 2005*; *Ray et al., 2008*; *Ray et al., 2007*). We found robust responses to several odorants in our panel in both the *wildtype* and *Ir25a^2* mutant flies, including odorants like 1-octen-3-ol typically considered as an OR ligand (*Figure 6B*), and IR ligands like pyrrolidine. Neither odor-evoked nor spontaneous activity was detected in the *Orco^2* mutant (*Figure 6B*, bottom row; see also *Figure 6—figure supplement 1A*). This was true of all sensilla tested in the palps. The SSR experiments in *Figure 6A–D* were performed at 4–8 DPE. We recently discovered that neurodegeneration of *Orco^2* mutant olfactory neurons occurs in the palps by ~6 DPE (*Task and Potter, 2021*), which could potentially confound our interpretation. We repeated the experiments in young (1–3 DPE) flies but similarly detected neither odor-evoked activity nor spontaneous activity in *Orco^2* mutant palpal neurons (*Figure 6—figure supplement 1B*). There was also no spontaneous or odor-evoked activity in an *Ir25a^2; Orco^2* double mutant (*Figure 6—figure supplement 1C*). This suggests one of three possibilities: first, *Orco^2* mutant neurons in the palps could already be dysfunctional at this early stage, despite not yet showing cell loss, and *Ir25a*-dependent activity is not sufficient to maintain either baseline or stimulus-induced activity; second, *Ir25a* function may be *Orco*-dependent in these cells, or act downstream of *Orco*, such that loss of *Orco* function affects *Ir25a* function; third, we did not stimulate neurons with an *Ir25a*-dependent odorant. The latter possibility would not, however, explain why there is no spontaneous activity in these cells. Future experiments will be needed to address these possibilities. Given the lack of neuronal activity in the *Orco^2* mutant, we focused subsequent analyses in the palps on the two other genotypes: *wildtype* and *Ir25a^2*.

The response in the pb1A neuron to 1-octen-3-ol was significantly higher in the *Ir25a^2* mutant compared to the *wildtype* (Mann–Whitney *U* test, p=0.0016), as was the response to methyl salicylate (p=0.0177), while the response to ethyl acetate (EA) was higher in *wildtype* (p=0.008) (*Figure 6C*; see *Figure 6—source data 1* for results of all statistical analyses). The differences in responses across all six OSN classes in the palps between *wildtype* and *Ir25a^2* mutant flies are summarized in *Figure 6D*. In each neuron class, we found 1–3 odorants whose response profiles differed between the two genotypes. However, the specific stimuli eliciting different responses, and the directionality of those responses, varied. For example, 2,3-butanedione elicited higher responses in the *Ir25a^2* mutant in both pb2B and pb3A neurons, but lower responses in the mutant (higher in the *wildtype*) in pb3B.
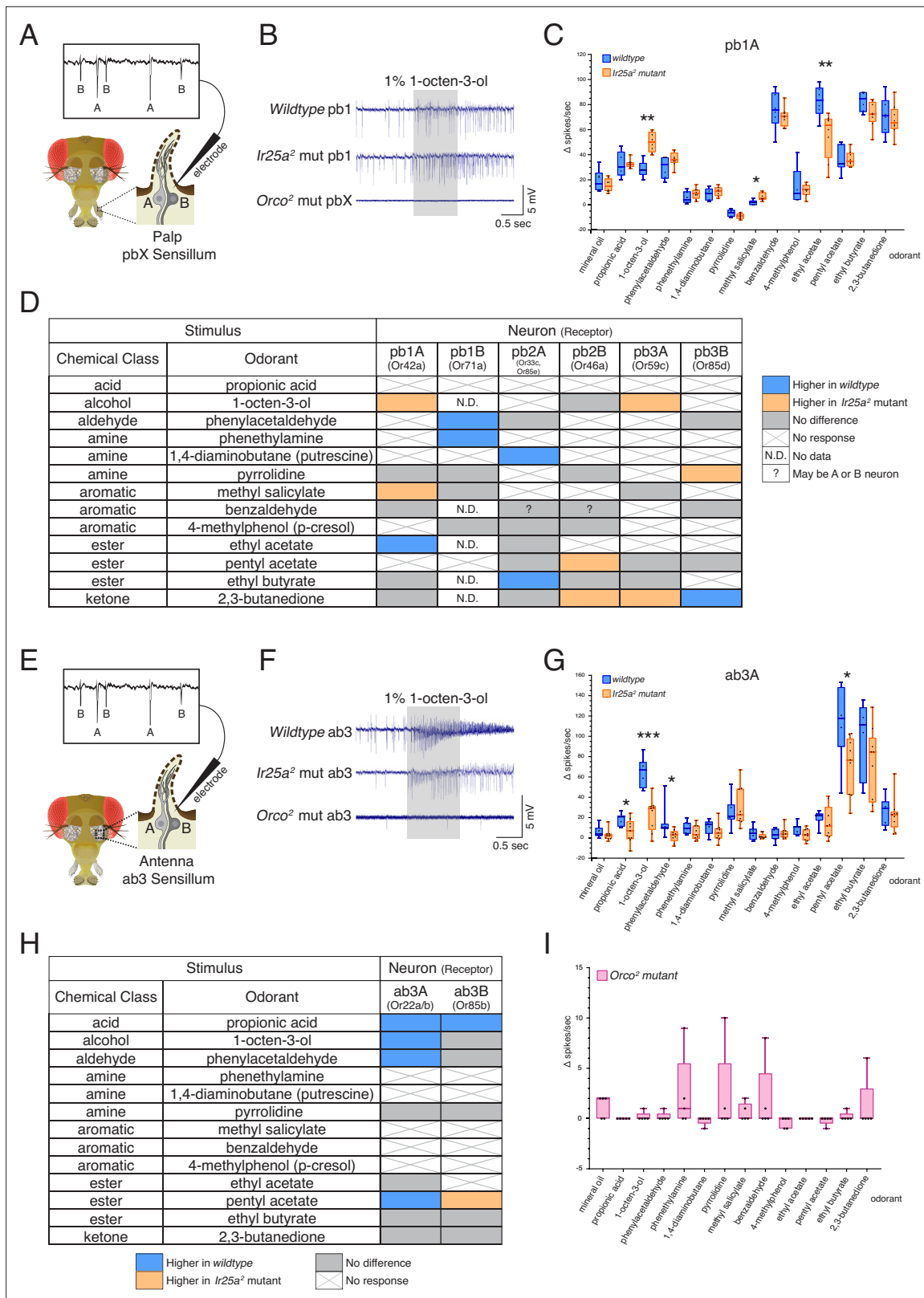
A

Palp
pbX Sensillum

B

1% 1-octen-3-ol

Wildtype pb1

Ir25a² mut pb1

Orco² mut pbX

5 mV

0.5 sec

C

pb1A

- wildtype
- Ir25a² mutant

Δ spikes/sec

odorant

D

Stimulus		Neuron (Receptor)					
Chemical Class	Odorant	pb1A (Or42a)	pb1B (Or71a)	pb2A (Or33c, Or85e)	pb2B (Or46a)	pb3A (Or59c)	pb3B (Or85d)
acid	propionic acid						
alcohol	1-octen-3-ol		N.D.				
aldehyde	phenylacetaldehyde						
amine	phenethylamine						
amine	1,4-diaminobutane (putrescine)						
amine	pyrrolidine						
aromatic	methyl salicylate						
aromatic	benzaldehyde		N.D.	?	?		
aromatic	4-methylphenol (p-cresol)						
ester	ethyl acetate		N.D.				
ester	pentyl acetate						
ester	ethyl butyrate		N.D.				
ketone	2,3-butanedione		N.D.				

- Higher in *wildtype*
- Higher in *Ir25a²* mutant
- No difference
- No response
- N.D. No data
- ? May be A or B neuron

E

Antenna
ab3 Sensillum

F

1% 1-octen-3-ol

Wildtype ab3

Ir25a² mut ab3

Orco² mut ab3

5 mV

0.5 sec

G

ab3A

- wildtype
- Ir25a² mutant

Δ spikes/sec

odorant

H

Stimulus		Neuron (Receptor)	
Chemical Class	Odorant	ab3A (Or22a/b)	ab3B (Or85b)
acid	propionic acid		
alcohol	1-octen-3-ol		
aldehyde	phenylacetaldehyde		
amine	phenethylamine		
amine	1,4-diaminobutane (putrescine)		
amine	pyrrolidine		
aromatic	methyl salicylate		
aromatic	benzaldehyde		
aromatic	4-methylphenol (p-cresol)		
ester	ethyl acetate		
ester	pentyl acetate		
ester	ethyl butyrate		
ketone	2,3-butanedione		

- Higher in *wildtype*
- Higher in *Ir25a²* mutant
- No difference
- No response

I

- Orco² mutant

Δ spikes/sec

odorant

Figure 6. Co-receptor contributions to olfactory neuron physiology. (**A–I**) Single sensillum recording (SSR) experiments were performed in three genetic backgrounds: *wildtype*, *Ir25a²* mutant, and *Orco²* mutant flies. A panel of 13 odorants was tested. In all box plots, *p<0.05, **p<0.01, and ***p<0.001. (**A**) Cartoon of a fly head, zooming in on a single sensillum in the palp. Each palpal sensillum (pbX) contains two neurons, A and B. An electrode is inserted into the sensillum, and neuronal activity is recorded in response to odorants. Activity of the A and B neurons can be distinguished based on

Figure 6 continued on next page

Figure 6 continued

their spike amplitudes (top). (**B**) Representative traces from recordings in palp basiconic pb1 sensilla in the three genotypes in response to 1% 1-octen-3-ol. Sensilla were identified based on responses to reference odorants (***de Bruyne et al., 1999***; see Materials and methods). The $Orco^2$ mutant did not exhibit odor-evoked activity nor spontaneous activity, making it difficult to determine the identity of the recorded sensillum. $Orco^2$ mutant sensilla are thus denoted pbX. (**C**) Quantification of responses to the panel of odorants in *wildtype* (blue; N = 5–9 flies) and $Ir25a^2$ mutant (orange; N = 6–10 flies) pb1A neurons. Responses were higher in the $Ir25a^2$ mutant than in the *wildtype* for 1-octen-3-ol and methyl salicylate, and lower in the $Ir25a^2$ mutant for ethyl acetate. Mann–Whitney U tests indicated these differences were statistically significant: 1-octen-3-ol: $Mdn_{Ir25amut}$ = 50, $Mdn_{wildtype}$ = 28, $U(N_{Ir25amut}$ = 8, $N_{wildtype}$ = 5) = 0, p=0.0016; methyl salicylate: $Mdn_{Ir25amut}$ = 5, $Mdn_{wildtype}$ = 2, $U(N_{Ir25amut}$ = 7, $N_{wildtype}$ = 5) = 3, p=0.0177; ethyl acetate: $Mdn_{Ir25amut}$ = 63.5, $Mdn_{wildtype}$ = 83.5, $U(N_{Ir25amut}$ = 8, $N_{wildtype}$ = 6) = 4, p=0.008. (**D**) Summary of differences in responses across all six neuron classes in the palps between *wildtype* and $Ir25a^2$ mutant flies. Comparisons were made using Mann–Whitney U tests. Orange indicates higher response in $Ir25a^2$ mutant, blue indicates higher response in *wildtype*. Gray is no difference between genotypes, X indicates no response to the given stimulus, and N.D. is no data (strong A neuron response obscured B neuron spikes preventing quantification). In the *wildtype*, for one sensillum-odorant combination (pb2 and benzaldehyde), it could not be distinguished if responses arose from the A or B neuron or both (indicated by a question mark). (**E**) Fly head cartoon, zooming in on a single sensillum in the antenna. We recorded from antennal ab3 sensilla, each of which contains two neurons, A and B. As in the palps, responses from these neurons can be distinguished based upon their spike amplitude (top). (**F**) Representative traces from recordings in antennal basiconic ab3 sensilla in the three genotypes in response to 1% 1-octen-3-ol. In $Orco^2$ mutant ab3 sensilla spontaneous activity was observed, but there was no significant odor-evoked activity. *Wildtype* N = 7 sensilla from five flies; $Ir25a^2$ mutant N = 10 sensilla from five flies. (**G**) Quantification of responses in *wildtype* (blue; N = 7) and $Ir25a^2$ mutant (orange; N = 9) ab3A neurons. Responses were significantly higher in *wildtype* compared to $Ir25a^2$ mutant ab3A neurons for four odorants (Mann–Whitney U results in parentheses; all $N_{wildtype}$ = 7 and $N_{Ir25amut}$ = 9): propionic acid ($Mdn_{wildtype}$ = 21, $Mdn_{Ir25amut}$ = 7, U = 12.5, p=0.0441); 1-octen-3-ol ($Mdn_{wildtype}$ = 67, $Mdn_{Ir25amut}$ = 29, U = 1.5, p=0.0004); phenylacetaldehyde ($Mdn_{wildtype}$ = 10, $Mdn_{Ir25amut}$ = 3, U = 9, p=0.015); and pentyl acetate ($Mdn_{wildtype}$ = 118, $Mdn_{Ir25amut}$ = 77, U = 9, p=0.0164). Difference between *wildtype* and $Ir25a^2$ mutant to phenylacetaldehyde is significant even with the large *wildtype* outlier removed (p=0.0336). (**H**) Summary of differences in responses in the two neuron classes in ab3 between *wildtype* and $Ir25a^2$ mutant flies. Comparisons were made using Mann–Whitney U tests. Orange indicates higher response in $Ir25a^2$ mutant, blue indicates higher response in *wildtype*, gray is no difference between genotypes, and X is no response to the given stimulus. One $Ir25a^2$ mutant fly was excluded from analyses as it had high responses to the mineral oil control (40–53 Δ spikes/s), not seen in any other animal of any genotype. (**I**) Weak responses in $Orco^2$ mutant flies to certain stimuli (≤10 Δ spikes/s) were occasionally detected. While there were some statistically significant differences from mineral oil control (pentyl acetate p=0.0109, propionic acid p=0.0434, ethyl acetate p=0.0434, 1,4-diaminobutane p=0.0109, p-cresol p=0.0021), these were not deemed biologically significant due to very small Δ spike values relative to zero. For more details, see Materials and methods. N = 5 flies. See also ***Figure 6—figure supplements 1–3*** and ***Figure 6—source data 1***.

The online version of this article includes the following source data and figure supplement(s) for figure 6:

Source data 1. Single sensillum recording (SSR) of *Ir25a* mutant, *Orco* mutant, and *wildtype* flies.

Figure supplement 1. Electrophysiological experiments to examine *Ir25a* function in Orco+ neurons.

Figure supplement 2. No IrX expression of the top candidates in the maxillary palps.

Figure supplement 3. Example traces for odorants eliciting differences between *wildtype* and *Ir25a* mutant sensilla.

Interestingly, when we examined a list of candidate IrX tuning receptors (***Li et al., 2021***) in the palps using in situs, we did not find expression (see ***Figure 6—figure supplement 2*** and Appendix 1—key resources table). This suggests that *Ir25a* may not be functioning as a traditional co-receptor in Orco+ olfactory neurons in the palps (an expanded role for *Ir25a* beyond co-reception has previously been suggested; see ***Budelli et al., 2019***; ***Chen et al., 2015***).

We next examined olfactory responses in antennal basiconic ab3 sensilla in *wildtype*, $Ir25a^2$ mutant, and $Orco^2$ mutant flies (***Figure 6E–I***). As in the palps, ab3 sensilla contain two neurons, A and B (***Figure 6E***). In contrast to the palps, $Orco^2$ mutant ab3 sensilla did occasionally show spontaneous activity (***Figure 6F***, bottom row; see ***Figure 6—figure supplement 1D*** and ***Figure 6—figure supplement 3*** for additional example traces). Although there are two Orco+ neurons in this sensillum, we consistently observed only a single spike amplitude in the $Orco^2$ mutant. Thus, we cannot determine at this time whether this activity arises from the A or B neuron. We occasionally observed small responses (≤10 Δ spikes/s) in the $Orco^2$ mutant; however, across all flies tested, these responses were not significantly different from the mineral oil control (***Figure 6I***; statistical analyses can be found in ***Figure 6—source data 1***). For these reasons, $Orco^2$ mutant flies were excluded from the analyses in ***Figure 6G and H***.

As in the palps, we found significant differences in the responses of both ab3A and ab3B neurons to some odorants between the two genotypes. A comparison of all ab3A responses between the *wildtype* and $Ir25a^2$ mutant genotypes is shown in ***Figure 6G***, and results from both the A and B neurons are summarized in ***Figure 6H*** (Mann–Whitney U, as in ***Figure 6A–C***; see ***Figure 6—source data 1*** for all analyses). In the ab3A neuron, the *wildtype* showed higher responses to propionic acid (p=0.0441),

1-octen-3-ol (p=0.0004), phenylacetaldehyde (p=0.015), and pentyl acetate (p=0.0164). Interestingly, two of these four odorants are typically associated with *IRs* (propionic acid and phenylacetaldehyde). In the ab3B neuron, only two odorants elicited significantly different responses between the *wildtype* and $Ir25a^2$ mutant: propionic acid (response higher in *wildtype*, as with ab3A; p=0.0388), and pentyl acetate (response higher in mutant, in contrast to ab3A; p=0.0385). While responses to propionic acid are small in both ab3 neurons, they are abolished in the $Ir25a^2$ mutant background (Kruskal–Wallis with uncorrected Dunn's comparing odorant responses to mineral oil control; ab3A p=0.3957; ab3B p=0.5184), suggesting that propionic acid detection in ab3 may be *Ir25a*-dependent.

Co-receptor co-expression in other insect olfactory organs

To determine if co-receptor co-expression might exist in other insects besides *D. melanogaster*, we used RNA in situ hybridization to examine expression of *Orco* and *Ir25a* orthologues in the fly *D. sechellia* and in the mosquito *A. coluzzii* (*Figure 7*). *D. melanogaster* and *D. sechellia* diverged approximately 5 million years ago (*Hahn et al., 2007*), while the *Drosophila* and *Anopheles* lineages diverged nearly 260 million years ago (*Gaunt and Miles, 2002*; *Figure 7A*). Because co-receptor sequences are highly conserved, we could use our *D. mel. Orco* and *Ir25a* in situ probes (*Figure 7B*) to examine the expression of these genes in the maxillary palps of *D. sechellia*. We found widespread co-expression of *Orco* and *Ir25a* (63% of all cells were double labeled), consistent with our findings in *D. melanogaster* (*Figure 7C*). For *A. coluzzii* mosquitoes, we designed *Anopheles*-specific *Orco* and *Ir25a* probes, and examined co-receptor co-expression in antennae (*Figure 7D*) and maxillary palps (*Figure 7E*). We observed broad co-expression of *AcOrco* and *AcIr25a* in the maxillary palp capitate peg sensilla (47% of all cells were double labeled), and narrower co-expression in the antennae (25% double labeled). Co-expression results for all tissues examined are summarized in *Figure 7F*, and cell counts can be found in *Table 5*. These results suggest that *Orco* and *Ir25a* co-receptor co-expression extends to other Drosophilid species as well as mosquitoes (see also *Ye et al., 2021*; *Younger et al., 2020*).

The co-receptor co-expression map of olfaction in *D. melanogaster*

Co-receptor co-expression of insect chemosensory receptors suggests that multiple receptors may influence the response properties of an olfactory neuron, as we have shown in ab3 and palpal sensilla. To aid future investigations of co-receptor co-expression signaling, we synthesized our results (*Table 3*) into a comprehensive new map of the AL. *Figure 8* summarizes the expression patterns of all the co-receptor knock-in lines and presents a new model for chemosensory receptor expression in *D. melanogaster*. In *Figure 8A*, the expression pattern of each knock-in line is presented separately (see also *Figure 3—source data 1*). The new AL map is updated with the recent reclassification of VP1 into three glomeruli (*Marin et al., 2020*) and indicates the new VM6 subdivisions. In *Figure 8A*, the original glomerular innervation pattern for each co-receptor is shown in green, with new innervation revealed by the *T2A-QF2* knock-in lines color coded by intensity: strongly labeled glomeruli are in orange, intermediate glomeruli in yellow, and weakly labeled glomeruli are in pink. Glomeruli labeled in <50% of brains examined are designated variable (gray), and glomeruli not labeled by the given knock-in are in white. The new VM6v, VM6m, and VM6l subdivisions are labeled with gray stripes.

In the previous model of olfaction in *Drosophila*, the Orco/OR domain primarily occupied the anterior AL, while the IR domains innervated more posterior glomeruli. While the former is still, for the most part, accurate (*Figure 8A*, *Orco*), the latter is not: both *Ir8a-T2A-QF2* and *Ir76b-T2A-QF2* label several more anterior glomeruli (such as VA3 or VA6), and *Ir25a-T2A-QF2* labels the majority of glomeruli throughout the anterior to posterior axis (*Figure 8A*, *Ir25a*). The expansion of the Ir25a+ domain is the most dramatic of the four co-receptors: previously, Ir25a+ glomeruli accounted for 21% of the AL (12/58 glomeruli) (*Enjin et al., 2016*; *Frank et al., 2017*; *Marin et al., 2020*; *Silbering et al., 2011*); the *Ir25a-T2A-QF2* knock-in consistently labels 88% of the AL (51/58 glomeruli, excluding variable). This represents a greater than fourfold expansion. Similarly, the number of Ir76b+ glomeruli increased more than threefold, from 7% of the AL (4/58 glomeruli) (*Silbering et al., 2011*) to 26% (15/58, excluding variable). The Ir8a+ domain has nearly doubled, from 17% of the AL originally (10/58 glomeruli) (*Silbering et al., 2011*) to 31% (18/58, excluding variable). The most modest increase in reported expression is in the Orco+ domain: from 66% of the AL (38/58 glomeruli) (*Couto et al., 2005*; *Fishilevich and Vosshall, 2005*) to 78% (45/58, excluding variable).
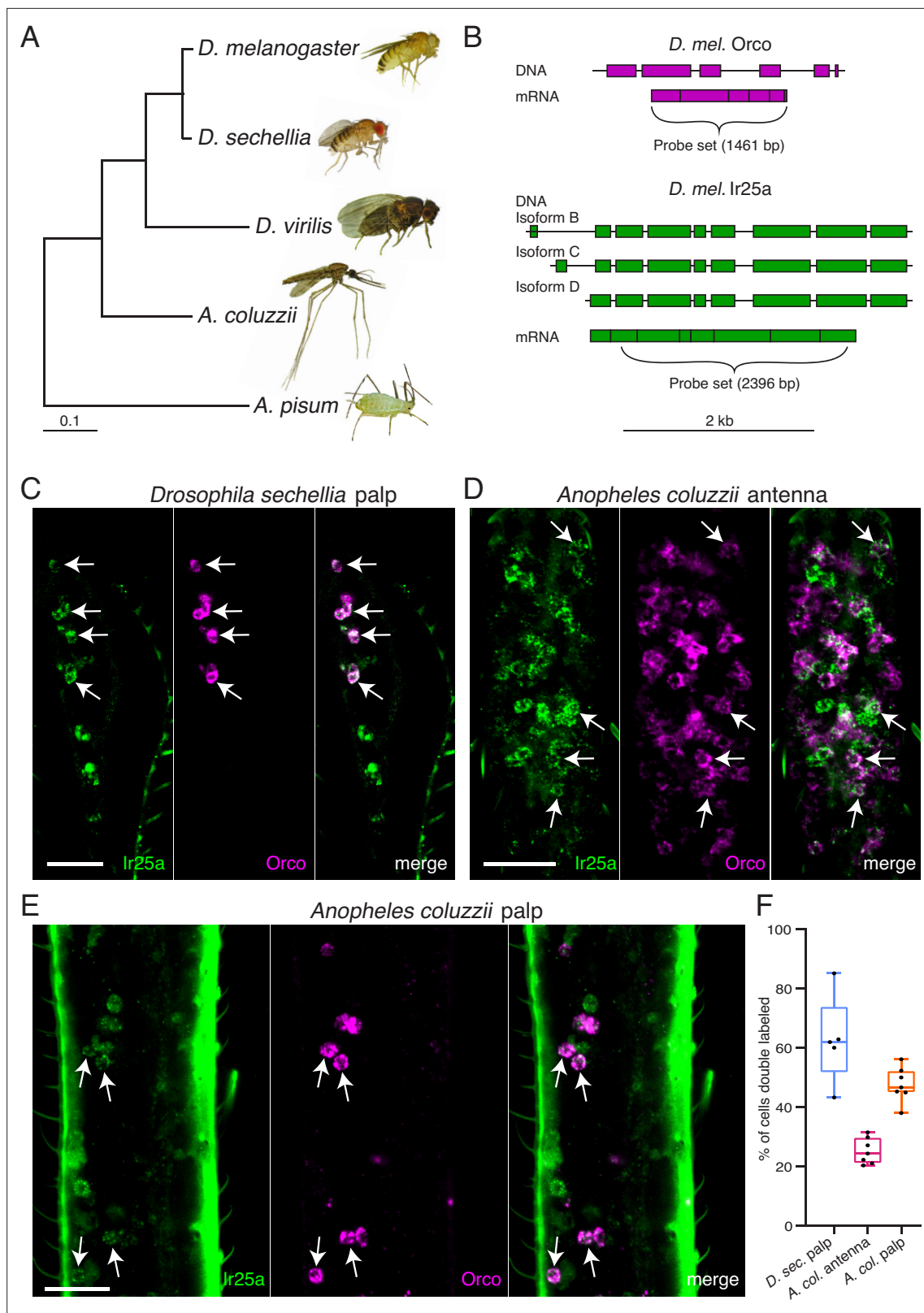
Figure 7. *Orco* and *Ir25a* are co-expressed in *Drosophila sechellia* and *Anopheles coluzzii* olfactory organs. (**A**) Phylogenetic tree based on the *Orco* sequences from the five insects shown (*D.* = *Drosophila*, *A. coluzzii* = *Anopheles coluzzii*, *A. pisum* = *Acyrthosiphon pisum*). Evolutionary history was inferred using the Maximum Likelihood method and Tamura–Nei model (***Tamura and Nei, 1993***). Pea aphid image **A** was reproduced from PLoS Biology Issue Image (2010). (**B**) The *Drosophila melanogaster Orco* in situ probe set, which covers the entire *Orco* coding sequence (top, magenta), was

Figure 7 continued on next page

Figure 7 continued

used to examine *Orco* expression in the maxillary palps of other *Drosophila* fly species. We designed a new probe set covering the most conserved portion of *D. mel. Ir25a* (bottom) as determined by analyzing the *Ir25a* sequences from multiple fly species and comparing them to the various *Drosophila melanogaster Ir25a* isoforms (three of which are illustrated in green). (**C**) Many olfactory sensory neurons (OSNs) in the *Drosophila sechellia* maxillary palps co-express both *Orco* and *Ir25a*, as revealed by in situ experiments (four example cells indicated with arrows). N = 5. (**D**) In situs in *Anopheles coluzzii* antennae reveal a small proportion of cells expressing both co-receptors (arrows). N = 7. (**E**) In situs in *Anopheles coluzzii* maxillary palps show many cells express both *Orco* and *Ir25a* (four examples indicated with arrows). N = 7. (**F**) Summary of co-expression analyses in (**C–E**). For each olfactory organ examined, we divided the number of Orco+ Ir25a+ double-labeled cells by the total number of cells labeled by either probe. We found that 63% of *D. sec.* palpal OSNs express both *Orco* and *Ir25a* (blue), 25% of *A. col.* antennal OSNs express both co-receptors (pink), and 47% of *A. col.* palpal OSNs are double labeled (orange). (**C–E**) are maximum intensity projections of partial z-stacks. See also ***Table 5***, and Appendix 1—key resources table.

The expression overlap in the AL of the four co-receptor families is summarized in the Venn diagram shown in ***Figure 8B*** (excluding the variably labeled glomeruli from ***Figure 8A***). The table at the right lists the names of the glomeruli that correspond to the sections of the Venn diagram. This analysis reveals nine glomeruli labeled by all four knock-in lines; furthermore, it shows that the Ir8a+ and Ir76b+ domains do not have glomeruli unique to them. Most of the AL is innervated by Orco+ Ir25a+ neurons (25 glomeruli that are only Orco+ Ir25a+, plus an additional 13 that have Orco, Ir25a, and one or both other co-receptors). The Orco+ and Ir25a+ domains reveal glomeruli unique to them (six glomeruli that are only Orco+, seven glomeruli that are only Ir25a+). Expression analyses also reveal that Ir8a does not co-express with Orco alone or Ir76b alone.

A unified AL map organized by chemosensory gene families (ORs, IRs, and GRs) is shown in ***Figure 8C*** (right panel), and the left two panels extend this information into the periphery. Here, we include the GR+innervation of the V glomerulus. However, a knock-in line for either *Gr21a* or *Gr63a* does not currently exist; thus, it is possible these receptors (as well as other poorly characterized antennal GRs) might also be more broadly expressed than previous transgenic lines indicate (***Fujii et al., 2015***; ***Menuz et al., 2014***). All four OR and IR co-receptors are expressed in the antenna, while olfactory neurons in the palps express *Orco* and *Ir25a* (***Figure 8C***, left panel). In the antennae, there are many different classes of OSNs expressing various combinations of chemosensory receptors and co-receptors: there are Orco+ only neurons (***Figure 8C***, middle panel, #2), such as those innervating the VM2 and VM3 glomeruli (teal); IrCo+ only neurons (purple), which include neurons expressing one, two, or all three *IR* co-receptors (such as VP2, VM6v, or DP1m, respectively) (***Figure 8C***, middle panel, #1); and neurons expressing both *Orco* and *IrCo(s)* (teal and purple stripe) (***Figure 8C***, middle panel, #3 and 4).

The expression data suggest that different subpopulations of olfactory neurons might be targeting a shared glomerulus. Our data indicate that both Orco+ and Ir25a+ neurons innervate the GR+ V glomerulus (dark blue; see also ***Figure 8A***). Based on the sparse innervation of the V glomerulus by the *Orco-T2A-QF2* knock-in (***Figure 3A***) and the lower expression levels in the snRNAseq data (***Figure 4A***), we hypothesize that *Orco* may be expressed in only a subset of Gr21a/Gr63a+ neurons. This contrasts with the *Ir25a-T2A-QF2* knock-in, which appears to label most Gr21a/Gr63a+ neurons. Thus, two subpopulations of neurons may be co-converging upon the same V glomerulus: neurons that express *Gr21a/Gr63a* and *Ir25a* (dark blue and purple stripes), and neurons that express *Gr21a/Gr63a, Ir25a,* and *Orco* (dark blue, purple, and teal stripes) (***Figure 8C***, middle panel, #5). Such co-convergence has recently been shown in the olfactory system of *Aedes aegypti* mosquitoes (***Younger et al., 2020***). Similarly, the sparse *Orco-T2A-QF2* knock-in innervation of the DP1l glomerulus suggests that there are OSN populations expressing mostly *IRs*, but with a subset of neurons that additionally express *Orco* (***Figure 8C***, middle panel, #3). The converse may also be possible (***Figure 8C***, middle panel, #4): OSN populations that have some neurons expressing only *Orco*, and a subset expressing both *Orco* and *IrCo(s)* co-converging onto the same glomerulus. There is some evidence for this in the palps, based on our anti-Orco and anti-Ir25a antibody staining (***Figure 2C and I***, ***Figure 4B***, ***Table 2***). The snRNAseq data suggest that this may also be the case in the antennae (see ***Figure 4—source data 1***).

Table 5. Co-expression of *Orco* and *Ir25a* in non-*melanogaster* insect olfactory organs (related to *Figure 7*).
Whole-mount palps from *Drosophila sechellia* flies, and whole-mount antennae and palps from *Anopheles coluzzii* mosquitoes, were examined using fluorescence in situ hybridization with probe sets against *Orco* and *Ir25a*. Co-expression between Orco and Ir25a co-receptors was observed in both insects, with *D. sec.* palps having the highest degree of co-expression (63% of cells double labeled) and *A. col.* antennae having the lowest (25% of cells double labeled). N = 5 for *D. sec.* and 7 for *A. col.*

Species	Sample	Orco+ cells	Ir25a+ cells	Double-labeled cells	Total cells
Drosophila sechellia	Palp 1	70	44	44	70
Drosophila sechellia	Palp 2	64	48	42	70
Drosophila sechellia	Palp 3	63	39	39	63
Drosophila sechellia	Palp 4	78	38	35	81
Drosophila sechellia	Palp 5	86	75	74	87
	Total across samples: 361		244	234	371
		Proportion of Orco+ cells that are Ir25a+:	Proportion of Ir25a+ cells that are Orco+:	Proportion of all cells that are double labeled:	
		0.65	0.96	0.63	
Anopheles coluzzii	Antenna 1	52	17	12	57
Anopheles coluzzii	Antenna 2	47	24	17	54
Anopheles coluzzii	Antenna 3	57	20	13	64
Anopheles coluzzii	Antenna 4	50	27	14	63
Anopheles coluzzii	Antenna 5	62	30	18	74
Anopheles coluzzii	Antenna 6	53	21	17	57
Anopheles coluzzii	Antenna 7	49	26	16	59
	Total across samples: 370		165	107	428
		Proportion of Orco+ cells that are Ir25a+:	Proportion of Ir25a+ cells that are Orco+:	Proportion of all cells that are double labeled:	
		0.29	0.65	0.25	
Anopheles coluzzii	Palp 1	34	30	23	41
Anopheles coluzzii	Palp 2	30	36	22	44
Anopheles coluzzii	Palp 3	26	35	19	42
Anopheles coluzzii	Palp 4	35	34	19	50
Anopheles coluzzii	Palp 5	32	39	22	49
Anopheles coluzzii	Palp 6	31	35	21	45
Anopheles coluzzii	Palp 7	30	37	23	44
	Total across samples: 218		246	149	315
		Proportion of Orco+ cells that are Ir25a+:	Proportion of Ir25a+ cells that are Orco+:	Proportion of all cells that are double labeled:	
		0.68	0.61	0.47	

Discussion

Here, we present evidence of widespread chemosensory co-receptor co-expression in the olfactory system of *D. melanogaster*, contrasting a previously accepted view of segregated, mutually exclusive olfactory domains. By generating targeted knock-ins of the four main chemosensory co-receptor genes (*Orco*, *Ir8a*, *Ir76b*, *Ir25a*), we demonstrate that all four co-receptors have broader olfactory neuron expression than previously appreciated. The *Ir25a* co-receptor was previously thought to be expressed only in a small subset of olfactory neurons (coeloconic, sacculus, and arista neurons), but we present evidence that it is expressed in subsets of all sensilla classes and in OSNs that innervate the majority of the fly's AL glomeruli. We further find that the *Ir25a* co-receptor may be involved in
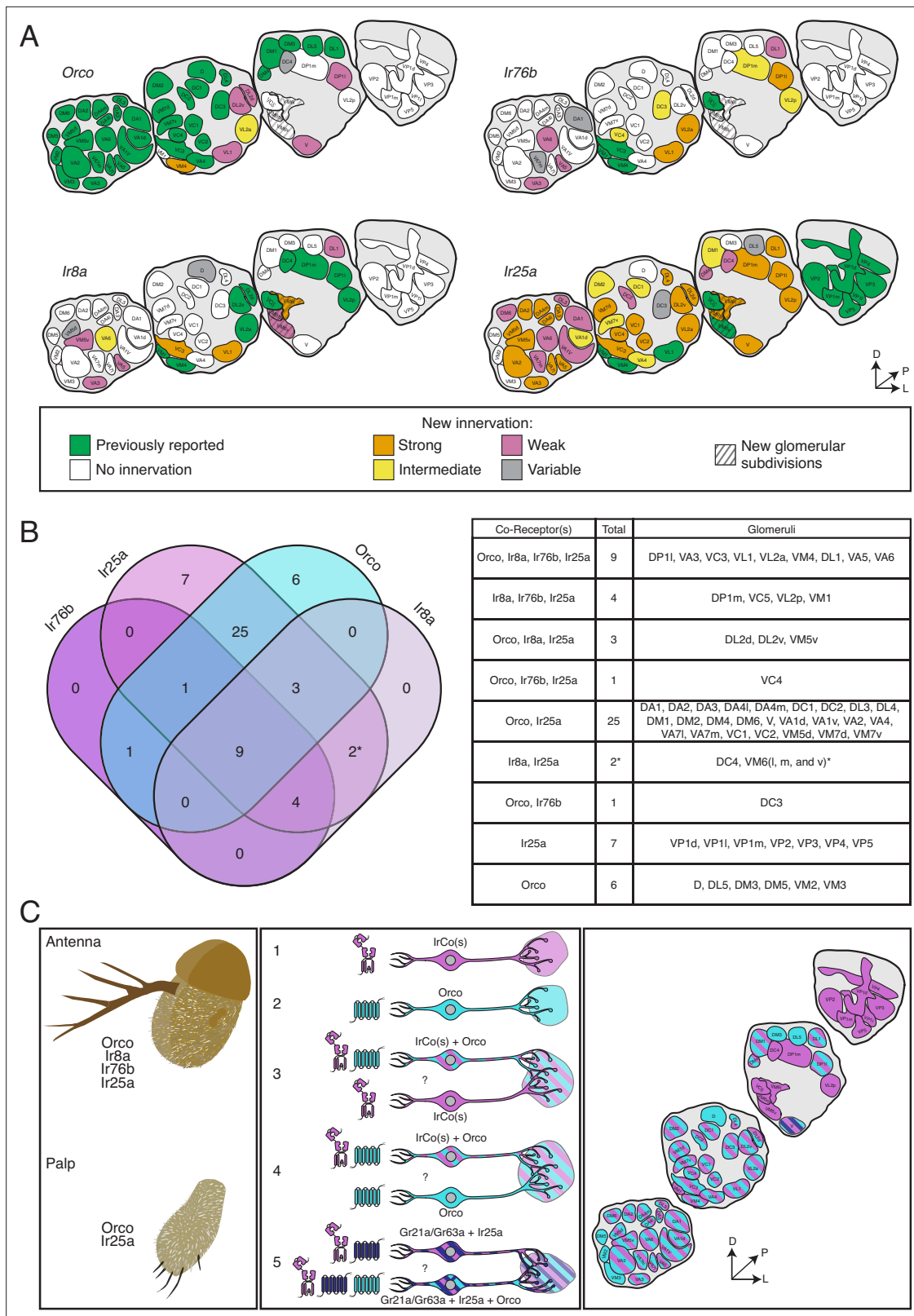
Figure 8. The co-receptor co-expression map of olfaction in *Drosophila melanogaster*. (**A**) Summary of antennal lobe (AL) expression for all co-receptor knock-in lines (from all brains examined in *Figures 3–5*; *Orco* N = 8, *Ir8a* N = 15, *Ir76b* N = 11, *Ir25a* N = 15). The previously reported innervation pattern for each co-receptor is shown in green; new innervation reported here is color-coded according to strength of glomerular labeling, from strong (orange), to intermediate (yellow), to weak (pink). Glomeruli labeled in <50% of brains examined for a given knock-in line are designated variable (gray); glomeruli

Figure 8 continued on next page

Figure 8 continued

not labeled are white. The novel VM6 glomerular subdivisions reported here are indicated by gray stripes. (**B**) Overlap of chemosensory modalities in the AL. In the Venn diagram (left), *IR* co-receptors are color-coded in shades of purple, while *Orco* is in teal, as in **Figure 1**. Numbers indicate how many glomeruli are found in the given intersection of co-receptors out of 58 total glomeruli. Variably labeled glomeruli were excluded from these analyses. The table lists the names of the glomeruli in each section of the Venn diagram. The new glomerular subdivisions are indicated with an asterisk. (**C**) New view of olfaction in *Drosophila*. Left: in the periphery, all four co-receptors are expressed in the antenna (top), while palpal neurons express *Orco* and *Ir25a* (bottom). Middle: many different classes of olfactory sensory neurons (OSNs) express various combinations of chemosensory receptors and co-receptors. While some neurons express only *IrCos* (purple, #1) or *Orco* (teal, #2), many neurons co-express these chemoreceptors (indicated with striped fill, #3 and 4). Within the latter group, there may be OSN populations in which *IRs* are the dominant receptors, and *OR* expression is sparse (#3), and other populations where *ORs* are the primary receptors and *IR* expression is infrequent (#4). GR+ neurons (dark blue) also express *Ir25a* (#5, dark blue and purple striped fill), and some of these neurons additionally express *Orco* (#5, dark blue, purple, and teal striped fill). Question marks indicate potential instances of co-convergence of different subtypes of OSNs onto the same glomeruli. Right: a comprehensive map of the antennal lobe shows that most glomeruli are innervated by OSNs that co-express multiple chemoreceptors. Compass in (**A**) and (**C**): D = dorsal, L = lateral, P = posterior. See also **Table 3** and **Figure 3—source data 1** and **Figure 3—source data 2**.

modulating the activity of some Orco+ OSNs, both in the antennae and maxillary palps. We present a new AL map that will aid future inquiries into the role that specific chemoreceptor co-expression plays in distinct OSN populations.

Based on the co-receptor innervation patterns in the ALs, we identified a glomerulus, VM6, that is uniquely partitioned by different OSNs (**Figure 5**; also see **Schlegel et al., 2021**). The co-receptor expression patterns allowed us to pinpoint the likely origin of the innervating OSNs. Since the VM6 glomerulus was labeled by both the *Ir25a-T2A-QF2* and *Ir8a-T2A-QF2* knock-in lines, the cell bodies of these neurons had to reside in the antenna; furthermore, since we did not find *Ir8a-T2A-QF2* labeling of the arista, these neurons were likely to be either in coeloconic sensilla or in the sacculus. Indeed, we determined the VM6 glomerulus to be innervated by the newly discovered Rh50+ Amt+ olfactory neurons that reside in the sacculus and ac1 sensilla (**Vulpe et al., 2021**). Based on our results, Rh50+ Amt+ sacculus neurons are further subdivided into those that strongly express Ir8a, which innervate the VM6l region, and those that weakly or infrequently express Ir8a, which innervate VM6m and VM6v. The functional consequences of this unusual subdivision by olfactory neurons for a glomerulus, and how this relates to the fly's olfactory perception of ammonia or other odorants, remain to be determined. These results also highlight the value of exploring chemosensory receptor expression patterns using knock-in lines even in the era of connectomics as the VM6 glomerulus and its subdivisions were not easily identifiable in prior electron microscopy reconstructions of the entire AL (**Bates et al., 2020**; **Scheffer et al., 2020**; **Schlegel et al., 2021**).

A model for OR/IR segregation was initially supported by developmental evidence. Two pro-neural genes specify the development of sensory structures on the antennae: *amos* and *atonal*. *Amos* mutants lack basiconic and trichoid sensilla, while *atonal* mutants do not develop coeloconic sensilla, the arista, or the sacculus (**Goulding et al., 2000**; **Gupta and Rodrigues, 1997**; **Jhaveri et al., 2000a**; **Jhaveri et al., 2000b**). It was observed that *amos* mutants lose *Orco* expression while retaining *Ir25a* expression (**Benton et al., 2009**). Our results generally do not conflict with this view. In the traditional segregated model of the fly olfactory system, it was presumed that *atonal* mutant antennae would show the reverse pattern: loss of *IrCo* expression but not *Orco* expression. However, our co-receptor knock-in expression results suggest that *atonal* mutants should have significant *IrCo* expression, particularly of *Ir25a*. This was indeed found to be the case in RNAseq analyses performed on *atonal* mutant antennae, which showed that both *Ir25a* and *Ir76b* expression, but not *Ir8a* expression, remained (**Menuz et al., 2014**). Based upon the strength of the corresponding glomerular innervations, it does appear that the previously reported Ir25a+ neurons have stronger or more consistent *Ir25a* expression, while the new Ir25a+ olfactory neurons in the antennae reported here (e.g., *OR*-expressing OSNs) are often weakly or stochastically labeled. This might also explain why *Ir25a* expression was initially overlooked in these Orco+ neural populations. The developmental pattern is different in the maxillary palps, where it is *atonal* and not *amos*, which is required for the development of the basiconic sensilla (**Gupta and Rodrigues, 1997**). Interestingly, the *Ir25a* knock-in expression corresponds well with the *atonal* developmental program across the olfactory appendages: the strongest expression of *Ir25a* is in coeloconic sensilla, but outside of these sensilla the strongest and most consistent *Ir25a* expression is in palp basiconic sensilla.

Chemosensory co-receptor co-expression may help clarify previously confounding observations regarding *D. melanogaster* odor coding. For example, olfactory neurons in the sacculus that express the *Ir64a* tuning receptor along with the *Ir8a* co-receptor project to two different glomeruli: DC4 and DP1m (*Ai et al., 2013*; *Ai et al., 2010*). These two glomeruli exhibit different olfactory response profiles, with DC4 being narrowly tuned to acids or protons, while DP1m is more broadly tuned. The molecular mechanism for these differences was previously unclear. However, the co-receptor knock-in data presented here reveals that the Ir64a+ OSN subpopulations express different combinations of co-receptors: in addition to the *Ir8a* co-receptor, neurons innervating DC4 express *Ir25a* (and occasionally *Orco*) (see *Figure 8*). In contrast, neurons innervating DP1m express *Ir8a*, *Ir25a*, and *Ir76b*. Thus, perhaps it is *Ir76b* expression in DP1m-targeting Ir64a+ neurons that makes them olfactory generalists. This idea is supported by experiments in which *Ir64a* was misexpressed in neurons targeting the VM4 glomerulus, conferring a DP1m-like, rather than a DC4-like, response profile to VM4 (*Ai et al., 2010*). We show here that VM4-targeting neurons express *Ir8a*, in addition to *Ir25a* and *Ir76b* (as well as *Orco*): thus, molecularly, the VM4 neuron profile is more similar to DP1m (co-expressing all *IrCos*) than DC4 (co-expressing two *IrCos*), and the key distinguishing component appears to be *Ir76b*. It would be interesting to repeat such misexpression experiments in an *Ir76b*⁻ mutant background to test this hypothesis.

While we demonstrate here that multiple chemosensory co-receptors can be co-expressed in the same olfactory neurons, it remains to be determined if this also applies to tuning (odor-binding) receptors. Previous studies suggest that OrX tuning receptors are generally limited to a single class of olfactory neurons (*Couto et al., 2005*; *Fishilevich and Vosshall, 2005*). However, many IrX tuning receptors remain to be fully characterized and could be co-expressed in multiple olfactory neurons. For example, recordings from ab1, ab3, and ab6 sensilla indicate responses to the typical IR odors 1,4-diaminobutane, ammonia, and butyric acid, respectively (*de Bruyne et al., 2001*), suggesting that tuning IrXs may be involved. We show that *Ir25a* plays a functional role in Orco+ neurons in the antennae and palps; this suggests that these Orco+ neurons could also express as yet unidentified ligand binding IrXs. The recent release of the whole fly single-cell atlas, which includes RNAseq data from maxillary palps, allowed us to identify six IRs that might be expressed in palpal OSNs (*Ir40a*, *Ir51a*, *Ir60a*, *Ir62a*, *Ir76a*, *Ir93a*) (*Li et al., 2021*). However, in situ analyses for these six IRs in the maxillary palps did not detect a signal (see *Figure 6—figure supplement 2* and Appendix 1—key resources table). This suggests that *Ir25a* in the palps may be playing a role independent of its role as a co-receptor, as discussed further below, or that a tuning IrX was missed by the RNAseq analyses. In antennal ab3 sensilla, we did find one odorant (propionic acid) that elicited a small response in *wild-type* neurons and no response in *Ir25a²* mutant neurons. It is possible that other antennal Orco+ OSNs might utilize IR chemoreceptors for signaling. For example, the ac3B neuron, which expresses Or35a/Orco and all IR co-receptors, has recently been suggested to utilize an unidentified IrX to mediate responses to phenethylamine (*Vulpe and Menuz, 2021*). The chemoreceptor expression patterns revealed in this work will help the search for olfactory neurons that may utilize multiple chemosensory families for odor detection.

The widespread expression of *Ir25a* in the fly olfactory system raises the possibility that it might have roles in addition to its function as an IrX co-receptor. For example, *Ir25a* has been found to play a developmental role in forming the unique structure of Cold Cells in the arista (*Budelli et al., 2019*). Evolutionary studies also suggest that *Ir25a* is the most ancient of all the insect chemosensory receptors (*Croset et al., 2010*), and the currently broad expression might reflect its previous ubiquitous role in chemosensory signaling.

Co-expression of chemosensory co-receptors might function to increase the signaling capabilities of an olfactory neuron. For example, the signaling of an Orco+ olfactory neuron may be guided primarily by the tuning OrX, and the sensitivity range extended to include odors detectable by an IrX. Co-expression might also allow synergism, such that weak activation of a co-expressed receptor could increase neuronal activity to levels sufficient to drive behavior. This might be useful in tuning behavioral response to complex odors, such that certain combinations of odors lead to stronger olfactory neuron responses. Alternatively, a co-expressed receptor inhibited by odorants might be able to attenuate a neuron's response to odor mixtures. The observed broad *Ir25a* co-expression might allow an Orco-positive olfactory neuron to be primed to express a functional IrX/Ir25a receptor complex. As suggested above, this could be an evolutionary advantage if the co-expressed IrX receptor improved

olfactory responses to a complex but crucial biologically relevant odor, such as host-seeking cues as observed in the *A. aegypti* mosquito olfactory system (*Younger et al., 2020*). Co-expression of chemosensory receptors could thereby be a mechanism to increase the functional flexibility of a numerically limited olfactory system.

Ir25a expression might further modulate chemosensory neuron activity levels driven by Orco/OrX signaling by altering membrane resistance. This might explain the modest activity changes we observed in *Ir25a* mutant Orco-expressing neurons (*Figure 6*). In this manner, altering Ir25a expression levels could be a neuronal mechanism to adjust Orco/OrX activity. Alternatively, *Ir25a* may contribute to olfactory signal transduction or amplification as has recently been shown for a pickpocket ion channel (*Ng et al., 2019*). Experiments addressing potentially expanded roles for *Ir25a* in olfactory neurons will be aided by the new chemosensory co-receptor map presented here.

D. melanogaster often serves as a model for many other insect olfactory systems, and information gleaned from vinegar flies is frequently extrapolated to other insects (e.g., *DeGennaro et al., 2013*; *Fandino et al., 2019*; *Riabinina et al., 2016*; *Trible et al., 2017*; *Yan et al., 2017*). Indeed, prompted by our findings of *Orco* and *Ir25a* co-expression in *D. melanogaster*, we extended our observations to two additional insect species. Using in situ hybridization, we found that olfactory neurons in the palps of *D. sechellia* flies, and in the antennae and palps of *A. coluzzii* mosquitoes, also co-express *Orco* and *Ir25a* co-receptors. The work presented here raises the possibility that many insects may also exhibit co-expression of chemosensory co-receptors. Recent work in *A. aegypti* mosquitoes suggests this is indeed the case: *A. aegypti* mosquito olfactory neurons can co-express Orco/IrCo/Gr receptors (*Younger et al., 2020*). Furthermore, *A. coluzzii* mosquitoes have recently been shown to co-express *Orco* and *Ir76b* co-receptors in their olfactory organs (*Ye et al., 2021*). This suggests that co-expression of chemosensory co-receptors may be an important feature of insect olfactory neurons.

Materials and methods
Key resources table
See Appendices 1 and 2.

Resource availability
Lead contact
Further information and requests for resources and reagents should be directed to and will be fulfilled by the lead contact, Christopher J. Potter (cpotter@jhmi.edu).

Materials availability
Fly lines generated in this study have been deposited to the Bloomington Drosophila Stock Center.

Data and code availability
The snRNAseq dataset analyzed in this paper is published in *McLaughlin et al., 2021*. Sequencing reads and preprocessed sequencing data are available in the NCBI Gene Expression Omnibus (GSE162121). Python code for generating figures is publicly available on GitHub (https://github.com/colleen-mclaughlin/ORN_seq/). VM6 reconstructions using FlyWire can be viewed at https://flywire.ai/#links/Task2021a/all. Raw data used to generate each figure is available at Dryad (https://doi.org/10.5061/dryad.9w0vt4bgp).

Experimental model and subject details
Fly husbandry
Fly stocks were maintained at 20–25°C on standard cornmeal-agar food. Male and female flies used for experiments were 3–11 days old, unless otherwise noted.

Fly stocks
Fly lines used in this paper can be found in the Appendix 1—key resources table.

While performing co-labeling experiments, we discovered that several *OrX-Gal4* lines label multiple glomeruli, and thus do not accurately represent single OSN classes. These lines were excluded from

analyses and should be used with caution: *Or33c-Gal4* (BDSC# 9966), *Or42a-Gal4* (BDSC# 9970), *Or43b-Gal4* (BDSC# 23894), *Or59b-Gal4* (BDSC# 23897), *Or65a-Gal4* (BDSC# 9994), *Or85a-Gal4* (BDSC# 23133), and *Or85b-Gal4* (BDSC# 23911). We also found that the following *Or35a* lines label the newly identified VM6l glomerulus in addition to VC3: *Or35a-Gal4* (BDSC# 9967), *Or35a-Gal4* (BDSC# 9968), *Or35a-mCD8.GFP* (BDSC# 52624), as well as an *Or35a-Gal4* line from the Carlson lab (*Yao et al., 2005*).

D. *sechellia* flies (strain: Cousin Island, Seychelles; SKU: 14021-0248.25) were obtained from the National *Drosophila* Species Stock Center (Cornell College of Agriculture and Life Sciences) and reared according to our *D. melanogaster* protocol.

Mosquito husbandry

A. gambiae mosquitoes were reared as previously described (*Riabinina et al., 2016*). The *wildtype* N'Gousso strain was a gift from the Insect Transformation Facility in Rockville, Maryland.

Generation of *QUAS-CsChrimson*

The sequence of CsChrimson.Venus was PCR amplified from the genomic DNA of *UAS-CsChrimson.mVenus* flies (*Klapoetke et al., 2014*) and cloned into the *10XQUAS* vector (Addgene #163629). A fly line was established through random *P*-element insertion. Cloning was confirmed with Sanger sequencing (Genewiz) before being sent for injection (Rainbow Transgenic Flies, Inc). Primers used for PCR amplification and In-Fusion cloning:

IVS-FOR:
TGGGTTGGACTCAGGGAATAGATCTAAAAGGTAGGTTCAACCACT
EcoRI-SV40-REV:
GCTTACGTCAGAATTCAGATCGATCCAGACATGATAAGA

Generation of HACK knock-in lines

The HACK knock-in approach requires two components: a donor construct and Cas9 (*Lin and Potter, 2016a*). The donor includes *gRNAs* specific to the target gene, as well as the template for HDR-mediated insertion of *T2A-QF2* into the genome (*Figure 2A*, middle row). This template includes ~1 kb homology arms directly up- and downstream of the gene's stop codon flanking a cassette containing *T2A-QF2* and a *3XP3-mCherry* fluorescent eye marker (see *Figure 2—figure supplement 1D and E* and *Figure 2—figure supplement 3A and B*). Outside of these homology arms, the construct has two *RNA polymerase III U6* promoters driving independent expression of two *gRNAs* specific to the region around the target gene's stop codon (*Port et al., 2014*). Two *gRNAs* were used to increase the probability of successfully inducing double-stranded breaks in the target (*Port et al., 2014*). The knock-in construct replaces the target gene's stop codon (*Figure 2A*, bottom row) and introduces a transcriptional stop at the end of *QF2*.

The donor construct can be supplied in one of two ways (*Figure 2—figure supplement 1*). The first is to inject the HACK construct directly into embryos expressing Cas9 in their germline (direct injection method) (*Figure 2—figure supplement 1A and B*). The second approach is to establish transgenic donor lines through random *P*-element insertion or *ΦC31* integration (*Bischof et al., 2007*; *Gloor et al., 1991*; *Groth et al., 2004*) of the construct into the genome, followed by genetic crosses with germline Cas9 flies for the generation of the knock-in (cross method) (*Figure 2—figure supplement 1C*). Only one (direct injection method) or two (cross method) generations of crosses are required for the creation of a knock-in line (*Figure 2—figure supplement 1B and C*). The HACK 3XP3-mCherry selection marker is bright but shows positional effects (*Figure 2—figure supplement 3A*). Potential knock-in flies can be screened at the adult stage (*Figure 2—figure supplement 3A*), or at the larval or pupal stages (*Figure 2—figure supplement 1D*). We generated *T2A-QF2* knock-in lines for all four co-receptor genes using the direct injection method. Additionally, we tested the feasibility of the cross approach with two genes: *Orco* and *Ir25a*. Knock-ins were confirmed by PCR genotyping and sequencing (*Figure 2—figure supplement 3B–D*), and by crosses to a *QUAS-GFP* reporter to check for expression in the brain (*QUAS-mCD8::GFP* was used only to establish the *Orco-T2A-QF2* knock-in line, after which the reporter was removed via genetic crosses; for all AL analyses, we used the

10XQUAS-6XGFP reporter line). We found no difference in expression pattern in the brain between these two approaches (*Figure 2—figure supplement 1G*). After establishing a knock-in line, the 3XP3-mCherry marker can be removed via *Cre* recombination (*Siegal and Hartl, 1996*). This can be useful as 3XP3-mCherry is expressed broadly throughout the fly nervous system and can interfere with red fluorescent reporters (*Figure 2—figure supplement 1E*). We produced two unmarked knock-in lines (for *Orco* and *Ir25a*) and confirmed no difference in brain GFP expression between marked and unmarked lines (*Figure 2—figure supplement 1F*).

Both approaches produced knock-ins at high rates (*Table 1*). Efficiency was calculated as the number of potentially HACKed knock-in flies (mCherry+), divided by the total number of flies from the given cross (G_1 or F_2 progeny; see *Figure 2—figure supplement 1A–C*). We further calculated the percentage of founders producing knock-in lines as this gives an indication of effort (how many initial crosses need to be set up to produce a knock-in). The aggregate efficiency rates for a given target locus ranged from 8% for Ir8a to 33% for Orco (*Table 1*); however, for individual crosses, efficiency rates were as high as 100% (see *Table 1—source data 1*), meaning that all progeny were potential mCherry+ knock-ins. For the two genes for which we created knock-in lines via both direct injection and genetic cross (*Orco* and *Ir25a*), we found efficiency rates comparable between approaches (*Orco*: 33% for direct injection, 28% for cross; *Ir25a*: 23% for direct injection, 24% for cross). For the direct injection approach, we tested 51 independent knock-in lines across the four target genes and found 100% to be correctly targeted events (*Table 1*). However, for the genetic cross approach, of the 32 independent knock-in lines tested for the two target genes, 6 (~19%) had the HACK mCherry eye marker but did not have *QF2*-driven GFP expression in the brain.

Information on plasmid construction can be found in the 'Method details' section. All *D. melanogaster* embryo injections were performed by Rainbow Transgenic Flies, Inc (Camarillo, CA). For HACKing via genetic cross, *Orco-T2A-QF2* and *Ir25a-T2A-QF2* constructs were injected into w^{1118} flies for *P*-element insertion, and donor lines were established on the second or third chromosomes by crossing to double balancers (see Appendix 1—key resources table). Donor lines were then crossed to *Vas-Cas9* (BDSC# 51323). Knock-in lines were established from *cis*-chromosomal HACK (donor line on same chromosome as target gene) (*Lin and Potter, 2016a*). For HACKing via direct injection, knock-in constructs were injected into the following lines: *Vas-Cas9* (BDSC# 51324) for *Ir8a*; *Act5C-Cas9* (BDSC# 54590) for *Orco*, *Ir76b*, and *Ir25a*. The following lines were used to verify knock-in expression: *QUAS-mCD8::GFP* (BDSC# 30003), *10XQUAS-6XGFP* (BDSC# 52264). Knock-in lines were confirmed by PCR genotyping (Phusion, NEB) and Sanger sequencing (Genewiz). Unmarked *Orco-T2A-QF2* and *Ir25a-T2A-QF2* knock-in lines were generated by crossing mCherry+ knock-in flies to the Crey+ 1B fly line (see Appendix 1—key resources table; *Siegal and Hartl, 1996*).

To investigate the effect of *T2A-QF2* knock-in on gene function, we performed SSR on homozygous flies for each co-receptor knock-in (*Figure 2—figure supplement 2*), comparing their responses to *wildtype* flies to panels of Orco- and Ir-dependent odorants (*Abuin et al., 2011*; *de Bruyne et al., 2001*; *Lin and Potter, 2015*). In ab2 basiconic sensilla, *Orco-T2A-QF2* knock-in flies had slightly lower baseline activity as compared to *wildtype* (*Figure 2—figure supplement 2A*); however, there were no significant differences in odor-evoked activity between these two genotypes across all stimuli tested (*Figure 2—figure supplement 2B*). In ac2 coeloconic sensilla, responses of *Ir8a-T2A-QF2* knock-in flies to hexanol and cadaverine were slightly lower than *wildtype* (*Figure 2—figure supplement 2D*); however, these are not typically considered Ir8a-dependent odorants. Responses of the *Ir8a-T2A-QF2* knock-in to Ir8a-dependent odorants (*Abuin et al., 2011*) were similar to *wildtype* controls (example trace in *Figure 2—figure supplement 2C*, quantification in *Figure 2—figure supplement 2D*). Responses of *Ir76b-T2A-QF2* knock-in ac2 neurons to phenethylamine and acetic acid differed slightly from *wildtype* controls (*Figure 2—figure supplement 2E and F*). The reasons for this are unclear. The largest difference in responses between a knock-in and *wildtype* were for *Ir25a-T2A-QF2* (*Figure 2—figure supplement 2G and H*); the knock-in has significantly reduced or abolished responses to Ir25a-dependent odorants, recapitulating an *Ir25a* mutant phenotype (*Abuin et al., 2011*; *Silbering et al., 2011*; see also *Figure 2—source data 1*).

Method details

Plasmid construction

The construction of *QF2*^{X-HACK} knock-in plasmids requires three steps of cloning, as previously described (**Lin and Potter, 2016a**). All knock-in constructs were created using the *pHACK-QF2* plasmid (Addgene #80274) as the backbone. The backbone was digested with the following enzymes for cloning: *MluI* for the 5′ homology arms; *SpeI* for the 3′ homology arms; and *BbsI* for the gRNAs. All cloning was performed using In-Fusion Cloning (Clontech #639645). The homology arms were PCR-amplified from genomic DNA extracted from *wildtype* flies using the DNeasy Blood and Tissue Kit (QIAGEN #69506), while the gRNAs were PCR-amplified using the *pHACK-QF2* backbone as a template, with the primers themselves containing the gRNA target sequences. All homology arms were approximately 1 kb (Orco: 5HA = 1012 bp, 3HA = 1027 bp; Ir8a: 5HA = 1027 bp, 3HA = 1079 bp; Ir76b: 5HA = 997 bp, 3HA = 956 bp; Ir25a: 5HA = 1119 bp, 3HA = 990 bp). gRNAs were selected by analyzing the region around the stop codon of each gene using an online tool (https://flycrispr.org/ *Gratz et al., 2014*). When possible, gRNAs were chosen to minimize potential off-target cleavage sites (zero predicted for *Orco*, *Ir8a*, and *Ir76b*; one predicted for *Ir25a*, discussed below). They were selected such that one gRNA targeted upstream of the stop codon, within the last exon of the gene; the second gRNA targeted downstream of the stop codon, within the 3′UTR; and the two gRNAs were <100 bp apart. In order to prevent the gRNAs from targeting the homology arms, three synonymous nucleotide substitutions were made in each homology arm. The final knock-in lines did not always have all three substitutions (see *Figure 2—figure supplement 3D*), possibly due to PCR or HDR error. Note that due to the way the primers are designed, each targeted gene loses a small portion of its native 3′UTR (Orco = 72 bp, Ir8a = 31 bp, Ir76b = 27 bp, Ir25a = 24 bp). Cloning was confirmed with Sanger sequencing (Genewiz) before being sent for injection (Rainbow Transgenic Flies, Inc). Below are the gRNAs used for each gene, with the PAM sequence in parentheses.

> Orco:
> CTGCACCAGCACCATAAAGT (AGG)
> GCACAGTGCGGAGGGGGCAA (GGG)
> Ir8a:
> GTTTGTTTGTTCGGCCATGT (TGG)
> GGTGCCTCTGACTCCCACAG (TGG)
> Ir76b:
> GCAGTGATGCGAACTTCATA (TGG)
> GTATTGAAAGAGGGCCGCCG (AGG)
> Ir25a:
> GCCGGATACTGATTAAAGCG (CGG)
> ATTATGGTAAAATGAGCACT (CGG)

Primers

Italics = In-Fusion Cloning 15 bp overhang; **bold** = gRNA; lowercase = adding back restriction site; <u>underline</u> = synonymous substitution to prevent Cas9 targeting of donor construct.

PCR primers for cloning

> Orco_gRNA_FOR:
> *TCCGGGTGAACTTC***GCACAGTGCGGAGGGGGCAA**GTTTTAGAGCTAGAAATAGCAAGTTA
> Orco_gRNA_REV:
> *TTCTAGCTCTAAAAC***ACTTTATGGTGCTGGTGCAG**CGACGTTAAATTGAAAATAGGTC
> Orco_5HA_FOR:
> *CCCTTACGTAACGCG*tCAGCTTGTTTGACTTACTTGATTAC
> Orco_5HA_REV:
> *CGCGGCCCTCACGCG*tCTTGAGCTGT<u>A</u>C<u>A</u>AG<u>T</u>ACCATAAAGT
> Orco_3HA_FOR:
> *GTTATAGATCACTAG*tCTC<u>A</u>GT<u>A</u>CT<u>A</u>TGCAACCAGCAATA
> Orco_3HA_REV:
> *AATTCAGATCACTAG*tGTTTTATGAAAGCTGCAAGAAATAA
> Ir8a_gRNA_FOR:
> *TCCGGGTGAACTTCG***TTTGTTTGTTCGGCCATGT**GTTTTAGAGCTAGAAATAGCAAGTTA

Ir8a_gRNA_REV:
*TTCTAGCTCTAAAAC***CTGTGGGAGTCAGAGGCAC**CGACGTTAAATTGAAAATAGGTC
Ir8a_5HA_FOR:
*CCCTTACGTAACGCG*tCTATTGGCTATTCGTCGTACTCATGC
Ir8a_5HA_REV:
*CGCGGCCCTCACGCG*tCTCCATGTAGCCACTAT<u>G</u>T<u>G</u>AGTCAGA<u>T</u>
Ir8a_3HA_FOR:
*GTTATAGATCACTAG*tGTTTCTTGTCGCACCTAATTAACAAGTG
Ir8a_3HA_REV:
*AATTCAGATCACTAG*tCATACTTAAGCTCCTTGAGGTCCAGC
Ir76b_gRNA_FOR:
*TCCGGGTGAACTTCG***CAGTGATGCGAACTTCATA**GTTTTAGAGCTAGAAATAGCAAGTTA
Ir76b_gRNA_REV:
*TTCTAGCTCTAAAAC***CGGCGGCCCTCTTTCAATAC**GACGTTAAATTGAAAATAGGTC
Ir76b_5HA_FOR:
*CCCTTACGTAACGCG*tACCAATGAATCCTTGTCCATGCTAAA
Ir76b_5HA_REV:
*CGCGGCCCTCACGCG*tCTCGGTGTAGCTGTC<u>T</u>TGAA<u>GG</u>A<u>A</u>
Ir76b_3HA_FOR:
*GTTATAGATCACTAG*tGCCTAATTGGAATACCTTCTACATAATGGA
Ir76b_3HA_REV:
*AATTCAGATCACTAG*tGGCAAGGCACAAAATAAAACGAAG
Ir25a_gRNA_FOR:
*TCCGGGTGAACTTC***GCCGGATACTGATTAAAGCG**GTTTTAGAGCTAGAAATAGCAAGTTA
Ir25a_gRNA_REV:
*TTCTAGCTCTAAAAC***AGTGCTCATTTTACCATAAT**CGACGTTAAATTGAAAATAGGTC
Ir25a_5HA_FOR:
*CCCTTACGTAACGCG*tTGCATGACTTCATTGACACCTCAAG
Ir25a_5HA_REV:
*CGCGGCCCTCACGCG*tGAAACGAGGCTTAAACGT<u>A</u>GC<u>T</u>GGATA<u>TT</u>
Ir25a_3HA_FOR:
*GTTATAGATCACTAG*tAATATTATGGT<u>T</u>AA<u>G</u>TGAGC<u>T</u>CTCGG
Ir25a_3HA_REV:
*AATTCAGATCACTAG*tCAAAGCTAAGTTCATCGTCATAGAGAC
Genotyping and sequencing primers (PCR fragment size):
Orco_Seq_FOR (~2 kb):
GATGTTCTGCTCTTGGCTGATATTC
Ir8a_Seq_FOR (~1.9 kb):
CATCGACTTCATCATCAGGCTTTCG
Ir76b_Seq_FOR (~1.9 kb):
CAACGATATCCTCACGAAGAACAAGC
Ir25a_Seq_FOR (~1.9 kb):
CGAAAGGATACAAAGGATACTGCAT
HACK_Seq_REV (same for all):
TGTATTCCGTCGCATTTCTCTC

Checking for off-target effects

One of the gRNAs for *QF2*[Ir25a-HACK] had one predicted potential off-target cut site in the genome, in the *tetraspanin 42ej* (*Tsp42Ej*) gene. We sequenced this locus in the *Ir25a-T2A-QF2* knock-in line and compared the sequence to our *wildtype* lab stock. We found no evidence of indels in the knock-in line. Primers used:

Tsp42Ej_FOR:
GAGAAGTCGTTTCCCATAACACCCT
Tsp42Ej_REV:
GAGGAGCAGTTTTCGGAGTCGCCTTC

HACK marker screening

Adult flies were anesthetized on a CO_2 pad and screened in one of two ways: either with a Nightsea Stereo Microscope Fluorescence Adapter with the green SFA-GR LED light source (Nightsea LLC, Lexington, MA) and viewed with a Zeiss Stemi SV6 stereo microscope; or illuminated with an X-Cite 120Q excitation light source and viewed with a Zeiss SteREO Discovery V8 microscope equipped with a ds-Red filter.

Whole-animal imaging

Whole adults were anesthetized on ice before imaging. Whole larvae, pupae, or freshly dissected adult heads were affixed to slides with clear nail polish before imaging. All animals were imaged on an Olympus SZX7 microscope equipped with GFP and RFP filters. Animals were illuminated with an X-Cite Series 120Q light source. Images were acquired using a QImaging QIClick Cooled digital CCD camera and Q-Capture Pro 7 software. Multiple images were taken at different focal planes and then merged in Photoshop (CS6). Gain was adjusted in Fiji. Images appear in the following figures/panels: *Figure 2B, D, F and H*; *Figure 2—figure supplement 1D*; *Figure 2—figure supplement 3A*; and *Figure 2—figure supplement 4*. For *Figure 7*, *D. melanogaster*, *D. sechellia*, *D. virilis*, and *A. coluzzii* animals were immobilized with clear nail polish and imaged on a Zeiss SteREO Discovery V8 microscope. Images were acquired with a smartphone camera attached to the microscope ocular and processed in Photoshop (CS6) to remove background.

Immunohistochemistry

All flies were used at 3–11 days old. Apart from the cryosection protocols and portions of the antennal whole-mount protocol, all immunostaining steps were done on a nutator. All steps involving or following the addition of fluorescently conjugated secondary antibodies were done in the dark.

Brain and VNC staining was performed as in *Xie et al., 2018*. The tissue was dissected in PBS and then fixed for 20 min at room temperature (RT) in 4% paraformaldehyde in PBT (1× PBS with 0.3% Triton X-100). After fixation, the tissue was quickly rinsed three times with PBT, then put through three longer washes in PBT at RT (at least 15 min each). The tissue was blocked in PBT + 5% normal goat serum (NGS) at RT for at least 30 min, then transferred to block + primary antibody solution, and incubated at 4°C in primary antibodies for 1–2 days. The tissue was then washed three times with PBT at RT (at least 15 min per wash) and incubated in a secondary antibody solution in block at 4°C for 1 day. The tissue was washed three final times with PBT at RT for 15 min each, and then mounted in SlowFade Gold (Thermo Fisher Scientific #S36936). For experiments in which the 10XQUAS-6XGFP or 20XUAS-6XGFP reporters were used, the endogenous, unstained GFP signal was visualized, and no secondary green antibodies were used. Primary antibodies used: mouse anti-nc82 (DSHB, 1:25) and rat anti-mCD8 (Thermo Fisher #14-0081-82, 1:100 or 1:200). Secondary antibodies used: Cy3 goat anti-rat (Jackson ImmunoResearch #112-165-167, 1:200), Cy3 goat anti-mouse (Jackson ImmunoResearch #115-165-166, 1:200), Alexa 647 goat anti-rat (Jackson ImmunoResearch #112-605-167, 1:200), and Alexa 647 goat anti-mouse (Jackson ImmunoResearch #115-605-166, 1:200).

Whole-mount staining of maxillary palps was performed according to the brain staining protocol above, with the exception of a shorter fixation step (15 min). Primary antibodies used: rabbit anti-Ir25a (gift from Richard Benton, University of Lausanne, 1:100), rabbit anti-Orco (gift from Leslie Vosshall, Rockefeller University, 1:100), and rat anti-elav (DSHB, 1:100). Secondary antibodies used: Cy3 goat anti-rabbit (Jackson ImmunoResearch #111-165-144, 1:200), Alexa 647 goat anti-rabbit (Jackson ImmunoResearch #111-605-144, 1:200), and Alexa 647 goat anti-rat (Jackson ImmunoResearch #112-605-167, 1:200). For whole-mount staining of *Orco²* mutant palps, 3-day-old flies were used to check for Orco expression before neurons degenerate (*Task and Potter, 2021*).

The protocol for whole-mount staining of antennae was adapted from *Karim et al., 2014*; *Saina and Benton, 2013*; *Younger et al., 2020*. Fly heads were dissected into CCD buffer (50 units chitinase, 1000 units chymotrypsin [25 mg of 40 units/mg], 10 mL HEPES larval buffer [119 mM NaCl, 48 mM KCl, 2 mM $CaCl_2$, 2 mM $MgCl_2$, 25 mM HEPES], 100 µL DMSO) on ice, then warmed on a 37°C heat block for 10 min. Heads were incubated in CCD buffer at 37°C while rotating for 1 hr 20 min. Antennae were subsequently dissected off heads into fixative solution (4% PFA in PBT). All subsequent steps were done without rotation to prevent antennae from sticking to the walls or lids of the tubes. The antennae were fixed at RT for 40 min, then washed with PBT three times at RT, at

least 15 min each time, and blocked in PBT plus 5% NGS for at least 1 hr at RT. The antennae were incubated in primary antibodies in blocking solution at 4°C for 4 days, washed three times for 15 min each at RT, and incubated in a secondary antibody solution at 4°C for 3 days. The antennae were then washed three times for 15 min each time at RT and mounted in SlowFade Gold. Primary antibody: rabbit anti-Orco (gift from Leslie Vosshall, 1:100). Secondary antibody: Cy3 goat anti-rabbit (Jackson ImmunoResearch #111-165-144, 1:200). The endogenous GFP signal was visualized.

The cryosection protocol was adapted from *Spletter et al., 2007*. Fly heads were dissected and lined up in cryomolds (Tissue-Tek #4565), covered with OCT compound (Tissue-Tek #4583), and frozen at –80°C. The samples were sectioned at ~12 µm on a Microm HM 500 cryostat (Microm International GmbH, Walldorf, Germany) and collected on SuperFrost Plus slides (Fisher #12-550-15). Slides were stored at –80°C until further processing. The slides were fixed at RT for 15 min in 4% paraformaldehyde in PBT (1× PBS with 0.3% Triton X-100), washed three times in PBT at RT (15 min each), blocked at RT for at least 30 min in PBT + 2.5% NGS + 2.5% normal donkey serum (NDS), then incubated overnight at 4°C in primary antibodies in fresh block solution in a special humidified chamber. On the next day, the slides were washed three times (15 min each) with PBT at RT and then incubated in secondary antibodies in block at 4°C overnight in the same humidified chamber covered in foil. Finally, the slides were washed three times (15 min each) with PBT at RT. DAPI (1:10,000) was included in the first wash as a nuclear counterstain. After washes, the slides were mounted in SlowFade Gold (Thermo Fisher Scientific #S36936). Primary antibody: guinea pig anti-Ir8a (gift from Richard Benton, University of Lausanne, 1:1000). Secondary antibody: Cy3 donkey anti-guinea pig (Jackson ImmunoResearch #706-165-148, 1:200).

For sacculus staining, 7- to 10-day-old flies were placed in an alignment collar. Their heads were encased in OCT (Tissue-Plus Fisher) in a silicone mold, frozen on dry ice, and snapped off. The head blocks were stored in centrifuge tubes at –80°C. A Leica cryostat was used to collect 20 µm sections of antennae. Immunohistochemical staining was carried out by fixing tissue in 4% paraformaldehyde for 10 min, followed by three 5 min washes in 1× PBS. The tissue was washed in 1× PBS containing 0.2% Triton-X (PBST) for 30 min to permeabilize the cuticle. Lastly, the tissue was washed in PBST containing 1% bovine serum albumin (BSA) to block nonspecific antibody binding. Primary antibody solution was made in PBST + 1% BSA, 200 µL was pipetted onto each slide under bridged coverslips, and slides were placed at 4°C overnight to incubate. The following day, the primary antibody was removed, and the slides were washed three times for 10 min each in PBST. Secondary antibody solution was made in PBST + 1% BSA, 200 µL was pipetted onto each slide under bridged coverslips, and left at RT in a dark box to incubate for 2 hr. After the 2 hr incubation, the slides were washed three times for 5 min each in PBST. After the last wash, the slides were allowed to dry in the dark staining box for ~30 min before being mounted in Vectashield, coverslipped, and stored at 4°C. Primary antibodies: rabbit anti-Ir25a (gift from Richard Benton, University of Lausanne, 1:100), guinea pig anti-Ir8a (gift from Richard Benton, University of Lausanne, 1:100), and rabbit anti-Ir64a (gift from Greg Suh, NYU/KAIST, 1:100). Secondary antibodies: Jackson Immuno Cy3 conjugated AffiniPure 568 goat anti-rabbit (111-165-144, 1:500) and Alexa Fluor 568 goat anti-guinea pig (A11075, 1:500).

In situ HCR

Cryosectioning for antennal in situs was performed as described above. The HCR protocol was adapted from Molecular Instruments HCR v3.0 protocol for fresh frozen or fixed frozen tissue sections (*Choi et al., 2018*). Slides were fixed in ice-cold 4% PFA in PBT for 15 min at 4°C, dehydrated in an ethanol series (50% EtOH, 70% EtOH, 100% EtOH, 100% EtOH, 5 min each step), and air dried for 5 min at RT. The slides were then incubated in proteinase K solution in a humidified chamber for 10 min at 37°C, rinsed twice with PBS and dried, then pre-hybridized for 10 min at 37°C in a humidified chamber. The slides were then incubated in probe solution (0.4 pmol Ir76b probe) overnight in the 37°C humidified chamber. On day 2, the slides were washed with a probe wash buffer/SSCT series (75% buffer/25% SSCT, 50% buffer/50% SSCT, 25% buffer/75% SSCT, 100% SSCT, 15 min each) at 37°C, then washed for 5 min at RT with SSCT and dried. The slides were pre-amplified for 30 min at RT in the humidified chamber while hairpins were snap cooled (6 pmol concentration). The slides were incubated in fresh amplification buffer with hairpins overnight in a dark humidified chamber at RT. On day 3, the slides were rinsed in SSCT at RT (2 × 30 min, 1 × 10 min with 1:10,000 DAPI, 1 × 5 min) and mounted in

SlowFade Diamond (Thermo Fisher S36972). For the overnight steps, the slides were covered with HybriSlips (Electron Microscopy Sciences 70329-62) to prevent solution evaporation.

The whole-mount palp in situ protocol for all *Drosophila* species tested in this paper was adapted from a combination of *Prieto-Godino et al., 2020*; *Saina and Benton, 2013*; *Younger et al., 2020* and the *D. melanogaster* whole-mount embryo protocol from Molecular Instruments (*Choi et al., 2016*). All steps after dissection were performed while rotating unless otherwise noted. Fly mouthparts (palps and proboscises) were dissected into CCD buffer (same as for whole-mount IHC on antennae above), incubated for 20–65 min in CCD at 37°C (5 min on heat block, 15 min to 1 hr rotating), then pre-fixed in 4% PFA in PBT for 20 min at RT. Tissue was washed with 0.1% PBS-Tween on ice (4 × 5 min), incubated for 1 hr at RT in 80% methanol/20% DMSO, and washed for 10 min in PBS-Tween at RT. The tissue was incubated in Proteinase K solution (1:1000) in PBS-Tween at RT for 30 min, then washed in PBS-Tween at RT (2 × 10 min) and post-fixed in 4% PFA in PBS-Tween at RT for 20 min. After post-fixation, the tissue was washed in PBS-Tween at RT (3 × 15 min), then pre-hybridized in a pre-heated probe hybridization buffer at 37°C for 30 min. The tissue was incubated in probe solution (2–30 pmol in hybridization buffer) at 37°C for 2–3 nights. After probe incubation, the tissue was washed in a pre-heated probe wash buffer at 37°C (5 × 10 min), then washed in SSCT (1× SSC plus 1% Tween) at RT (2 × 5 min). The tissue was pre-amplified with RT-equilibrated amplification buffer at RT for 10 min, then incubated in hairpin mixture (6–30 pmol snap-cooled hairpins in amplification buffer) in the dark at RT for 1–2 nights. After hairpin incubation, the tissue was washed at RT with SSCT (2 × 5 min, 2 × 30 min, 1 × 5 min), then mounted in SlowFade Diamond (Thermo Fisher S36972). Sequences for all in situ probes can be found in Appendix 2. In addition to *D. sechellia* (Cousin Island, Seychelles genome line, SKU: 14021-0248.25; *Figure 7*), we also tested the same in situ probes for six other species of *Drosophila* (apart from *D. virilis*, all species were ordered from the National *Drosophila* Species Stock Center): *Drosophila simulans* (genome line w[501], SKU: 14021-0251.195), *Drosophila erecta* (wild-type genome line, SKU: 14021-0224.01), *Drosophila ananassae* (wildtype line, Queensland, Australia, SKU: 14024-0371.11), *Drosophila pseudoobscura* (genome line, Anderson, Mesa Verde, CO, SKU: 14011-0121.94), *Drosophila mojavensis* (wildtype line, Catalina Island, CA [2002], SKU: 15081-1352.22), and *Drosophila virilis* (wildtype, Carolina Biological Supply, item# 172890). While we could detect a clean signal for the *D. mel. Orco* probe in these other fly species, the high background and poor signal-to-noise ratio for *D. mel. Ir25a* prevented co-localization analyses for all species but *D. sechellia*.

Anopheles in situs were performed essentially as described above, with the following modifications: olfactory appendages were dissected from 5- to 6-day-old female mosquitoes and incubated in CCD buffer for either 20 min (antennae) or 1.5 hr (maxillary palps) at 37°C while rotating. The tissue was then pre-fixed for 24 hr at 4°C. After the PBS-Tween and methanol/DMSO washes, the tissue was incubated overnight at –20°C in absolute methanol. The next day, the tissue was rehydrated in a graded methanol/PBS-Tween series. Subsequent steps follow the *Drosophila* whole-mount palp protocol. Probe concentration was 8 pmol in hybridization buffer (two night incubation), and hairpin concentration was 18 pmol in amplification buffer (one night incubation). The tissue was rinsed three times in SlowFade Diamond before being mounted.

For two-color in situs, we used the Molecular Instruments B2 amplifier conjugated to Alexa 647 for *Orco* and the B4 amplifier conjugated to Alexa 488 for *Ir25a*. For single-color in situs (*Orco*, *Ir76b* or tuning *IrXs*), we used the B2 amplifier conjugated to Alexa 647.

Confocal imaging and analysis

Brains, VNCs, antennae, maxillary palps, and antennal cryosections were imaged on a Zeiss LSM 700 confocal microscope equipped with Fluar 10×/0.50 air M27, LCI Plan-Neofluar 25×/0.8 water Korr DIC M27, Plan-Apochromat 40×/1.3 Oil DIC M27, and C-Apochromat 63×/1.2 water Korr M27 objectives. Images were acquired at either 512 × 512 or 1024 × 1024-pixel resolution with 0.43, 0.58, 2.37, or 6.54 µm z-steps. For illustration purposes, confocal images were processed in Fiji/ImageJ to collapse Z-stacks into a single image using maximum intensity projection. Where noted, single slices or partial z projections were used as opposed to full stacks. For co-labeling experiments, Fiji was used to convert red Look-Up Tables (LUTs) to orange for a colorblind-friendly palette. Similarly, in *Figure 2—figure supplement 1E*, Fiji was used to convert magenta LUT to blue for clarity. For *Figure 4B*, Fiji was used to convert the two-channel maximum intensity projection to a gray LUT, and the cell-counting plug-in was used in separate channels to identify single- and double-labeled cells. Fiji was also used to adjust

the gain in separate channels in all figures/images; no other image processing was performed on the confocal data. For *Figure 8A*, glomeruli were assigned to the categories strong, intermediate, and weak by visual inspection of the strength of their innervation compared to the previously reported glomeruli for each respective knock-in line. Strong glomeruli generally have similar brightness/intensity of GFP signal as most of the originally reported glomeruli for the given knock-in line.

For sacculus staining (*Figure 5C–E*), slides were imaged on a Nikon A1R confocal microscope in the UConn Advanced Light Microscopy Facility with a 40× oil immersion objective at 1024 × 1024-pixel resolution. Stacks of images (0.5 μm z-step size) were gathered and analyzed with ImageJ/Fiji software. Image processing was performed as described above.

Magnification used:

10×: *Figure 1D* (brain), *Figure 2—figure supplement 1E*
25×: *Figure 2—figure supplement 1F and G*, *Figure 3—figure supplement 1A and B*
40×: *Figures 5C–E and 7D and E*
63×: *Figure 2C, E, G, and I*, *Figure 3A–D*, *Figure 4B and C*, *Figure 5A and B*, *Figure 2—figure supplement 3E–H*, *Figure 3—figure supplement 2A–E*, *Figure 5—figure supplement 1*, *Figure 6—figure supplement 2*, *Figure 7C*

Note regarding *Ir8a* knock-in expression: in the ALs, we found that the sparse Ir8a+ expression in olfactory neurons targeting VM6m and VM6v could potentially be sexually dimorphic. Male brains generally had stronger and more frequent Ir8a+ innervation in these two glomeruli compared to female brains, as shown in *Figure 3—source data 2* (see *Figure 3—source data 1* for a summary of AL analyses). However, we did not find corresponding evidence for sexual dimorphism in Ir8a+ expression in the periphery. The reason for this discrepancy is currently unclear, and future work will be needed to determine whether there are functional male/female differences in Ir8a+ neurons.

Basiconic single sensillum recordings

Flies were immobilized and visualized as previously described (*Lin and Potter, 2015*). Basiconic sensilla were identified either using fluorescent-guided SSR (for ab3 sensilla) or using the strength of the A and B neuron responses to the reference odorants 1% ethyl acetate (EA) (Sigma #270989) and 1% pentyl acetate (PA) (Sigma #109584) (for ab2 and pb1-3 sensilla) (*de Bruyne et al., 1999*; *Lin and Potter, 2015*). For example, pb1A has strong responses to both odorants, while pb3A does not respond to EA. Similarly, ab2 sensilla were distinguished from ab3 based on the A neuron responses: ab2A responds strongly to EA and weakly to PA, while ab3A neurons have the reverse response (weak EA and strong PA response). The glass recording electrode was filled with Beadle–Ephrussi Ringer's solution (7.5 g of NaCl + 0.35 g of KCl + 0.279 g of CaCl$_2$-2H$_2$O in 1 L H$_2$O). Extracellular activity was recorded by inserting the glass electrode into the shaft or base of the sensillum of 3- to 10-day-old flies (unless otherwise specified in the young *Orco^2* mutant experiments). A tungsten reference electrode was inserted into the fly eye. Signals were amplified 100× (USB-IDAC System; Syntech, Hilversum, the Netherlands), input into a computer via a 16-bit analog-digital converter, and analyzed offline with AUTOSPIKE software (USB-IDAC System; Syntech). The low cutoff filter setting was 50 Hz, and the high cutoff was 5 kHz. Stimuli consisted of 1000 ms air pulses passed over odorant sources. The Δ spikes/s was calculated by counting the spikes in a 1000 ms window from ~500 ms after odorant stimuli were triggered, subtracting the spikes in a 1000 ms window prior to each stimulation. For ab3 recordings from *wildtype*, *Orco^2* mutant, and *Ir25a^2* mutant flies, spikes were counted in a 500 ms window from the start of the response and multiplied by 2. Then, the spikes in the 1000 ms window prior to stimulation were subtracted from this to calculate the Δ spikes/s. Stimuli used: mineral oil (Sigma CAS# 8042-47-5), EA (Sigma CAS# 141-78-6), PA (Sigma CAS# 628-63-7), benzaldehyde (Sigma CAS# 100-52-7), ethyl butyrate (Sigma CAS# 105-54-4), hexanol (Sigma CAS# 111-27-3), e2-hexenal (Sigma CAS# 6728-26-3), geranyl acetate (Sigma CAS# 105-87-3), 2-heptanone (Sigma CAS# 110-43-0), 1-octen-3-ol (Sigma CAS#3391-86-4), 2,3-butanedione (Sigma CAS#431-03-8), phenylacetaldehyde (Sigma CAS# 122-78-1), phenethylamine (Sigma CAS# 64-04-0), propionic acid (Sigma CAS# 79-09-4), 1,4-diaminobutane (Sigma CAS# 110-60-1), pyrrolidine (Sigma CAS# 123-75-1), p-cresol (Sigma CAS# 106-44-5), and methyl salicylate (Sigma CAS# 119-36-8). Odorants were dissolved in mineral oil at a concentration of 1%, and 20 μL of solution was pipetted onto filter paper in a glass Pasteur pipette. Stimuli were delivered by placing the tip of the Pasteur pipette through a hole in a plastic pipette (Denville Scientific Inc, 10 mL pipette) that carried a purified continuous

air stream (8.3 mL/s) directed at the antenna or maxillary palp. A solenoid valve (Syntech) diverted delivery of a 1000 ms pulse of charcoal-filtered air (5 mL/s) to the Pasteur pipette containing the odorant dissolved on filter paper. Fresh odorant pipettes were used for no more than five odorant presentations. *Ir25a²* and *Orco²* mutant fly lines were outcrossed into the *w¹¹¹⁸ wildtype* genetic background for at least five generations. Full genotypes for ab3 fgSSR were *Pin/CyO;Or22a-Gal4,15XUAS-IVS-mcd8GFP/TM6B (wildtype)*, *Ir25a²;Or22a-Gal4,15XUAS-IVS-mcd8GFP/TM6B (Ir25a² mutant)*, and *Or22a-Gal4/10XUAS-IVS-mcd8GFP (attp40);Orco² (Orco² mutant)*. These stocks were made from the following Bloomington Stocks (outcrossed to the Potter lab *w¹¹¹⁸* genetic background): BDSC# 9951, 9952, 23130, 32186, 32193, and 41737.

Coeloconic single sensillum recordings

Coeloconic SSR was performed similarly as for basiconic sensilla. Three- to five-day-old female flies were wedged in the tip of a 200 µL pipette, with the antennae and half the head exposed. A tapered glass electrode was used to stabilize the antenna against a coverslip. A BX51WI microscope (Olympus) was used to visualize the prep, which was kept under a 2000 mL/min humidified and purified air stream. A borosilicate glass electrode was filled with sensillum recording solution (*Kaissling and Thorson, 1980*) and inserted into the eye as a reference electrode. An aluminosilicate glass electrode was filled with the same recording solution and inserted into individual sensilla. Different classes of coeloconic sensilla were identified by their known location on the antenna and confirmed with their responses to a small panel of diagnostic odorants: in *wildtype* flies, ac2 sensilla were identified by their strong responses to 1,4-diaminobutane and 2,3-butanedione. The absence of a strong response to ammonia was used to rule out ac1 sensilla, the absence of a hexanol response was used to rule out ac3 sensilla, and the absence of a phenethylamine response was used to rule out ac4 sensilla. In *Ir25a* mutant flies in which amine responses were largely abolished, ac2 and ac4 sensilla were distinguished based on anatomical location, as well as the strong response of ac2 to 2,3-butanedione and the moderate response to propanal (both absent in ac4). ac1 and ac3 sensilla were excluded similarly in the mutant and wildtype flies. No more than four sensilla per fly were recorded. Each sensillum was tested with multiple odorants, with a rest time of at least 10 s between applications. The odorants used were acetic acid (Fisher, 1%, CAS# 64-19-7), ammonium hydroxide (Fisher, 0.1%, CAS# 7664-41-7), cadaverine (Sigma-Aldrich, 1%, CAS# 462-94-2), hexanol (ACROS Organics, 0.001%, CAS# 111-27-3), 2,3-butanedione (ACROS Organics, 1%, CAS# 431-03-8), phenethylamine (ACROS Organics, 1%, CAS# 64-04-0), propanal (ACROS Organics, 1%, CAS# 123-38-6), and 1,4-diaminobutane (ACROS Organics, 1%, CAS# 110-60-1). Odorants were diluted in water or paraffin oil. Odorant cartridges were made by placing a 13 mm antibiotic assay disc (Whatman) into a Pasteur pipette, pipetting 50 µL odorant onto the disc, and closing the end with a 1 mL plastic pipette tip. Each odorant cartridge was used a maximum of four times. The tip of the cartridge was inserted into a hole in the main airflow tube, and odorants were applied at 500 mL/min for 500 ms. Delivery was controlled via LabChart Pro v8 software (ADInstruments), which directed the opening and closing of a Lee valve (02-21-08i) linked to a ValveBank 4 controller (AutoMate Scientific). Extracellular action potentials were collected with an EXT-02F amplifier (NPI) with a custom 10X head stage. Data were acquired and AC filtered (300–1700 Hz) at 10 kHz with a PowerLab 4/35 digitizer and LabChart Pro v8 software. Spikes were summed in coeloconic recordings due to their similar sizes, and they were counted over a 500 ms window, starting at 100 ms after stimulus onset.

Optogenetics

Ir25a-T2A-QF2 was crossed to *QUAS-CsChrimson* #11C and double balanced to establish a stable stock (*Ir25a-T2A-QF2/CyO; QUAS-CsChrimson* #11C/*TM6B*). Newly eclosed flies (age <1 day old) were transferred to fly vials containing 0.4 mM all trans-retinal in fly food (Sigma-Aldrich #R2500, dissolved in pure DMSO with stock concentration of 0.4 M). Vials with flies were kept in the dark for at least 4 days before experiments. 627 nm LED light source (1-up LED Lighting Kit, Part# ALK-1UP-EH-KIT) powered by an Arduino Uno (https://docs.arduino.cc/hardware/uno-rev3/) was used to activate CsChrimson. By setting the voltage to 2 V and the distance of the light source to 20 cm between the LED and the fly antenna, the light intensity was equivalent to 1.13 W/m². The antenna was stimulated for 500 ms followed by 5 s of recovery period for the total recording length of 20 s (three stimulations). The identity of ab2 and ab3 sensilla were first verified with 1% EA (Sigma #270989) and

1% PA (Sigma #109584) before optogenetic experiments. Identification of ab9 sensilla was assisted by fluorescence-guided SSR (fgSSR) (*Lin and Potter, 2015*) using *Or67b-Gal4* (BDSC #9995) recombined with *15XUAS-IVS-mCD8::GFP* (BDSC #32193). The Δ spikes/s was calculated as for other basiconic SSR. For all optogenetic experiments, the control flies were of the same genotype as experimental flies but had not been fed all-trans retinal.

Single-nucleus RNA-sequencing analyses

Dataset analyzed in this paper was published in *McLaughlin et al., 2021*. The expression levels for the *Ir co-receptors* across all OSNs were lower than for *Orco*, even for their corresponding 'canonical' glomeruli. To account for these differences and facilitate comparisons, we performed within-gene normalization in *Figure 4—source data 1* and used the normalized values to generate the AL maps in *Figure 4A*. The normalization was performed as follows: first, we determined the fraction of cells within each cluster expressing the given co-receptor (read counts per million, CPM threshold ≥3). The cluster with the highest fraction value was taken as the maximum. Then, the fraction for each cluster was divided by this maximum value. The normalized value shows the relative strength of expression within each cluster for the given co-receptor gene.

EM neuron reconstruction

VM6 OSNs (*Figure 5F and G*) were reconstructed in the FAFB EM volume (*Zheng et al., 2018*) using FlyWire (https://flywire.ai/; *Dorkenwald et al., 2020*). Initial candidates were selected based on either being upstream of the VM6 (previously called VC5 in *Bates et al., 2020*) projection neurons or based on co-fasciculation with already identified VM6 OSNs. Analyses were performed in Python using the open-source packages *navis* (https://github.com/schlegelp/navis) and *fafbseq* (https://github.com/flyconnectome/fafbseg-py). OSNs were clustered using FAFB synapse predictions (*Buhmann et al., 2021*) for a synapse-based NBLAST ('syNBLAST,' implemented in *navis*). The reconstructions can be viewed at https://flywire.ai/#links/Task2021a/all.

Phylogenetic analysis

D. melanogaster, *D. sechellia*, and *D. virilis Orco* sequences were compared using the FlyBase (https://flybase.org/) BLAST tool (reference sequences examined: XM_002038370.1, XM_032721743.1, XM_002056720.3). The *A. coluzzii Orco* sequence was downloaded from VectorBase (https://vectorbase.org/) (sequence reference UniProtKB/TrEMBL;Acc:A0A182LER8). The pea aphid *Orco* sequence was acquired from the European Nucleotide Archive (https://www.ebi.ac.uk/ena/browser/view/AQS60741) (sequence reference ENA|AQS60741|AQS60741.1). Sequences were aligned using MUSCLE in MEGA11 software. This alignment was used to generate the phylogenetic tree shown in *Figure 7A*. The tree with the highest log likelihood (–6037.19) was used. Initial trees for the heuristic search were obtained automatically by applying Neighbor-Join and BioNJ algorithms to a matrix of pairwise distances estimated using the Tamura–Nei model, and then selecting the topology with superior log likelihood value. The tree in *Figure 7A* is drawn to sale, with branch lengths measured in the number of substitutions per site (scale bar = 0.1). Codon positions included were 1st + 2nd + 3rd + Noncoding. There were a total of 1488 positions in the final dataset. Evolutionary analyses were conducted in MEGA11 (*Tamura et al., 2021*). The tree is rooted to the pea aphid (*Acyrthosiphon pisum*) outgroup, thought to represent one of the most ancient examples of functional Orco/Or complexes (*Missbach et al., 2014*; *Smadja et al., 2009*; *Soffan et al., 2018*).

Quantification and statistical analysis

Cell counting

To quantify knock-in co-expression with the corresponding antibodies (*Figure 2*), the 3D reconstruction software Amira (FEI, OR) was used to manually mark individual cell bodies throughout the z-stack in each channel (antibody in far red channel, knock-in in green channel), and the cell markers between channels were compared. We also used Amira for the *D. sechellia* palp cell counts (*Figure 7C*). Cells were first marked in the far red (Orco) channel, then subsequently in the green (Ir25a) channel.

For sacculus cell counts (*Figure 5C–E*), cells were counted within ImageJ/Fiji using the cell counter tool. Counts were done manually by going through each stack within an image and using different colored markers for each cell type.

For *Anopheles* cell counts (*Figure 7D and E*), cells were counted in the Zeiss software (Zen Black) with the help of a manual cell counter.

All cell count data were gathered in Excel and analyzed for percent colocalization.

Statistics

Statistical analyses on SSR data were done in GraphPad Prism (version 8), except for optogenetic experiments, which were analyzed in Microsoft Excel. Box plots were made using GraphPad Prism; bar graphs were made in Excel. For all analyses, significance level α = 0.05. The following analyses were performed on all SSR data (excluding optogenetics): within genotype, Kruskal–Wallis test with uncorrected Dunn's to determine which odorant responses were significantly different from mineral oil or paraffin oil control; between genotype, Mann–Whitney *U* to compare responses of two genotypes to the same odorant (e.g., *wildtype* vs. *Ir25a²* mutant, or *wildtype* vs. *Orco-T2A-QF2* knock-in). Summary tables in *Figure 6* are filled in based on the following criteria: no response means neither *wildtype* nor *Ir25a²* mutant odor-evoked activity for given odorant was significantly different from its respective mineral oil control, nor was the difference between the genotypes statistically significant; no difference means that either *wildtype* or mutant or both had a significantly different odor-evoked response to the stimulus compared to mineral oil control, but the difference between the two genotypes was not statistically significant; higher response (in either *wildtype* or mutant) means that there was a statistically significant difference between genotypes for the given odorant. This could mean that (a) one genotype did not have a response, while the other did; (b) both genotypes had a response, and one was higher; (c) responses are different from each other, but not from their respective mineral oil controls; or (d) neural activity was inhibited by the odorant in one genotype compared to mineral oil control, and either not inhibited in the other genotype or inhibited to a lesser degree. Nonparametric tests were chosen due to small sample sizes and/or data that were not normally distributed.

In *Figure 6I*, stimulus responses that were statistically significantly different from mineral oil control were those whose Δ spike values were zero due to the fact that the mineral oil control Δ spike value was nonzero (median = 1.2, range = 0–2). Because of this, we did not deem these differences as biologically relevant. Nevertheless, p-values are reported in the figure legend of *Figure 6*, and detailed information can be found in *Figure 6—source data 1*.

Acknowledgements

Additional information

Author contributions

Darya Task, Conceptualization, Formal analysis, Investigation, Methodology, Visualization, Writing – original draft, Writing – review and editing; Chun-Chieh Lin, Maria Brbic, Philipp Schlegel, Hongjie Li, Conceptualization, Formal analysis, Investigation, Methodology, Visualization, Writing – review and editing; Alina Vulpe, Conceptualization, Formal analysis, Investigation, Methodology, Writing – review and editing; Ali Afify, Sydney Ballou, Joshua Raji, Formal analysis, Investigation, Methodology, Writing – review and editing; Gregory Jefferis, Supervision, Writing – review and editing; Karen Menuz, Conceptualization, Methodology, Supervision, Writing – review and editing; Christopher J Potter, Conceptualization, Funding acquisition, Methodology, Supervision, Visualization, Writing – original draft, Writing – review and editing

Author ORCIDs

Darya Task http://orcid.org/0000-0003-0166-3626
Philipp Schlegel http://orcid.org/0000-0002-5633-1314
Gregory Jefferis http://orcid.org/0000-0002-0587-9355
Christopher J Potter http://orcid.org/0000-0002-5223-8112

Decision letter and Author response

Decision letter https://doi.org/10.7554/eLife.72599.sa1
Author response https://doi.org/10.7554/eLife.72599.sa2

Additional files

Supplementary files
• Transparent reporting form

Data availability

All data generated or analyzed during this study are included in the manuscript and supporting files; Source Data files have been provided for Table 1, Figure 2, Figure 3, Figure 4, Figure 6, and Figure 7.

The following previously published datasets were used:

Author(s)	Year	Dataset title	Dataset URL	Database and Identifier
McLaughlin CN, Brbić M, Xie Q, Li T, Horns F, Kolluru SS, Kebschull JM, Vacek D, Xie A, Li J, Jones RC, Leskovec J, Quake SR, Luo L Li H	2021	Single-cell transcriptomes of developing and adult olfactory receptor neurons in Drosophila	https://github.com/colleen-mclaughlin/ORN_seq/	Omnibus ID, GSE162121
Task D, Potter CJ	2021	Raw and analyzed data from Task et al 2022	https://doi.org/10.5061/dryad.9w0vt4bgp	Dryad Digital Repository, 10.5061/dryad.9w0vt4bgp
Schlegal P, Gsxe J	2021	EM Reconstructions of VM6 OSNs	https://flywire.ai/#links/Task2021a/all	FAFB EM volume, FAFB

References

Abuin L, Bargeton B, Ulbrich MH, Isacoff EY, Kellenberger S, Benton R. 2011. Functional architecture of olfactory ionotropic glutamate receptors *Neuron* **69**:44–60. DOI: https://doi.org/10.1016/j.neuron.2010.11.042, PMID: 21220098

Abuin L, Prieto-Godino LL, Pan H, Gutierrez C, Huang L, Jin R, Benton R. 2019. In vivo assembly and trafficking of olfactory Ionotropic Receptors. *BMC Biology* **17**:0651-7. DOI: https://doi.org/10.1186/s12915-019-0651-7, PMID: 30995910

Ache BW, Young JM. 2005. Olfaction: diverse species, conserved principles *Neuron* **48**:417–430. DOI: https://doi.org/10.1016/j.neuron.2005.10.022, PMID: 16269360

Ai M, Min S, Grosjean Y, Leblanc C, Bell R, Benton R, Suh GSB. 2010. Acid sensing by the *Drosophila* olfactory system *Nature* **468**:691–695. DOI: https://doi.org/10.1038/nature09537, PMID: 21085119

Ai M, Blais S, Park JY, Min S, Neubert TA, Suh GSB. 2013. Ionotropic glutamate receptors IR64a and IR8a form a functional odorant receptor complex in vivo in *Drosophila The Journal of Neuroscience* **33**:10741–10749. DOI: https://doi.org/10.1523/JNEUROSCI.5419-12.2013, PMID: 23804096

Auer TO, Khallaf MA, Silbering AF, Zappia G, Ellis K, Álvarez-Ocaña R, Arguello JR, Hansson BS, Jefferis G, Caron SJC, Knaden M, Benton R. 2020. Olfactory receptor and circuit evolution promote host specialization *Nature* **579**:402–408. DOI: https://doi.org/10.1038/s41586-020-2073-7, PMID: 32132713

Awasaki T, Huang Y, O'Connor MB, Lee T. 2011. Glia instruct developmental neuronal remodeling through TGF-β signaling *Nature Neuroscience* **14**:821–823. DOI: https://doi.org/10.1038/nn.2833, PMID: 21685919

Baena-Lopez LA, Alexandre C, Mitchell A, Pasakarnis L, Vincent JP. 2013. Accelerated homologous recombination and subsequent genome modification in *Drosophila Development (Cambridge, England)* **140**:4818–4825. DOI: https://doi.org/10.1242/dev.100933, PMID: 24154526

Bates AS, Schlegel P, Roberts RJV, Drummond N, Tamimi IFM, Turnbull R, Zhao X, Marin EC, Popovici PD, Dhawan S, Jamasb A, Javier A, Serratosa Capdevila L, Li F, Rubin GM, Waddell S, Bock DD, Costa M, Jefferis G. 2020. Complete Connectomic Reconstruction of Olfactory Projection Neurons in the Fly Brain *Current Biology* **30**:3183–3199. DOI: https://doi.org/10.1016/j.cub.2020.06.042, PMID: 32619485

Benton R, Sachse S, Michnick SW, Vosshall LB. 2006. Atypical membrane topology and heteromeric function of *Drosophila* odorant receptors in vivo *PLOS Biology* **4**:e20. DOI: https://doi.org/10.1371/journal.pbio.0040020, PMID: 16402857

Benton R, Vannice KS, Gomez-Diaz C, Vosshall LB. 2009. Variant ionotropic glutamate receptors as chemosensory receptors in *Drosophila Cell* **136**:149–162. DOI: https://doi.org/10.1016/j.cell.2008.12.001, PMID: 19135896

Berck ME, Khandelwal A, Claus L, Hernandez-Nunez L, Si G, Tabone CJ, Li F, Truman JW, Fetter RD, Louis M, Samuel AD, Cardona A. 2016. The wiring diagram of a glomerular olfactory system *eLife* **5**:e14859. DOI: https://doi.org/10.7554/eLife.14859, PMID: 27177418

Bhalerao S, Sen A, Stocker R, Rodrigues V. 2003. Olfactory neurons expressing identified receptor genes project to subsets of glomeruli within the antennal lobe of *Drosophila melanogaster Journal of Neurobiology* **54**:577–592. DOI: https://doi.org/10.1002/neu.10175, PMID: 12555270

Bischof J, Maeda RK, Hediger M, Karch F, Basler K. 2007. An optimized transgenesis system for *Drosophila* using germ-line-specific phiC31 integrases *PNAS* **104**:3312–3317. DOI: https://doi.org/10.1073/pnas.0611511104, PMID: 17360644

Bosch JA, Knight S, Kanca O, Zirin J, Yang-Zhou D, Hu Y, Rodiger J, Amador G, Bellen HJ, Perrimon N, Mohr SE. 2020. Use of the CRISPR-Cas9 System in *Drosophila* Cultured Cells to Introduce Fluorescent Tags into Endogenous Genes *Current Protocols in Molecular Biology* **130**:e112. DOI: https://doi.org/10.1002/cpmb.112, PMID: 31869524

Brand AH, Perrimon N. 1993. Targeted gene expression as a means of altering cell fates and generating dominant phenotypes *Development (Cambridge, England)* **118**:401–415. DOI: https://doi.org/10.1242/dev.118.2.401, PMID: 8223268

Budelli G, Ni L, Berciu C, van Giesen L, Knecht ZA, Chang EC, Kaminski B, Silbering AF, Samuel A, Klein M, Benton R, Nicastro D, Garrity PA. 2019. Ionotropic receptors specify the morphogenesis of phasic sensors controlling rapid thermal preference in *drosophila Neuron* **101**:738–747. DOI: https://doi.org/10.1016/j.neuron.2018.12.022, PMID: 30654923

Buhmann J, Sheridan A, Malin-Mayor C, Schlegel P, Gerhard S, Kazimiers T, Krause R, Nguyen TM, Heinrich L, Lee W-CA, Wilson R, Saalfeld S, Jefferis GSXE, Bock DD, Turaga SC, Cook M, Funke J. 2021. Automatic detection of synaptic partners in a whole-brain *Drosophila* electron microscopy data set *Nature Methods* **18**:771–774. DOI: https://doi.org/10.1038/s41592-021-01183-7, PMID: 34168373

Butterwick JA, Del Mármol J, Kim KH, Kahlson MA, Rogow JA, Walz T, Ruta V. 2018. Cryo-EM structure of the insect olfactory receptor Orco *Nature* **560**:447–452. DOI: https://doi.org/10.1038/s41586-018-0420-8, PMID: 30111839

Carey AF, Carlson JR. 2011. Insect olfaction from model systems to disease control *PNAS* **108**:12987–12995. DOI: https://doi.org/10.1073/pnas.1103472108, PMID: 21746926

Chai PC, Cruchet S, Wigger L, Benton R. 2019. Sensory neuron lineage mapping and manipulation in the *Drosophila* olfactory system *Nature Communications* **10**:643. DOI: https://doi.org/10.1038/s41467-019-08345-4, PMID: 30733440

Chen C, Buhl E, Xu M, Croset V, Rees JS, Lilley KS, Benton R, Hodge JJL, Stanewsky R. 2015. *Drosophila* Ionotropic Receptor 25a mediates circadian clock resetting by temperature *Nature* **527**:516–520. DOI: https://doi.org/10.1038/nature16148, PMID: 26580016

Chen Y, Amrein H. 2017. Ionotropic receptors mediate *Drosophila* oviposition preference through sour gustatory receptor neurons *Current Biology* **27**:2741–2750. DOI: https://doi.org/10.1016/j.cub.2017.08.003, PMID: 28889974

Chen Y-CD, Dahanukar A. 2017. Molecular and Cellular Organization of Taste Neurons in Adult *Drosophila* Pharynx *Cell Reports* **21**:2978–2991. DOI: https://doi.org/10.1016/j.celrep.2017.11.041, PMID: 29212040

Chen HM, Yao X, Ren Q, Chang CC, Liu LY, Miyares RL, Lee T. 2020. Enhanced Golic+: highly effective CRISPR gene targeting and transgene HACKing in *Drosophila Development (Cambridge, England)* **147**:dev181974. DOI: https://doi.org/10.1242/dev.181974, PMID: 32467238

Choi HMT, Calvert CR, Husain N, Huss D, Barsi JC, Deverman BE, Hunter RC, Kato M, Lee SM, Abelin ACT, Rosenthal AZ, Akbari OS, Li Y, Hay BA, Sternberg PW, Patterson PH, Davidson EH, Mazmanian SK, Prober DA, van de Rijn M, et al. 2016. Mapping a multiplexed zoo of mRNA expression *Development (Cambridge, England)* **143**:3632–3637. DOI: https://doi.org/10.1242/dev.140137, PMID: 27702788

Choi HMT, Schwarzkopf M, Fornace ME, Acharya A, Artavanis G, Stegmaier J, Cunha A, Pierce NA. 2018. Third-generation in situ hybridization chain reaction: multiplexed, quantitative, sensitive, versatile, robust *Development (Cambridge, England)* **145**:dev165753. DOI: https://doi.org/10.1242/dev.165753, PMID: 29945988

Clyne PJ, Warr CG, Freeman MR, Lessing D, Kim J, Carlson JR. 1999. A novel family of divergent seven-transmembrane proteins: candidate odorant receptors in *Drosophila Neuron* **22**:327–338. DOI: https://doi.org/10.1016/s0896-6273(00)81093-4, PMID: 10069338

Couto A, Alenius M, Dickson BJ. 2005. Molecular, anatomical, and functional organization of the *Drosophila* olfactory system *Current Biology* **15**:1535–1547. DOI: https://doi.org/10.1016/j.cub.2005.07.034, PMID: 16139208

Croset V, Rytz R, Cummins SF, Budd A, Brawand D, Kaessmann H, Gibson TJ, Benton R. 2010. Ancient protostome origin of chemosensory ionotropic glutamate receptors and the evolution of insect taste and olfaction *PLOS Genetics* **6**:e1001064. DOI: https://doi.org/10.1371/journal.pgen.1001064, PMID: 20808886

de Bruyne M, Clyne PJ, Carlson JR. 1999. Odor Coding in a Model Olfactory Organ: The *Drosophila* Maxillary Palp *The Journal of Neuroscience* **19**:4520–4532. DOI: https://doi.org/10.1523/JNEUROSCI.19-11-04520.1999, PMID: 10341252

de Bruyne M, Foster K, Carlson JR. 2001. Odor Coding in the *Drosophila* Antenna *Neuron* **30**:537–552. DOI: https://doi.org/10.1016/s0896-6273(01)00289-6, PMID: 11395013

DeGennaro M, McBride CS, Seeholzer L, Nakagawa T, Dennis EJ, Goldman C, Jasinskiene N, James AA, Vosshall LB. 2013. orco mutant mosquitoes lose strong preference for humans and are not repelled by volatile DEET *Nature* **498**:487–491. DOI: https://doi.org/10.1038/nature12206, PMID: 23719379

Depetris-Chauvin A, Galagovsky D, Grosjean Y. 2015. Chemicals and chemoreceptors: ecologically relevant signals driving behavior in *Drosophila*. *Frontiers in Ecology and Evolution* **3**:41. DOI: https://doi.org/10.3389/fevo.2015.00041

Diao F, White BH. 2012. A novel approach for directing transgene expression in *Drosophila*: T2A-Gal4 in-frame fusion *Genetics* **190**:1139–1144. DOI: https://doi.org/10.1534/genetics.111.136291, PMID: 22209908

Diao F, Ironfield H, Luan H, Diao F, Shropshire WC, Ewer J, Marr E, Potter CJ, Landgraf M, White BH. 2015. Plug-and-play genetic access to *Drosophila* cell types using exchangeable exon cassettes *Cell Reports* **10**:1410–1421. DOI: https://doi.org/10.1016/j.celrep.2015.01.059, PMID: 25732830

Dorkenwald S, McKellar C, Macrina T, Kemnitz N, Lee K, Lu R, Wu J, Popovych S, Mitchell E, Nehoran B, Jia Z, Bae JA, Mu S, Ih D, Castro M, Ogedengbe O, Halageri A, Ashwood Z, Zung J, Brittain D, et al. 2020. FlyWire: Online Community for Whole-Brain Connectomics. *bioRxiv*. DOI: https://doi.org/10.1101/2020.08.30.274225

Du L, Zhou A, Sohr A, Roy S. 2018. An efficient strategy for generating tissue-specific binary transcription systems in *drosophila* by genome editing. *Journal of Visualized Experiments* **10**:58268. DOI: https://doi.org/10.3791/58268, PMID: 30295654

Dunipace L, Meister S, McNealy C, Amrein H. 2001. Spatially restricted expression of candidate taste receptors in the *Drosophila* gustatory system *Current Biology* **11**:822–835. DOI: https://doi.org/10.1016/s0960-9822(01)00258-5, PMID: 11516643

Dweck HKM, Ebrahim SAM, Thoma M, Mohamed AAM, Keesey IW, Trona F, Lavista-Llanos S, Svatoš A, Sachse S, Knaden M, Hansson BS. 2015. Pheromones mediating copulation and attraction in *Drosophila. PNAS* **112**:E2829. DOI: https://doi.org/10.1073/pnas.1504527112, PMID: 25964351

Ebrahim SAM, Dweck HKM, Stökl J, Hofferberth JE, Trona F, Weniger K, Rybak J, Seki Y, Stensmyr MC, Sachse S, Hansson BS, Knaden M. 2015. *Drosophila* avoids parasitoids by sensing their semiochemicals via a dedicated olfactory circuit. *PLOS Biology* **13**:1002318. DOI: https://doi.org/10.1371/journal.pbio.1002318, PMID: 26674493

Endo K, Aoki T, Yoda Y, Kimura K, Hama C. 2007. Notch signal organizes the *Drosophila* olfactory circuitry by diversifying the sensory neuronal lineages. *Nature Neuroscience* **10**:153–160. DOI: https://doi.org/10.1038/nn1832, PMID: 17220884

Enjin A, Zaharieva EE, Frank DD, Mansourian S, Suh GSB, Gallio M, Stensmyr MC. 2016. Humidity Sensing in *Drosophila Current Biology* **26**:1352–1358. DOI: https://doi.org/10.1016/j.cub.2016.03.049, PMID: 27161501

Fandino RA, Haverkamp A, Bisch-Knaden S, Zhang J, Bucks S, Nguyen TAT, Schröder K, Werckenthin A, Rybak J, Stengl M, Knaden M, Hansson BS, Große-Wilde E. 2019. Mutagenesis of odorant coreceptor Orco fully disrupts foraging but not oviposition behaviors in the hawkmoth Manduca sexta *PNAS* **116**:15677–15685. DOI: https://doi.org/10.1073/pnas.1902089116, PMID: 31320583

Fishilevich E, Vosshall LB. 2005. Genetic and functional subdivision of the *Drosophila* antennal lobe *Current Biology* **15**:1548–1553. DOI: https://doi.org/10.1016/j.cub.2005.07.066, PMID: 16139209

Frank DD, Enjin A, Jouandet GC, Zaharieva EE, Para A, Stensmyr MC, Gallio M. 2017. Early integration of temperature and humidity stimuli in the *drosophila* brain *Current Biology* **27**:2381–2388. DOI: https://doi.org/10.1016/j.cub.2017.06.077, PMID: 28736172

Frechter S, Bates AS, Tootoonian S, Dolan MJ, Manton J, Jamasb AR, Kohl J, Bock D, Jefferis G. 2019. Functional and anatomical specificity in a higher olfactory centre *eLife* **8**:e44590. DOI: https://doi.org/10.7554/eLife.44590, PMID: 31112127

Fujii S, Yavuz A, Slone J, Jagge C, Song X, Amrein H. 2015. *Drosophila* sugar receptors in sweet taste perception, olfaction, and internal nutrient sensing *Current Biology* **25**:621–627. DOI: https://doi.org/10.1016/j.cub.2014.12.058, PMID: 25702577

Ganguly A, Pang L, Duong VK, Lee A, Schoniger H, Varady E, Dahanukar A. 2017. A Molecular and Cellular Context-Dependent Role for Ir76b in Detection of Amino Acid Taste *Cell Reports* **18**:737–750. DOI: https://doi.org/10.1016/j.celrep.2016.12.071, PMID: 28099851

Gao Q, Chess A. 1999. Identification of candidate *Drosophila* olfactory receptors from genomic DNA sequence *Genomics* **60**:31–39. DOI: https://doi.org/10.1006/geno.1999.5894, PMID: 10458908

Gao Q, Yuan B, Chess A. 2000. Convergent projections of *Drosophila* olfactory neurons to specific glomeruli in the antennal lobe *Nature Neuroscience* **3**:780–785. DOI: https://doi.org/10.1038/77680, PMID: 10903570

Gaunt MW, Miles MA. 2002. An Insect Molecular Clock Dates the Origin of the Insects and Accords with Palaeontological and Biogeographic Landmarks *Molecular Biology and Evolution* **19**:748–761. DOI: https://doi.org/10.1093/oxfordjournals.molbev.a004133, PMID: 11961108

Gloor GB, Nassif NA, Johnson-Schlitz DM, Preston CR, Engels WR. 1991. Targeted gene replacement in *Drosophila* via P element-induced gap repair *Science (New York, N.Y.)* **253**:1110–1117. DOI: https://doi.org/10.1126/science.1653452, PMID: 1653452

Gnerer JP, Venken KJT, Dierick HA. 2015. Gene-specific cell labeling using MiMIC transposons. *Nucleic Acids Research* **43**:gkv113. DOI: https://doi.org/10.1093/nar/gkv113, PMID: 25712101

Goldman AL, Van der Goes W, Lessing D, Warr CG, Carlson JR. 2005. Coexpression of two functional odor receptors in one neuron. *Neuron* **45**:661–666. DOI: https://doi.org/10.1016/j.neuron.2005.01.025, PMID: 15748842

Gomez-Diaz C, Martin F, Garcia-Fernandez JM, Alcorta E. 2018. The two main olfactory receptor families in *drosophila*, ORs and IRs: A comparative approach *Frontiers in Cellular Neuroscience* **12**:253. DOI: https://doi.org/10.3389/fncel.2018.00253, PMID: 30214396

Goulding SE, zur Lage P, Jarman AP. 2000. amos, a Proneural Gene for *Drosophila* Olfactory Sense Organs that Is Regulated by lozenge *Neuron* **25**:69–78. DOI: https://doi.org/10.1016/s0896-6273(00)80872-7, PMID: 10707973

Grabe V, Baschwitz A, Dweck HKM, Lavista-Llanos S, Hansson BS, Sachse S. 2016. Elucidating the Neuronal Architecture of Olfactory Glomeruli in the *Drosophila* Antennal Lobe *Cell Reports* **16**:3401–3413. DOI: https://doi.org/10.1016/j.celrep.2016.08.063, PMID: 27653699

Grabe V, Sachse S. 2018. Fundamental principles of the olfactory code *Bio Systems* **164**:94–101. DOI: https://doi.org/10.1016/j.biosystems.2017.10.010, PMID: 29054468

Gratz SJ, Ukken FP, Rubinstein CD, Thiede G, Donohue LK, Cummings AM, O'Connor-Giles KM. 2014. Highly specific and efficient CRISPR/Cas9-catalyzed homology-directed repair in *Drosophila Genetics* **196**:961–971. DOI: https://doi.org/10.1534/genetics.113.160713, PMID: 24478335

Groth AC, Fish M, Nusse R, Calos MP. 2004. Construction of transgenic *Drosophila* by using the site-specific integrase from phage phiC31 *Genetics* **166**:1775–1782. DOI: https://doi.org/10.1534/genetics.166.4.1775, PMID: 15126397

Gupta BP, Rodrigues V. 1997. Atonal is a proneural gene for a subset of olfactory sense organs in *Drosophila. Genes to Cells* **2**:225–233. DOI: https://doi.org/10.1046/j.1365-2443.1997.d01-312.x, PMID: 9189759

Hahn MW, Han MV, Han SG. 2007. Gene family evolution across 12 *Drosophila* genomes. *PLOoS Genetics* **3**:e197. DOI: https://doi.org/10.1371/journal.pgen.0030197, PMID: 17997610

Hallem EA, Ho MG, Carlson JR. 2004. The molecular basis of odor coding in the *Drosophila* antenna *Cell* **117**:965–979. DOI: https://doi.org/10.1016/j.cell.2004.05.012, PMID: 15210116

Hallem EA, Carlson JR. 2006. Coding of odors by a receptor repertoire *Cell* **125**:143–160. DOI: https://doi.org/10.1016/j.cell.2006.01.050, PMID: 16615896

Hansson BS, Stensmyr MC. 2011. Evolution of insect olfaction *Neuron* **72**:698–711. DOI: https://doi.org/10.1016/j.neuron.2011.11.003, PMID: 22153368

Harris WA. 1972. The maxillae of *Drosophila melanogaster* as revealed by scanning electron microscopy *Journal of Morphology* **138**:451–456. DOI: https://doi.org/10.1002/jmor.1051380405, PMID: 4629324

Haverkamp A, Hansson BS, Knaden M. 2018. Combinatorial codes and labeled lines: How insects use olfactory cues to find and judge food, mates, and oviposition sites in complex environments *Frontiers in Physiology* **9**:49. DOI: https://doi.org/10.3389/fphys.2018.00049, PMID: 29449815

Horne JA, Langille C, McLin S, Wiederman M, Lu Z, Xu CS, Plaza SM, Scheffer LK, Hess HF, Meinertzhagen IA. 2018. A resource for the *Drosophila* antennal lobe provided by the connectome of glomerulus VA1v *eLife* **7**:e37550. DOI: https://doi.org/10.7554/eLife.37550, PMID: 30382940

Hussain A, Zhang M, Üçpunar HK, Svensson T, Quillery E, Gompel N, Ignell R, Grunwald Kadow IC. 2016. Ionotropic Chemosensory Receptors Mediate the Taste and Smell of Polyamines. *PLOS Biology* **14**:1002454. DOI: https://doi.org/10.1371/journal.pbio.1002454, PMID: 27145030

Jaeger AH, Stanley M, Weiss ZF, Musso PY, Chan RC, Zhang H, Feldman-Kiss D, Gordon MD. 2018. A complex peripheral code for salt taste in *Drosophila eLife* **7**:e37167. DOI: https://doi.org/10.7554/eLife.37167, PMID: 30307393

Jhaveri D, Sen A, Reddy GV, Rodrigues V. 2000a. Sense organ identity in the *Drosophila* antenna is specified by the expression of the proneural gene atonal *Mechanisms of Development* **99**:101–111. DOI: https://doi.org/10.1016/s0925-4773(00)00487-1, PMID: 11091078

Jhaveri D, Sen A, Rodrigues V. 2000b. Mechanisms underlying olfactory neuronal connectivity in *Drosophila*-the atonal lineage organizes the periphery while sensory neurons and glia pattern the olfactory lobe *Developmental Biology* **226**:73–87. DOI: https://doi.org/10.1006/dbio.2000.9855, PMID: 10993675

Jinek M, Chylinski K, Fonfara I, Hauer M, Doudna JA, Charpentier E. 2012. A programmable dual-RNA-guided DNA endonuclease in adaptive bacterial immunity *Science (New York, N.Y.)* **337**:816–821. DOI: https://doi.org/10.1126/science.1225829, PMID: 22745249

Jones WD, Cayirlioglu P, Kadow IG, Vosshall LB. 2007. Two chemosensory receptors together mediate carbon dioxide detection in *Drosophila Nature* **445**:86–90. DOI: https://doi.org/10.1038/nature05466, PMID: 17167414

Kaissling KE, Thorson J. 1980. Insect olfactory sensilla: structural, chemical and electrical aspects of the functional organisation Kaissling KE (Ed). *In Receptors for Neurotransmitters, Hormones and Pheromones in Insects.* Elsevier/North-Holland Biomedical Press. p. 261–282.

Kanca O, Zirin J, Garcia-Marques J, Knight SM, Yang-Zhou D, Amador G, Chung H, Zuo Z, Ma L, He Y, Lin WW, Fang Y, Ge M, Yamamoto S, Schulze KL, Hu Y, Spradling AC, Mohr SE, Perrimon N, Bellen HJ. 2019. An efficient CRISPR-based strategy to insert small and large fragments of DNA using short homology arms *eLife* **8**:e51539. DOI: https://doi.org/10.7554/eLife.51539, PMID: 31674908

Karim MR, Endo K, Moore AW, Taniguchi H. 2014. Whole mount immunolabeling of olfactory receptor neurons in the *Drosophila* antenna *Journal of Visualized Experiments* **1**:51245. DOI: https://doi.org/10.3791/51245, PMID: 24834898

Klapoetke NC, Murata Y, Kim SS, Pulver SR, Birdsey-Benson A, Cho YK, Morimoto TK, Chuong AS, Carpenter EJ, Tian Z, Wang J, Xie Y, Yan Z, Zhang Y, Chow BY, Surek B, Melkonian M, Jayaraman V, Constantine-Paton M, Wong GK-S, et al. 2014. Independent optical excitation of distinct neural populations *Nature Methods* **11**:338–346. DOI: https://doi.org/10.1038/nmeth.2836, PMID: 24509633

Knecht ZA, Silbering AF, Ni L, Klein M, Budelli G, Bell R, Abuin L, Ferrer AJ, Samuel AD, Benton R, Garrity PA. 2016. Distinct combinations of variant ionotropic glutamate receptors mediate thermosensation and hygrosensation in *Drosophila*. *eLife* **5**:e17879. DOI: https://doi.org/10.7554/eLife.17879, PMID: 27656904

Knecht ZA, Silbering AF, Cruz J, Yang L, Croset V, Benton R, Garrity PA. 2017. Ionotropic Receptor-dependent moist and dry cells control hygrosensation in *Drosophila eLife* **6**:e26654. DOI: https://doi.org/10.7554/eLife.26654, PMID: 28621663

Koh TW, He Z, Gorur-Shandilya S, Menuz K, Larter NK, Stewart S, Carlson JR. 2014. The *Drosophila* IR20a clade of ionotropic receptors are candidate taste and pheromone receptors *Neuron* **83**:850–865. DOI: https://doi.org/10.1016/j.neuron.2014.07.012, PMID: 25123314

Kondoh K, Lu Z, Ye X, Olson DP, Lowell BB, Buck LB. 2016. A specific area of olfactory cortex involved in stress hormone responses to predator odours *Nature* **532**:103–106. DOI: https://doi.org/10.1038/nature17156, PMID: 27001694

Kurtovic A, Widmer A, Dickson BJ. 2007. A single class of olfactory neurons mediates behavioural responses to a *Drosophila* sex pheromone *Nature* **446**:542–546. DOI: https://doi.org/10.1038/nature05672, PMID: 17392786

Kwon JY, Dahanukar A, Weiss LA, Carlson JR. 2007. The molecular basis of CO2 reception in *Drosophila PNAS* **104**:3574–3578. DOI: https://doi.org/10.1073/pnas.0700079104, PMID: 17360684

Lai SL, Lee T. 2006. Genetic mosaic with dual binary transcriptional systems in *Drosophila Nature Neuroscience* **9**:703–709. DOI: https://doi.org/10.1038/nn1681, PMID: 16582903

Laissue PP, Reiter CH, Hiesinger PR, Halter S, Fischbach KF, Stocker RF. 1999. Three-dimensional reconstruction of the antennal lobe in *Drosophila melanogaster The Journal of Comparative Neurology* **405**:543–552 PMID: 10098944.,

Larsson MC, Domingos AI, Jones WD, Chiappe ME, Amrein H, Vosshall LB. 2004. Or83b encodes a broadly expressed odorant receptor essential for *Drosophila* olfaction *Neuron* **43**:703–714. DOI: https://doi.org/10.1016/j.neuron.2004.08.019, PMID: 15339651

Lee T, Luo L. 1999. Mosaic analysis with a repressible cell marker for studies of gene function in neuronal morphogenesis *Neuron* **22**:451–461. DOI: https://doi.org/10.1016/s0896-6273(00)80701-1, PMID: 10197526

Lee P-T, Zirin J, Kanca O, Lin W-W, Schulze KL, Li-Kroeger D, Tao R, Devereaux C, Hu Y, Chung V, Fang Y, He Y, Pan H, Ge M, Zuo Z, Housden BE, Mohr SE, Yamamoto S, Levis RW, Spradling AC, et al. 2018. A gene-specific T2A-GAL4 library for *Drosophila eLife* **7**:e35574. DOI: https://doi.org/10.7554/eLife.35574

Li Q, Barish S, Okuwa S, Maciejewski A, Brandt AT, Reinhold D, Jones CD, Volkan PC. 2016. A functionally conserved gene regulatory network module governing olfactory neuron diversity. *PLOS Genetics* **12**:e1005780. DOI: https://doi.org/10.1371/journal.pgen.1005780, PMID: 26765103

Li H, Janssens J, De Waegeneer M, Kolluru SS, Davie K, Gardeux V, Saelens W, David F, Brbić M, Leskovec J, McLaughlin CN, Xie Q, Jones RC, Brueckner K, Shim J, Tattikota SG, Schnorrer F, Rust K, Nystul TG, Carvalho-Santos Z, et al. 2021. Fly Cell Atlas: A Single-Cell Transcriptomic Atlas of the Adult Fruit Fly. *bioRxiv*. DOI: https://doi.org/10.1101/2021.07.04.451050

Li-Kroeger D, Kanca O, Lee PT, Cowan S, Lee MT, Jaiswal M, Salazar JL, He Y, Zuo Z, Bellen HJ. 2018. An expanded toolkit for gene tagging based on MiMIC and scarless CRISPR tagging in *Drosophila*. *eLife* **7**:e38709. DOI: https://doi.org/10.7554/eLife.38709, PMID: 30091705

Lin CC, Potter CJ. 2015. Re-Classification of *Drosophila melanogaster* Trichoid and Intermediate Sensilla Using Fluorescence-Guided Single Sensillum Recording *PLOS ONE* **10**:e0139675. DOI: https://doi.org/10.1371/journal.pone.0139675, PMID: 26431203

Lin CC, Potter CJ. 2016a. Editing transgenic DNA components by inducible gene replacement in *drosophila melanogaster Genetics* **203**:1613–1628. DOI: https://doi.org/10.1534/genetics.116.191783, PMID: 27334272

Lin CC, Potter CJ. 2016b. Non-mendelian dominant maternal effects caused by CRISPR/Cas9 transgenic components in *Drosophila melanogaster*. *G3: Genes, Genomes, Genetics* **6**:3685–3691. DOI: https://doi.org/10.1534/g3.116.034884, PMID: 27638686

Mansourian S, Corcoran J, Enjin A, Löfstedt C, Dacke M, Stensmyr MC. 2016. Fecal-Derived Phenol Induces Egg-Laying Aversion in *Drosophila Current Biology* **26**:2762–2769. DOI: https://doi.org/10.1016/j.cub.2016.07.065, PMID: 27641770

Marin EC, Büld L, Theiss M, Sarkissian T, Roberts RJV, Turnbull R, Tamimi IFM, Pleijzier MW, Laursen WJ, Drummond N, Schlegel P, Bates AS, Li F, Landgraf M, Costa M, Bock DD, Garrity PA, Jefferis GSXE. 2020. Connectomics Analysis Reveals First-, Second-, and Third-Order Thermosensory and Hygrosensory Neurons in the Adult *Drosophila* Brain *Current Biology* **30**:3167-3182.. DOI: https://doi.org/10.1016/j.cub.2020.06.028

McLaughlin CN, Brbić M, Xie Q, Li T, Horns F, Kolluru SS, Kebschull JM, Vacek D, Xie A, Li J, Jones RC, Leskovec J, Quake SR, Luo L, Li H. 2021. Single-cell transcriptomes of developing and adult olfactory receptor neurons in *Drosophila eLife* **10**:e63856. DOI: https://doi.org/10.7554/eLife.63856, PMID: 33555999

Menuz K, Larter NK, Park J, Carlson JR. 2014. An RNA-seq screen of the *Drosophila* antenna identifies a transporter necessary for ammonia detection *PLOS Genetics* **10**:e1004810. DOI: https://doi.org/10.1371/journal.pgen.1004810, PMID: 25412082

Min S, Ai M, Shin SA, Suh GSB. 2013. Dedicated olfactory neurons mediating attraction behavior to ammonia and amines in *Drosophila PNAS* **110**:E1321–E1329. DOI: https://doi.org/10.1073/pnas.1215680110, PMID: 23509267

Missbach C, Dweck HK, Vogel H, Vilcinskas A, Stensmyr MC, Hansson BS, Grosse-Wilde E. 2014. Evolution of insect olfactory receptors. *eLife* **3**:e02115. DOI: https://doi.org/10.7554/eLife.02115, PMID: 24670956

Miwa Y, Koganezawa M, Yamamoto D. 2018. Antennae sense heat stress to inhibit mating and promote escaping in *Drosophila* females. *Journal of Neurogenetics* **32**:353–363. DOI: https://doi.org/10.1080/01677063.2018.1513507, PMID: 30231794

Ng R, Salem SS, Wu ST, Wu M, Lin HH, Shepherd AK, Joiner WJ, Wang JW, Su CY. 2019. Amplification of *Drosophila* Olfactory Responses by a DEG/ENaC Channel. *Neuron* **104**:947–959. DOI: https://doi.org/10.1016/j.neuron.2019.08.041, PMID: 31629603

Ni L, Bronk P, Chang EC, Lowell AM, Flam JO, Panzano VC, Theobald DL, Griffith LC, Garrity PA. 2013. A gustatory receptor paralogue controls rapid warmth avoidance in *Drosophila*. *Nature* **500**:580–584. DOI: https://doi.org/10.1038/nature12390, PMID: 23925112

Papes F, Logan DW, Stowers L. 2010. The Vomeronasal Organ Mediates Interspecies Defensive Behaviors through Detection of Protein Pheromone Homologs *Cell* **141**:692–703. DOI: https://doi.org/10.1016/j.cell.2010.03.037, PMID: 20478258

Park JH, Kwon JY. 2011. A systematic analysis of *Drosophila* gustatory receptor gene expression in abdominal neurons which project to the central nervous system *Molecules and Cells* **32**:375–381. DOI: https://doi.org/10.1007/s10059-011-0128-1, PMID: 21870111

Pask GM, Ray A. 2016. Insect Olfactory Receptors: An Interface between Chemistry and Biology. Akabas MH (Ed). *Chemosensory Transduction*. Elsevier. p. 101–122.

Pinto L, Stocker RF, Rodrigues V. 1988. Anatomical and neurochemical classification of the antennal glomeruli in *Drosophila melanogaster* meigen (Diptera: Drosophilidae) *International Journal of Insect Morphology and Embryology* **17**:335–344. DOI: https://doi.org/10.1016/0020-7322(88)90014-1

Port F, Chen HM, Lee T, Bullock SL. 2014. Optimized CRISPR/Cas tools for efficient germline and somatic genome engineering in *Drosophila*. *PNAS* **111**:E2967–E2976. DOI: https://doi.org/10.1073/pnas.1405500111, PMID: 25002478

Potter CJ, Tasic B, Russler EV, Liang L, Luo L. 2010. The Q system: a repressible binary system for transgene expression, lineage tracing, and mosaic analysis *Cell* **141**:536–548. DOI: https://doi.org/10.1016/j.cell.2010.02.025, PMID: 20434990

Prieto-Godino LL, Rytz R, Cruchet S, Bargeton B, Abuin L, Silbering AF, Ruta V, Dal Peraro M, Benton R. 2017. Evolution of Acid-Sensing Olfactory Circuits in Drosophilids *Neuron* **93**:661-676.. DOI: https://doi.org/10.1016/j.neuron.2016.12.024, PMID: 28111079

Prieto-Godino LL, Silbering AF, Khallaf MA, Cruchet S, Bojkowska K, Pradervand S, Hansson BS, Knaden M, Benton R. 2020. Functional integration of "undead" neurons in the olfactory system *Science Advances* **6**:eaaz7238. DOI: https://doi.org/10.1126/sciadv.aaz7238, PMID: 32195354

Ray A, van Naters W, Shiraiwa T, Carlson JR. 2007. Mechanisms of odor receptor gene choice in *Drosophila*. *Neuron* **53**:353–369. DOI: https://doi.org/10.1016/j.neuron.2006.12.010, PMID: 17270733

Ray A, van der Goes van Naters W, Carlson JR. 2008. A regulatory code for neuron-specific odor receptor expression. *PLOS Biology* **6**:0060125. DOI: https://doi.org/10.1371/journal.pbio.0060125, PMID: 18846726

Riabinina O, Luginbuhl D, Marr E, Liu S, Wu MN, Luo L, Potter CJ. 2015. Improved and expanded Q-system reagents for genetic manipulations *Nature Methods* **12**:219–222. DOI: https://doi.org/10.1038/nmeth.3250, PMID: 25581800

Riabinina O, Task D, Marr E, Lin C-C, Alford R, O'Brochta DA, Potter CJ. 2016. Organization of olfactory centres in the malaria mosquito Anopheles gambiae. *Nature Communications* **7**:13010. DOI: https://doi.org/10.1038/ncomms13010, PMID: 27694947

Saina M, Benton R. 2013. Visualizing olfactory receptor expression and localization in *drosophila Methods in Molecular Biology (Clifton, N.J.)* **1003**:211–228. DOI: https://doi.org/10.1007/978-1-62703-377-0_16, PMID: 23585045

Sánchez-Alcañiz JA, Silbering AF, Croset V, Zappia G, Sivasubramaniam AK, Abuin L, Sahai SY, Münch D, Steck K, Auer TO, Cruchet S, Neagu-Maier GL, Sprecher SG, Ribeiro C, Yapici N, Benton R. 2018. An expression atlas of variant ionotropic glutamate receptors identifies a molecular basis of carbonation sensing. *Nature Communications* **9**:4252. DOI: https://doi.org/10.1038/s41467-018-06453-1, PMID: 30315166

Sato K, Pellegrino M, Nakagawa T, Nakagawa T, Vosshall LB, Touhara K. 2008. Insect olfactory receptors are heteromeric ligand-gated ion channels *Nature* **452**:1002–1006. DOI: https://doi.org/10.1038/nature06850, PMID: 18408712

Scheffer LK, Xu CS, Januszewski M, Lu Z, Takemura S-Y, Hayworth KJ, Huang GB, Shinomiya K, Maitlin-Shepard J, Berg S, Clements J, Hubbard PM, Katz WT, Umayam L, Zhao T, Ackerman D, Blakely T, Bogovic J, Dolafi T, Kainmueller D, et al. 2020. A connectome and analysis of the adult *Drosophila* central brain *eLife* **9**:e57443. DOI: https://doi.org/10.7554/eLife.57443, PMID: 32880371

Schindelin J, Arganda-Carreras I, Frise E, Kaynig V, Longair M, Pietzsch T, Preibisch S, Rueden C, Saalfeld S, Schmid B, Tinevez J-Y, White DJ, Hartenstein V, Eliceiri K, Tomancak P, Cardona A. 2012. Fiji: an open-source platform for biological-image analysis *Nature Methods* **9**:676–682. DOI: https://doi.org/10.1038/nmeth.2019, PMID: 22743772

Schlegel P, Bates AS, Stürner T, Jagannathan SR, Drummond N, Hsu J, Serratosa Capdevila L, Javier A, Marin EC, Barth-Maron A, Tamimi IF, Li F, Rubin GM, Plaza SM, Costa M, Jefferis GSXE. 2021. Information flow, cell types and stereotypy in a full olfactory connectome *eLife* **10**:e66018. DOI: https://doi.org/10.7554/eLife.66018

Scott K, Brady R, Cravchik A, Morozov P, Rzhetsky A, Zuker C, Axel R. 2001. A Chemosensory Gene Family Encoding Candidate Gustatory and Olfactory Receptors in *Drosophila Cell* **104**:661–673. DOI: https://doi.org/10.1016/s0092-8674(01)00263-x, PMID: 11257221

Scott K. 2018. Gustatory Processing in *Drosophila melanogaster Annual Review of Entomology* **63**:15–30. DOI: https://doi.org/10.1146/annurev-ento-020117-043331, PMID: 29324046

Seki Y, Dweck HKM, Rybak J, Wicher D, Sachse S, Hansson BS. 2017. Olfactory coding from the periphery to higher brain centers in the *Drosophila* brain. *BMC Biology* **15**:0389-z. DOI: https://doi.org/10.1186/s12915-017-0389-z, PMID: 28666437

Shearin HK, Macdonald IS, Spector LP, Stowers RS. 2014. Hexameric GFP and mCherry reporters for the *Drosophila* GAL4, Q, and LexA transcription systems *Genetics* **196**:951–960. DOI: https://doi.org/10.1534/genetics.113.161141, PMID: 24451596

Siddiqi O. 1987. Neurogenetics of olfaction in *Drosophila melanogaster Trends in Genetics* **3**:137–142. DOI: https://doi.org/10.1016/0168-9525(87)90204-6

Siegal ML, Hartl DL. 1996. Transgene Coplacement and high efficiency site-specific recombination with the Cre/loxP system in *Drosophila Genetics* **144**:715–726. DOI: https://doi.org/10.1093/genetics/144.2.715, PMID: 8889532

Silbering AF, Rytz R, Grosjean Y, Abuin L, Ramdya P, Jefferis GSXE, Benton R. 2011. Complementary function and integrated wiring of the evolutionarily distinct *Drosophila* olfactory subsystems *The Journal of Neuroscience* **31**:13357–13375. DOI: https://doi.org/10.1523/JNEUROSCI.2360-11.2011, PMID: 21940430

Smadja C, Shi P, Butlin RK, Robertson HM. 2009. Large Gene Family Expansions and Adaptive Evolution for Odorant and Gustatory Receptors in the Pea Aphid, Acyrthosiphon pisum *Molecular Biology and Evolution* **26**:2073–2086. DOI: https://doi.org/10.1093/molbev/msp116, PMID: 19542205

Soffan A, Subandiyah S, Makino H, Watanabe T, Horiike T. 2018. Evolutionary Analysis of the Highly Conserved Insect Odorant Coreceptor (Orco) Revealed a Positive Selection Mode, Implying Functional Flexibility. *Journal of Insect Science (Online)* **18**:120. DOI: https://doi.org/10.1093/jisesa/iey120, PMID: 30535416

Spletter ML, Liu J, Liu J, Su H, Giniger E, Komiyama T, Quake S, Luo L. 2007. Lola regulates *Drosophila* olfactory projection neuron identity and targeting specificity. *Neural Development* **2**:14. DOI: https://doi.org/10.1186/1749-8104-2-14, PMID: 17634136

Stengl M. 2010. Pheromone transduction in moths. *Frontiers in Cellular Neuroscience* **4**:133. DOI: https://doi.org/10.3389/fncel.2010.00133, PMID: 21228914

Stensmyr MC, Dweck HKM, Farhan A, Ibba I, Strutz A, Mukunda L, Linz J, Grabe V, Steck K, Lavista-Llanos S, Wicher D, Sachse S, Knaden M, Becher PG, Seki Y, Hansson BS. 2012. A Conserved Dedicated Olfactory Circuit for Detecting Harmful Microbes in *Drosophila Cell* **151**:1345–1357. DOI: https://doi.org/10.1016/j.cell.2012.09.046, PMID: 23217715

Stocker RF. 1994. The organization of the chemosensory system in *Drosophila melanogaster*: a review *Cell and Tissue Research* **275**:3–26. DOI: https://doi.org/10.1007/BF00305372, PMID: 8118845

Stocker RF. 2001. *Drosophila* as a focus in olfactory research: mapping of olfactory sensilla by fine structure, odor specificity, odorant receptor expression, and central connectivity. *Microscopy Research and Technique* **55**:284–296. DOI: https://doi.org/10.1002/jemt.1178, PMID: 11754508

Su CY, Menuz K, Carlson JR. 2009. Olfactory perception: receptors, cells, and circuits *Cell* **139**:45–59. DOI: https://doi.org/10.1016/j.cell.2009.09.015, PMID: 19804753

Tamura K, Nei M. 1993. Estimation of the number of nucleotide substitutions in the control region of mitochondrial DNA in humans and chimpanzees *Molecular Biology and Evolution* **10**:512–526. DOI: https://doi.org/10.1093/oxfordjournals.molbev.a040023, PMID: 8336541

Tamura K, Stecher G, Kumar S. 2021. MEGA11: Molecular Evolutionary Genetics Analysis Version 11 *Molecular Biology and Evolution* **38**:3022–3027. DOI: https://doi.org/10.1093/molbev/msab120, PMID: 33892491

Task D, Lin CC, Vulpe A, Afify A, Ballou S, Brbić M, Schlegel P, Jefferis G, Li H, Menuz K, Potter CJ. 2020. Chemoreceptor Co-Expression in *Drosophila* Olfactory Neurons. *bioRxiv*. DOI: https://doi.org/10.1101/2020.11.07.355651

Task D, Potter CJ. 2021. Rapid degeneration of *Drosophila* olfactory neurons in Orco mutant maxillary palps. *MicroPublication Biology* **14**:000398. DOI: https://doi.org/10.17912/micropub.biology.000398

Thurmond J, Goodman JL, Strelets VB, Attrill H, Gramates LS, Marygold SJ, Matthews BB, Millburn G, Antonazzo G, Trovisco V, Kaufman TC, Calvi BR, FlyBase Consortium. 2019. FlyBase 2.0: the next generation *Nucleic Acids Research* **47**:D759–D765. DOI: https://doi.org/10.1093/nar/gky1003, PMID: 30364959

Trible W, Olivos-Cisneros L, McKenzie SK, Saragosti J, Chang NC, Matthews BJ, Oxley PR, Kronauer DJC. 2017. Orco mutagenesis causes loss of antennal lobe glomeruli and impaired social behavior in ants *Cell* **170**:727-735.. DOI: https://doi.org/10.1016/j.cell.2017.07.001

Van der Maaten L, Hinton G. 2008. Visualizing data using t-SNE. *Journal of Machine Learning Research: JMLR* **9**:2579–2605.

Venkatesh S, Naresh Singh R. 1984. Sensilla on the third antennal segment of *Drosophila melanogaster* meigen (Diptera: Drosophilidae) *International Journal of Insect Morphology and Embryology* **13**:51–63. DOI: https://doi.org/10.1016/0020-7322(84)90032-1

Vilain S, Vanhauwaert R, Maes I, Schoovaerts N, Zhou L, Soukup S, da Cunha R, Lauwers E, Fiers M, Verstreken P. 2014. Fast and efficient *Drosophila melanogaster* gene knock-ins using MiMIC transposons. *G3: Genes, Genomes, Genetics* **4**:2381–2387. DOI: https://doi.org/10.1534/g3.114.014803, PMID: 25298537

Vosshall LB, Amrein H, Morozov PS, Rzhetsky A, Axel R. 1999. A Spatial Map of Olfactory Receptor Expression in the *Drosophila* Antenna *Cell* **96**:725–736. DOI: https://doi.org/10.1016/s0092-8674(00)80582-6, PMID: 10089887

Vosshall LB, Wong AM, Axel R. 2000. An Olfactory Sensory Map in the Fly Brain *Cell* **102**:147–159. DOI: https://doi.org/10.1016/s0092-8674(00)00021-0, PMID: 10943836

Vosshall LB, Stocker RF. 2007. Molecular architecture of smell and taste in *Drosophila Annual Review of Neuroscience* **30**:505–533. DOI: https://doi.org/10.1146/annurev.neuro.30.051606.094306, PMID: 17506643

Vosshall LB, Hansson BS. 2011. A unified nomenclature system for the insect olfactory coreceptor *Chemical Senses* **36**:497–498. DOI: https://doi.org/10.1093/chemse/bjr022, PMID: 21441366

Vulpe A, Kim HS, Ballou S, Wu ST, Grabe V, Nava Gonzales C, Liang T, Sachse S, Jeanne JM, Su CY, Menuz K. 2021. An ammonium transporter is a non-canonical olfactory receptor for ammonia. *Current Biology* **31**:3382–3390. DOI: https://doi.org/10.1016/j.cub.2021.05.025, PMID: 34111404

Vulpe A, Menuz K. 2021. Ir76b is a Co-receptor for Amine Responses in *Drosophila* Olfactory Neurons. *Frontiers in Cellular Neuroscience* **15**:759238. DOI: https://doi.org/10.3389/fncel.2021.759238, PMID: 34867202

Wilson RI. 2013. Early olfactory processing in *Drosophila*: mechanisms and principles *Annual Review of Neuroscience* **36**:217–241. DOI: https://doi.org/10.1146/annurev-neuro-062111-150533, PMID: 23841839

Xie T, Ho MCW, Liu Q, Horiuchi W, Lin CC, Task D, Luan H, White BH, Potter CJ, Wu MN. 2018. A genetic toolkit for dissecting dopamine circuit function in *Drosophila Cell Reports* **23**:652–665. DOI: https://doi.org/10.1016/j.celrep.2018.03.068, PMID: 29642019

Xue Z, Ren M, Wu M, Dai J, Rong YS, Gao G. 2014. Efficient gene knock-out and knock-in with transgenic Cas9 in *Drosophila*. *G3: Genes, Genomes, Genetics* **4**:925–929. DOI: https://doi.org/10.1534/g3.114.010496, PMID: 24657904

Yan H, Opachaloemphan C, Mancini G, Yang H, Gallitto M, Mlejnek J, Leibholz A, Haight K, Ghaninia M, Huo L, Perry M, Slone J, Zhou X, Traficante M, Penick CA, Dolezal K, Gokhale K, Stevens K, Fetter-Pruneda I, Bonasio R, et al. 2017. An Engineered orco Mutation Produces Aberrant Social Behavior and Defective Neural Development in Ants. *Cell* **170**:736–747. DOI: https://doi.org/10.1016/j.cell.2017.06.051, PMID: 28802043

Yan H., Jafari S, Pask G, Zhou X, Reinberg D, Desplan C. 2020. Evolution, developmental expression and function of odorant receptors in insects *The Journal of Experimental Biology* **223**:jeb208215. DOI: https://doi.org/10.1242/jeb.208215, PMID: 32034042

Yao CA, Ignell R, Carlson JR. 2005. Chemosensory Coding by Neurons in the Coeloconic Sensilla of the *Drosophila* Antenna *The Journal of Neuroscience* **25**:8359–8367. DOI: https://doi.org/10.1523/JNEUROSCI.2432-05.2005, PMID: 16162917

Ye Z, Liu F, Sun H, Baker A, Zwiebel LJ. 2021. Discrete Roles of the Ir76b Ionotropic Co-Receptor Impact Olfaction, Blood Feeding, and Mating in the Malaria Vector Mosquito Anopheles Coluzzii. *bioRxiv*. DOI: https://doi.org/10.1101/2021.07.05.451160

Younger MA, Herre M, Goldman OV, Lu TC, Caballero-Vidal G, Qi Y, Gilbert ZN, Gong Z, Morita T, Rahiel S, Ghaninia M, Ignell R, Matthews BJ, Li H, Vosshall LB. 2020. Non-Canonical Odor Coding in the Mosquito. *bioRxiv*. DOI: https://doi.org/10.1101/2020.11.07.368720

Zhang YV, Ni J, Montell C. 2013. The molecular basis for attractive salt-taste coding in *Drosophila Science (New York, N.Y.)* **340**:1334–1338. DOI: https://doi.org/10.1126/science.1234133, PMID: 23766326

Zheng Z, Lauritzen JS, Perlman E, Robinson CG, Nichols M, Milkie D, Torrens O, Price J, Fisher CB, Sharifi N, Calle-Schuler SA, Kmecova L, Ali IJ, Karsh B, Trautman ET, Bogovic JA, Hanslovsky P, Jefferis G, Kazhdan M, Khairy K, et al. 2018. A complete electron microscopy volume of the brain of adult *Drosophila melanogaster Cell* **174**:730–743. DOI: https://doi.org/10.1016/j.cell.2018.06.019, PMID: 30033368

Appendix 1

Appendix 1—key resources table

Reagent type (species) or resource	Designation	Source or reference	Identifiers	Additional information
Antibody	Anti-nc82 (mouse monoclonal)	DSHB	Cat# nc82; RRID:AB_2314866	IHC (1:25)
Antibody	Anti-cd8 (rat monoclonal)	Thermo Fisher Scientific	Cat# 14-0081-82; RRID:AB_467087	IHC (1:100 or 1:200)
Antibody	Anti-elav (rat monoclonal)	DSHB	Cat# Rat-Elav-7E8A10; RRID:AB_528218	IHC (1:100)
Antibody	Anti-Orco (rabbit polyclonal)	Gift from Leslie Vosshall *Larsson et al., 2004*		IHC (1:100)
Antibody	Anti-Ir25a (rabbit polyclonal)	Gift from *Benton et al., 2009*	RRID:AB_2567027	IHC (1:100)
Antibody	Anti-Ir8a (guinea pig polyclonal)	Gift from Richard Benton *Abuin et al., 2011*	RRID:AB_2566833	IHC (1:100 for whole-mount, 1:1000 for cryosections)
Antibody	Anti-Ir64a (rabbit polyclonal)	Gift from Greg Suh *Ai et al., 2010*	RRID:AB_2566854	IHC (1:100)
Antibody	Anti-guinea pig Alexa 568 (goat polyclonal)	Thermo Fisher Scientific	Cat# A11075; RRID:AB_141954	IHC (1:500)
Antibody	Anti-rabbit Cy3 conjugated AffiniPure 568 (goat polyclonal)	Jackson ImmunoResearch	Cat# 111-165-144; RRID:AB_2338006	IHC (1:500)
Antibody	Anti-mouse Cy3 (goat polyclonal)	Jackson ImmunoResearch	Cat# 115-165-166; RRID:AB_2338692	IHC (1:200)
Antibody	Anti-mouse Alexa 647 (goat polyclonal)	Jackson ImmunoResearch	Cat# 115-605-166; RRID:AB_2338914	IHC (1:200)
Antibody	Anti-guinea pig Cy3 (donkey polyclonal)	Jackson ImmunoResearch	Cat# 706-165-148; RRID:AB_2340460	IHC (1:200)
Antibody	Anti-rat Cy3 (goat polyclonal)	Jackson ImmunoResearch	Cat# 112-165-167; RRID:AB_2338251	IHC (1:200)
Antibody	Anti-rat Alexa 647 (goat polyclonal)	Jackson ImmunoResearch	Cat# 112-605-167; RRID:AB_2338404	IHC (1:200)
Antibody	Anti-rabbit Cy3 (goat polyclonal)	Jackson ImmunoResearch	Cat# 111-165-144; RRID:AB_2338006	IHC (1:200)
Antibody	Anti-rabbit Alexa 647 (goat polyclonal)	Jackson ImmunoResearch	Cat# 111-605-144; RRID:AB_2338078	IHC (1:200)
Recombinant DNA reagent	pHACK-QF2 (plasmid)	Addgene *Lin and Potter, 2016a*	Plasmid# 80274; RRID:Addgene_80274	QF2 HACK backbone Contains QF2-hsp70, but no gRNAs
Recombinant DNA reagent	p10XQUAS-CsChrimson-SV40 (plasmid)	This paper	Plasmid# 163629; RRID:Addgene_163629	For red-shifted optogenetic activation of neurons under control of the Q-system; see 'Fly stocks'
Recombinant DNA reagent	pHACK-QF2^{Orco} (plasmid)	This paper		HACK construct targeting the *Orco* gene; see 'Plasmid construction'
Recombinant DNA reagent	pHACK-QF2^{Ir8a} (plasmid)	This paper		HACK construct targeting the *Ir8a* gene; see 'Plasmid construction'
Recombinant DNA reagent	pHACK-QF2^{Ir76b} (plasmid)	This paper		HACK construct targeting the *Ir76b* gene; see 'Plasmid construction'
Recombinant DNA reagent	pHACK-QF2^{Ir25a} (plasmid)	This paper		HACK construct targeting the *Ir25a* gene; see 'Plasmid construction'
Genetic reagent (*Drosophila melanogaster*)	Orco-T2A-QF2 knock-in	This paper	BDSC 92400, 92401, 92402	See 'Generation of HACK knock-in lines'
Genetic reagent (*D. melanogaster*)	Ir8a-T2A-QF2 knock-in	This paper	BDSC 92398, 92399	See 'Generation of HACK knock-in lines'
Genetic reagent (*D. melanogaster*)	Ir76b-T2A-QF2 knock-in	This paper	BDSC 92396, 92397	See 'Generation of HACK knock-in lines'

Appendix 1 Continued on next page

Appendix 1 Continued

Reagent type (species) or resource	Designation	Source or reference	Identifiers	Additional information
Genetic reagent (*D. melanogaster*)	*Ir25a-T2A-QF2 knock-in*	This paper	BDSC 92392, 92393, 92394, 92395	See 'Generation of HACK knock-in lines'
Genetic reagent (*D. melanogaster*)	*10XQUAS-CsChrimson (y[1] w[*]; Pin[1]/ CyO; P(w[+mC] = 10XQUAS-CsChrimson. mVenus)11c)*	This paper	BDSC 91996, FlyBase FBst0091996	See 'Fly stocks'
Genetic reagent (*D. melanogaster*)	*Ir21a-T2A-Gal4 knock-in*	Gift from Paul Garrity **Marin et al., 2020**		
Genetic reagent (*D. melanogaster*)	*Ir68a-T2A-Gal4 knock-in*	Gift from Paul Garrity **Marin et al., 2020**		
Genetic reagent (*D. melanogaster*)	*Or7a-Gal4 knock-in (y[1] w[*] TI(GAL4)Or7a[KI-GAL4.w-])*	Potter lab	BDSC 91991, FlyBase FBti0214362	
Genetic reagent (*D. melanogaster*)	*Ir64a-Gal4*	Gift from Greg Suh lab **Ai et al., 2010**		
Genetic reagent (*D. melanogaster*)	*Rh50-Gal4*	Menuz lab **Vulpe et al., 2021**		
Genetic reagent (*D. melanogaster*)	*Amt-Gal4*	Menuz lab **Menuz et al., 2014**		
Genetic reagent (*D. melanogaster*)	*Repo-Gal80*	**Awasaki et al., 2011**	FlyBase FBtp0067904	
Genetic reagent (*D. melanogaster*)	*wCS (Cantonized w[1118])*	**Koh et al., 2014**	FlyBase FBrf0226011	
Genetic reagent (*D. melanogaster*)	*Or35a-Gal4*	**Yao et al., 2005**		
Genetic reagent (*D. melanogaster*)	*Crey +1B (y[1] w[67c23] P(y[+mDint2] = Crey)1b; sna[Sco]/CyO)*	Bloomington Drosophila Stock Center	BDSC 766, FlyBase FBti0012692	
Genetic reagent (*D. melanogaster*)	*Gr21a-GAL4 (w[*]; P(w[+ mC] = Gr21a-GAL4.9.323)2/CyO; Dr[1]/TM3, Sb[+])*	Bloomington Drosophila Stock Center	BDSC 57600, FlyBase FBti0162643	
Genetic reagent (*D. melanogaster*)	*Gr28b.d-GAL4 (w[*]; P(w[+mC] = Gr28b.d-GAL4)B27; Dr[1]/TM3, Sb[1])*	Bloomington Drosophila Stock Center	BDSC 57620, FlyBase FBst0057620	
Genetic reagent (*D. melanogaster*)	*Ir25a-GAL4 (w[*]; P(w[+ mC] = Ir25a-GAL4.A)236.1; TM2/ TM6B, Tb[1])*	Bloomington Drosophila Stock Center	BDSC 41728, FlyBase FBti0148895	
Genetic reagent (*D. melanogaster*)	*Ir40a-GAL4 (w[*]; P(w[+ mC] = Ir40a-GAL4.3011)214.1; TM2/ TM6B, Tb[1])*	Bloomington Drosophila Stock Center	BDSC 41727, FlyBase FBst0041727	
Genetic reagent (*D. melanogaster*)	*Ir41a-GAL4 (w[*]; P(y[+ t7.7] w[+mC] = Ir41a-GAL4.2474)attP40; TM2/ TM6B, Tb[1])*	Bloomington Drosophila Stock Center	BDSC 41749, FlyBase FBst0041749	
Genetic reagent (*D. melanogaster*)	*Ir64a-GAL4 (w[*]; P(w[+mC] = Ir64a-GAL4.A)183.8; TM2/ TM6B, Tb[1])*	Bloomington Drosophila Stock Center	BDSC 41732, FlyBase FBti0148898	
Genetic reagent (*D. melanogaster*)	*Ir76a-GAL4 (w[*]; P(w[+ mC] = Ir76a-GAL4. PB)292.3B; TM2/TM6B, Tb[1])*	Bloomington Drosophila Stock Center	BDSC 41735, FlyBase FBst0041735	
Genetic reagent (*D. melanogaster*)	*Ir76b-GAL4 (w[*]; P(w[+ mC] = Ir76b-GAL4.916)226.8; TM2/ TM6B, Tb[+])*	Bloomington Drosophila Stock Center	BDSC 41730, FlyBase FBti0153291	

Appendix 1 Continued on next page

Appendix 1 Continued

Reagent type (species) or resource	Designation	Source or reference	Identifiers	Additional information
Genetic reagent (*D. melanogaster*)	Ir8a-GAL4 (w[*]; P(w[+ mC] = Ir8a-GAL4.A)204.8; TM2/TM6B, Tb[1])	Bloomington Drosophila Stock Center	BDSC 41731, FlyBase FBti0148897	
Genetic reagent (*D. melanogaster*)	Or10a-Gal4 (w[*]; l(2)*[*]/CyO; P(w[+ mC] = Or10a-GAL4.C)134t1.3)	Bloomington Drosophila Stock Center	BDSC 23885, FlyBase FBti0102042	
Genetic reagent (*D. melanogaster*)	Or13a-Gal4 (w[*]; P(w[+ mC] = Or13a-GAL4.C)229t56.2/TM3, Sb[1])	Bloomington Drosophila Stock Center	BDSC 23886, FlyBase FBti0102056	
Genetic reagent (*D. melanogaster*)	Or22a-Gal4 (w[*]; P(w[+ mC] = Or22a-GAL4.7.717)14.2)	Bloomington Drosophila Stock Center	BDSC 9951, FlyBase FBti0101805	
Genetic reagent (*D. melanogaster*)	Or22a-Gal4 (w[*]; P(w[+ mC] = Or22a-GAL4.7.717)14.21)	Bloomington Drosophila Stock Center	BDSC 9952, FlyBase FBti0101805	
Genetic reagent (*D. melanogaster*)	Or33c-Gal4 (w[*]; P(w[+ mC] = Or33c-GAL4.F)78.3)	Bloomington Drosophila Stock Center	BDSC 9966, FlyBase FBti0101843	
Genetic reagent (*D. melanogaster*)	Or35a-cd8GFP (w[*]; P(w[+ mC] = Or35a-Mmus\Cd8a.GFP)3/TM3, Sb[1])	Bloomington Drosophila Stock Center	BDSC 52624, FlyBase FBti0156834	
Genetic reagent (*D. melanogaster*)	Or35a-Gal4 (w[*]; P(w[+ mC] = Or35a-GAL4.F)109.2A)	Bloomington Drosophila Stock Center	BDSC 9967, FlyBase FBti0101810	
Genetic reagent (*D. melanogaster*)	Or35a-Gal4 (w[*]; P(w[+ mC] = Or35a-GAL4.F)109.3)	Bloomington Drosophila Stock Center	BDSC 9968, FlyBase FBti0101844	
Genetic reagent (*D. melanogaster*)	Or42a-Gal4 (w[*]; P(w[+ mC] = Or42a-GAL4.F)48.3B)	Bloomington Drosophila Stock Center	BDSC 9970, FlyBase FBti0101811	
Genetic reagent (*D. melanogaster*)	Or42b-Gal4 (w[*]; P(w[+ mC] = Or42b-GAL4.F)64.3)	Bloomington Drosophila Stock Center	BDSC 9971, FlyBase FBti0101812	
Genetic reagent (*D. melanogaster*)	Or43b-Gal4 (w[*]; P(w[+ mC] = Or43b-GAL4.C)110t8.1)	Bloomington Drosophila Stock Center	BDSC 23894, FlyBase FBti0102047	
Genetic reagent (*D. melanogaster*)	Or46a-Gal4 (w[1,118]; P(w[+ mC] = Or46a-GAL4.G)32.1.y)	Bloomington Drosophila Stock Center	BDSC 23291, FlyBase FBti0076800	
Genetic reagent (*D. melanogaster*)	Or47a-Gal4 (w[*]; P(w[+ mC] = Or47a-GAL4.8.239)15.4A)	Bloomington Drosophila Stock Center	BDSC 9982, FlyBase FBti0101851	
Genetic reagent (*D. melanogaster*)	Or49b-Gal4 (w[*]; P(w[+ mC] = Or49b-GAL4.F)80.1)	Bloomington Drosophila Stock Center	BDSC 9986, FlyBase FBti0101853	
Genetic reagent (*D. melanogaster*)	Or59b-Gal4 (w[*]; P(w[+ mC] = Or59b-GAL4.C)114t2.2)	Bloomington Drosophila Stock Center	BDSC 23897, FlyBase FBti0102060	
Genetic reagent (*D. melanogaster*)	Or59c-Gal4 (w[*]; P(w[+ mC] = Or59c-GAL4.C)129t1.1)	Bloomington Drosophila Stock Center	BDSC 23899, FlyBase FBti0102061	
Genetic reagent (*D. melanogaster*)	Or65a-Gal4 (w[*]; Bl[1]/SM1; P(w[+ mC] = Or65a-GAL4.F)72.1)	Bloomington Drosophila Stock Center	BDSC 9994, FlyBase FBti0101857	
Genetic reagent (*D. melanogaster*)	Or67a-Gal4 (w[*]; P(w[+ mC] = Or67a-GAL4.C)137t3.3)	Bloomington Drosophila Stock Center	BDSC 23904, FlyBase FBti0102049	

Appendix 1 Continued on next page

Appendix 1 Continued

Reagent type (species) or resource	Designation	Source or reference	Identifiers	Additional information
Genetic reagent (*D. melanogaster*)	Or67b-Gal4 (w[*]; P(w[+ mC] = Or67b-GAL4.F)68.3/TM6B, Tb[1])	Bloomington Drosophila Stock Center	BDSC 9995, FlyBase FBti0101858	
Genetic reagent (*D. melanogaster*)	Or67c-Gal4 (w[*]; P(w[+ mC] = Or67c-GAL4.C)116t3.2/CyO)	Bloomington Drosophila Stock Center	BDSC 23905, FlyBase FBti0102050	
Genetic reagent (*D. melanogaster*)	Or71a-Gal4 (w[*]; P(w[+ mC] = Or71a-GAL4.F)30.4)	Bloomington Drosophila Stock Center	BDSC 23122, FlyBase FBti0101860	
Genetic reagent (*D. melanogaster*)	Or83c-Gal4 (w[*]; P(w[+ mC] = Or83c-GAL4.F)73.3B)	Bloomington Drosophila Stock Center	BDSC 23131, FlyBase FBti0101829	
Genetic reagent (*D. melanogaster*)	Or85a-Gal4 (w[*]; P(w[+ mC] = Or85a-GAL4.F)67.2)	Bloomington Drosophila Stock Center	BDSC 23133, FlyBase FBti0101830	
Genetic reagent (*D. melanogaster*)	Or85b-Gal4 (w[*]; P(w[+ mC] = Or85b-GAL4.C)179t5.1)	Bloomington Drosophila Stock Center	BDSC 23911, FlyBase FBti0102053	
Genetic reagent (*D. melanogaster*)	Or85d-Gal4 (w[*]; P(w[+ mC] = Or85d-GAL4.C)143t2.1)	Bloomington Drosophila Stock Center	BDSC 24148, FlyBase FBti0102066	
Genetic reagent (*D. melanogaster*)	Or92a-Gal4 (w[*]; P(w[+ mC] = Or92a-GAL4.F)62.1)	Bloomington Drosophila Stock Center	BDSC 23139, FlyBase FBti0101867	
Genetic reagent (*D. melanogaster*)	Or98a-Gal4 (w[*]; P(w[+ mC] = Or98a-GAL4.F)115.1)	Bloomington Drosophila Stock Center	BDSC 23141, FlyBase FBti0101868	
Genetic reagent (*D. melanogaster*)	Orco-Gal4 (w[*]; P(w[+ mC] = Orco-GAL4.W)11.17; TM2/TM6B, Tb[1])	Bloomington Drosophila Stock Center	BDSC 26818, FlyBase FBti0101150	
Genetic reagent (*D. melanogaster*)	QUAS reporter (y[1] w[1,118]; P(w[+ mC] = QUAS-mCD8::GFP.P)5B/TM6B, Tb[1])	Bloomington Drosophila Stock Center	BDSC 30003, FlyBase FBti0129937	
Genetic reagent (*D. melanogaster*)	QUAS reporter (y[1] w[*]; PBac(y[+ mDint2] w[+ mC] = 10XQUAS-6XGFP)VK00018/CyO, P(Wee-P.ph0)Bacc[Wee-P20])	Bloomington Drosophila Stock Center	BDSC 52264, FlyBase FBti0162759	
Genetic reagent (*D. melanogaster*)	UAS reporter (w[*]; P(y[+ t7.7] w[+ mC] = 10XUAS-IVS-mCD8::GFP)attP40)	Bloomington Drosophila Stock Center	BDSC 32186, FlyBase FBti0131963	
Genetic reagent (*D. melanogaster*)	UAS reporter (w[*]; P(y[+ t7.7] w[+ mC] = 15XUAS-IVS-mCD8::GFP)attP2)	Bloomington Drosophila Stock Center	BDSC 32193, FlyBase FBti0131935	
Genetic reagent (*D. melanogaster*)	UAS reporter (w[*]; P(y[+ t7.7] w[+ mC] = 10XUAS-IVS-mCD8::RFP)attP2)	Bloomington Drosophila Stock Center	BDSC 32218, FlyBase FBti0131950	
Genetic reagent (*D. melanogaster*)	UAS reporter (w[*]; P(y[+ t7.7] w[+ mC] = 10XUAS-IVS-mCD8::RFP)attP40)	Bloomington Drosophila Stock Center	BDSC 32219, FlyBase FBti0131967	
Genetic reagent (*D. melanogaster*)	UAS reporter (y[1] w[*]; PBac(y[+ mDint2] w[+ mC] = 20XUAS-6XGFP)VK00018/CyO, P(Wee-P.ph0)Bacc[Wee-P20])	Bloomington Drosophila Stock Center	BDSC 52261, FlyBase FBti0162758	

Appendix 1 Continued on next page

Appendix 1 Continued

Reagent type (species) or resource	Designation	Source or reference	Identifiers	Additional information
Genetic reagent (*D. melanogaster*)	*UAS* reporter, sacculus experiments (*UAS-mCD8::GFP (2nd)*)	*Lee and Luo, 1999*	FlyBase FBti0012685	
Genetic reagent (*D. melanogaster*)	*UAS* reporter, sacculus experiments (*UAS-mCD8::GFP (3rd)*)	*Lee and Luo, 1999*	FlyBase FBti0012686	
Genetic reagent (*D. melanogaster*)	*Orco²* mutant (*w[*]; TI(w[+ m*] = TI)Orco[2]*)	Bloomington Drosophila Stock Center	BDSC 23130, FlyBase FBti0168777	
Genetic reagent (*D. melanogaster*)	*Ir25a²* mutant (*w[*]; TI(w[+ m*] = TI)Ir25a[2]/CyO*)	Bloomington Drosophila Stock Center	BDSC 41737, FlyBase FBti0168524	
Genetic reagent (*D. melanogaster*)	*Ir8a¹* mutant (*w[*] TI(w[+ mW.hs] = TI)Ir8a[1]; Bl[1] L[2]/CyO*)	Bloomington Drosophila Stock Center	BDSC 41744, FlyBase FBst0041744	
Genetic reagent (*D. melanogaster*)	*Ir76b¹* mutant (*w[*]; Ir76b[1]*)	Bloomington Drosophila Stock Center	BDSC 51309, FlyBase FBst0051309	
Genetic reagent (*D. melanogaster*)	Germline *Cas9* (*y[1] M(RFP[3xP3.PB] GFP[E.3xP3] = vas-Cas9) ZH-2A w[1,118]/FM7c*)	Bloomington Drosophila Stock Center	BDSC 51323, FlyBase FBti0154823	
Genetic reagent (*D. melanogaster*)	Germline *Cas9* (*w[1,118]; PBac(y[+ mDint2] = vas-Cas9) VK00027*)	Bloomington Drosophila Stock Center	BDSC 51324, FlyBase FBti0154822	
Genetic reagent (*D. melanogaster*)	Germline *Cas9* (*y[1] M(w[+ mC] = Act5C-Cas9.P)ZH-2A w[*]*)	Bloomington Drosophila Stock Center	BDSC 54590, FlyBase FBti0159182	
Genetic reagent (*D. melanogaster*)	Double balancer (*19ADrok/FM7c; Pin/CyO*)	Potter lab stock	Derived from BDSC 6666, FBba0000009, FBal0013831, FBba0000025	
Genetic reagent (*D. melanogaster*)	Double balancer (*y,w; Pin/CyO; Dh/TM6B*)	Potter lab stock	Derived from FBal0013831, FBba0000025, FBti0004009, FBba0000057, FBal0016730	
Genetic reagent (*D. melanogaster*)	Double balancer (*y,w; S/CyO; Pr/TM6B*)	Potter lab stock	Derived from FBal0015108, FBba0000025, FBal0013944, FBba0000057, FBal0016730	
Genetic reagent (*D. melanogaster*)	Single balancer (*y,w; +/+; Pr/TM6B*)	Potter lab stock	Derived from FBal0013944, FBba0000057, FBal0016730	
Genetic reagent (*D. melanogaster*)	Single balancer (*y,w; S/CyO; +/+*)	Potter lab stock	Derived from FBal0015108, FBba0000025	
Genetic reagent (*D. melanogaster*)	Wildtype (*w1118 IsoD1*)	Gift from Thomas R. Clandinin	Derived from FBal0018186	
Genetic reagent (*Drosophila sechellia*)	*Wildtype*, genome Cousin Island, Seychelles	National *Drosophila* Species Stock Center	SKU:14021-0248.25	
Genetic reagent (*Anopheles coluzzii*)	*Wildtype*, N'Gousso strain	Gift from Insect Transformation Facility (Rockville, MD) *Riabinina et al., 2016*		
Chemical compound, drug	Mineral oil	Sigma-Aldrich	CAS# 8042-47-5, Cat# 330779-1L	

Appendix 1 Continued on next page

Appendix 1 Continued

Reagent type (species) or resource	Designation	Source or reference	Identifiers	Additional information
Chemical compound, drug	Ethyl acetate	Sigma-Aldrich	CAS# 141-78-6, Cat# 650528-1L, Cat# 270989-100ML	
Chemical compound, drug	Pentyl acetate	Sigma-Aldrich	CAS# 628-63-7, Cat# 109584-250ML	
Chemical compound, drug	Benzaldehyde	Sigma-Aldrich	CAS# 100-52-7, Cat# 418099-100ML, Cat# B1334-100G	
Chemical compound, drug	Ethyl butyrate	Sigma-Aldrich	CAS# 105-54-4, Cat# E15701-500M, Cat# E15701-25ML	
Chemical compound, drug	Hexanol	Sigma-Aldrich	CAS# 111-27-3, Cat# H13303-100ML	
Chemical compound, drug	E2-hexenal	Sigma-Aldrich	CAS# 6728-26-3, Cat# W256005-1KG-K	
Chemical compound, drug	Geranyl acetate	Sigma-Aldrich	CAS# 105-87-3, Cat# 173495-25G, Cat# 45896-1ML-F	
Chemical compound, drug	2-Heptanone	Sigma-Aldrich	CAS# 110-43-0, Cat# 537683-100ML	
Chemical compound, drug	1-Octen-3-ol	Sigma-Aldrich	CAS# 3391-86-4, Cat# O5284-25G, Cat# W280518-SAMPLE-K	
Chemical compound, drug	2,3-Butanedione	Sigma-Aldrich	CAS# 431-03-8, Cat# 11038-1ML-F	
Chemical compound, drug	Phenylacetaldehyde	Sigma-Aldrich	CAS# 122-78-1, Cat# 107395-100ML	
Chemical compound, drug	Phenethylamine	Sigma-Aldrich	CAS# 64-04-0, Cat# 241008-50ML	
Chemical compound, drug	Propionic acid	Sigma-Aldrich	CAS# 79-09-4, Cat# 402907-100ML	
Chemical compound, drug	1,4-Diaminobutane	Sigma-Aldrich	CAS# 110-60-1, Cat# D13208-100G	
Chemical compound, drug	Pyrrolidine	Sigma-Aldrich	CAS# 123-75-1, Cat# P73803-100ML, Cat# P73803-5ML	
Chemical compound, drug	P-cresol	Sigma-Aldrich	CAS# 106-44-5, Cat# 42429-5G-F, Cat# C85751-5G	
Chemical compound, drug	Methyl salicylate	Sigma-Aldrich	CAS# 119-36-8, Cat# M6752-250ML	
Chemical compound, drug	Paraffin Oil	ACROS Organics	CAS# 8012-95-1, Cat# 171400010	
Chemical compound, drug	Water	SIGMA Life Science	CAS# 7732-18-5, Cat# W3500	
Chemical compound, drug	Acetic acid	Fisher Scientific	CAS# 64-19-7, Cat# A38S	
Chemical compound, drug	Ammonium hydroxide	Fisher Scientific	CAS# 7664-41-7, Cat# A669S	
Chemical compound, drug	Cadaverine	Sigma-Aldrich	CAS# 462-94-2, Cat# 33211-10ML-F	
Chemical compound, drug	Hexanol	ACROS Organics	CAS# 111-27-3, Cat# AC43386	
Chemical compound, drug	2,3-Butanedione	ACROS Organics	CAS# 431-03-8, Cat# AC10765	
Chemical compound, drug	Phenethylamine	ACROS Organics	CAS# 64-04-0, Cat# AC156491000	

Appendix 1 Continued on next page

Appendix 1 Continued

Reagent type (species) or resource	Designation	Source or reference	Identifiers	Additional information
Chemical compound, drug	Propanal	ACROS Organics	CAS# 123-38-6, Cat# AC220511000	
Chemical compound, drug	1,4-Diaminobutane	ACROS Organics	CAS# 110-60-1, Cat# AC11212-250	
Chemical compound, drug	All trans-retinal	Sigma-Aldrich	CAS# 116-31-4, Cat# R2500	
Commercial assay or kit	HCR v3.0	Molecular Instruments		
Commercial assay or kit	In-Fusion Cloning	Clontech Labs	Cat# 639645	
Commercial assay or kit	DNeasy Blood and Tissue Kit	QIAGEN	Cat# 69506	
Software, algorithm	Fiji (ImageJ)	*Schindelin et al., 2012*	https://imagej.net/Fiji	
Software, algorithm	GraphPad Prism 8.0	GraphPad Software	http://www.graphpad.com/	
Software, algorithm	AutoSpike	Syntech	http://www.ockenfels-syntech.com/products/signal-acquisition-systems-2/	
Software, algorithm	LabChart Pro v8	ADInstruments	https://www.adinstruments.com/support/downloads/windows/labchart	
Software, algorithm	Adobe Illustrator CS6	Adobe, Inc	https://www.adobe.com/products/illustrator.html	
Software, algorithm	Adobe Photoshop CS6	Adobe, Inc	https://www.adobe.com/products/photoshop.html	
Software, algorithm	MacVector 16.0	MacVector, Inc	https://macvector.com/	
Software, algorithm	MEGA11	*Tamura et al., 2021*	https://www.megasoftware.net/	
Software, algorithm	Zen Black	Carl Zeiss Microscopy	https://www.zeiss.com/microscopy/us/products/microscope-software/zen.html	
Software, algorithm	Venn Diagram web tool	VIB/UGent Bioinformatics & Evolutionary Genomics	http://bioinformatics.psb.ugent.be/webtools/Venn/	
Software, algorithm	Amira	Thermo Fisher Scientific	https://www.thermofisher.com/us/en/home/industrial/electron-microscopy/electron-microscopy-instruments-workflow-solutions/3d-visualization-analysis-software/amira-life-sciences-biomedical.html	
Software, algorithm	Python packages	*Schlegel et al., 2021*	https://github.com/schlegelp/navis, https://github.com/flyconnectome/fafbseg-py	
Software, algorithm	Q-Capture Pro 7	Teledyne QImaging	https://www.qimaging.com/home	

Appendix 1 Continued on next page

Appendix 1 Continued

Reagent type (species) or resource	Designation	Source or reference	Identifiers	Additional information
Other	DAPI stain	Invitrogen	D1306	IHC (1:10,000)
Sequence-based reagent	Orco_gRNA_FOR	This paper, Integrated DNA Technologies	PCR primers	TCCGGGTGAACT TCGCACAGTGCG GAGGGGGCAAG TTTTAGAGCT AGAAATAGCAAGTTA
Sequence-based reagent	Orco_gRNA_REV	This paper, Integrated DNA Technologies	PCR primers	TTCTAGCTCTAAAAC ACTTTATGGTGCT GGTGCAGCGACGTTA AATTGAAAATAGGTC
Sequence-based reagent	Orco_5HA_FOR	This paper, Integrated DNA Technologies	PCR primers	CCCTTACGTAACGCGTCAGCTT GTTTGACTTACTTGATTAC
Sequence-based reagent	Orco_5HA_REV	This paper, Integrated DNA Technologies	PCR primers	CGCGGCCCTCACGCGTCTTGA GCTGTACAAGTACCATAAAGT
Sequence-based reagent	Orco_3HA_FOR	This paper, Integrated DNA Technologies	PCR primers	GTTATAGATCACTAGTCTCAG TACTATGCAACCAGCAATA
Sequence-based reagent	Orco_3HA_REV	This paper, Integrated DNA Technologies	PCR primers	AATTCAGATCACTAGTGTTTT ATGAAAGCTGCAAGAAATAA
Sequence-based reagent	Ir8a_gRNA_FOR	This paper, Integrated DNA Technologies	PCR primers	TCCGGGTGAACTTCGTTTGT TTGTTCGGCCATGTGTTTTAG AGCTAGAAATAGCAAGTTA
Sequence-based reagent	Ir8a_gRNA_REV	This paper, Integrated DNA Technologies	PCR primers	TTCTAGCTCTAAAACCTGTGG GAGTCAGAGGCACCGACGT TAAATTGAAAATAGGTC
Sequence-based reagent	Ir8a_5HA_FOR	This paper, Integrated DNA Technologies	PCR primers	CCCTTACGTAACGCGtCTATT GGCTATTCGTCGTACTCATGC
Sequence-based reagent	Ir8a_5HA_REV	This paper, Integrated DNA Technologies	PCR primers	CGCGGCCCTCACGCGtCTCCA TGTAGCCACTATGTGAGTCAGAT
Sequence-based reagent	Ir8a_3HA_FOR	This paper, Integrated DNA Technologies	PCR primers	GTTATAGATCACTAGtGTTTCTT GTCGCACCTAATTAACAAGTG
Sequence-based reagent	Ir8a_3HA_REV	This paper, Integrated DNA Technologies	PCR primers	AATTCAGATCACTAGtCATAC TTAAGCTCCTTGAGGTCCAGC
Sequence-based reagent	Ir76b_gRNA_FOR	This paper, Integrated DNA Technologies	PCR primers	TCCGGGTGAACTTCGCAGT GATGCGAACTTCATAGTTTT AGAGCTAGAAATAGCAAGTTA
Sequence-based reagent	Ir76b_gRNA_REV	This paper, Integrated DNA Technologies	PCR primers	TTCTAGCTCTAAAACCGGCG GCCCTCTTTCAATACGACG TTAAATTGAAAATAGGTC
Sequence-based reagent	Ir76b_5HA_FOR	This paper, Integrated DNA Technologies	PCR primers	CCCTTACGTAACGCGtACCAATG AATCCTTGTCCATGCTAAA
Sequence-based reagent	Ir76b_5HA_REV	This paper, Integrated DNA Technologies	PCR primers	CGCGGCCCTCACGCGtCTC GGTGTAGCTGTCTTGAAGGAA
Sequence-based reagent	Ir76b_3HA_FOR	This paper, Integrated DNA Technologies	PCR primers	GTTATAGATC ACTAGtGCCTA ATTGGAATACC TTCTACATAATGGA
Sequence-based reagent	Ir76b_3HA_REV	This paper, Integrated DNA Technologies	PCR primers	AATTCAGATCACTAGtGGCAA GGCACAAAATAAAACGAAG
Sequence-based reagent	Ir25a_gRNA_FOR	This paper, Integrated DNA Technologies	PCR primers	TCCGGGTGAACTTCGCCGGA TACTGATTAAAGCGGTTTTA GAGCTAGAAATAGCAAGTTA
Sequence-based reagent	Ir25a_gRNA_REV	This paper, Integrated DNA Technologies	PCR primers	TTCTAGCTCTAAAACAGTG CTCATTTTACCATAATCGA CGTTAAATTGAAAATAGGTC
Sequence-based reagent	Ir25a_5HA_FOR	This paper, Integrated DNA Technologies	PCR primers	CCCTTACGTAACGCGtTGC ATGACTTCATTGACACCTCAAG
Sequence-based reagent	Ir25a_5HA_REV	This paper, Integrated DNA Technologies	PCR primers	CGCGGCCCTCACGCGtGAA ACGAGGCTTAAACGTAGCTGGATATT

Appendix 1 Continued on next page

Appendix 1 Continued

Reagent type (species) or resource	Designation	Source or reference	Identifiers	Additional information
Sequence-based reagent	Ir25a_3HA_FOR	This paper, Integrated DNA Technologies	PCR primers	GTTATAGATCACTAGtAATAT TATGGTTAAGTGAGCTCTCGG
Sequence-based reagent	Ir25a_3HA_REV	This paper, Integrated DNA Technologies	PCR primers	AATTCAGATCACTAGtCAAA GCTAAGTTCATCGTCATAGAGAC
Sequence-based reagent	Orco_Seq_FOR	This paper, Integrated DNA Technologies	PCR primers	GATGTTCTGCTCTTGGCTGATATTC
Sequence-based reagent	Ir8a_Seq_FOR	This paper, Integrated DNA Technologies	PCR primers	CATCGACTTCATCATCAGGCTTTCG
Sequence-based reagent	Ir76b_Seq_FOR	This paper, Integrated DNA Technologies	PCR primers	CAACGATATCCTCACGAAGAACAAGC
Sequence-based reagent	Ir25a_Seq_FOR	This paper, Integrated DNA Technologies	PCR primers	CGAAAGGATACAAAGGATACTGCAT
Sequence-based reagent	HACK_Seq_REV	This paper, Integrated DNA Technologies	PCR primers	TGTATTCCGTCGCATTTCTCTC
Sequence-based reagent	IVS-FOR	This paper, Integrated DNA Technologies	PCR primers	TGGGTTGGACTCAGGGAATA GATCTAAAAGGTAGGTTCAACCACT
Sequence-based reagent	EcoRI-SV40-REV	This paper, Integrated DNA Technologies	PCR primers	GCTTACGTCAGAATTCAGA TCGATCCAGACATGATAAGA
Sequence-based reagent	Tsp42Ej_FOR	This paper, Integrated DNA Technologies	PCR primers	GAGAAGTCGTTTCCCATAACACCCT
Sequence-based reagent	Tsp42Ej_REV	This paper, Integrated DNA Technologies	PCR primers	GAGGAGCAGTTTTCGGAGTCGCCTTC
Sequence-based reagent	*D. melanogaster Orco*	This paper, Molecular Instruments	RNA in situ HCR probe set	See Appendix 2 'In situ probe sequences'
Sequence-based reagent	*D. melanogaster Ir25a*	This paper, Molecular Instruments	RNA in situ HCR probe set	See Appendix 2 'In situ probe sequences'
Sequence-based reagent	*D. melanogaster Ir40a*	This paper, Molecular Instruments	RNA in situ HCR probe set	See Appendix 2 'In situ probe sequences'
Sequence-based reagent	*D. melanogaster Ir51a*	This paper, Molecular Instruments	RNA in situ HCR probe set	See Appendix 2 'In situ probe sequences'
Sequence-based reagent	*D. melanogaster Ir60a*	This paper, Molecular Instruments	RNA in situ HCR probe set	See Appendix 2 'In situ probe sequences'
Sequence-based reagent	*D. melanogaster Ir62a*	This paper, Molecular Instruments	RNA in situ HCR probe set	See Appendix 2 'In situ probe sequences'
Sequence-based reagent	*D. melanogaster Ir76a*	This paper, Molecular Instruments	RNA in situ HCR probe set	See Appendix 2 'In situ probe sequences'
Sequence-based reagent	*D. melanogaster Ir76b*	This paper, Molecular Instruments	RNA in situ HCR probe set	See Appendix 2 'In situ probe sequences'
Sequence-based reagent	*D. melanogaster Ir93a*	This paper, Molecular Instruments	RNA in situ HCR probe set	See Appendix 2 'In situ probe sequences'
Sequence-based reagent	*Anopheles coluzzii Orco*	This paper, Molecular Instruments	RNA in situ HCR probe set	See Appendix 2 'In situ probe sequences'
Sequence-based reagent	*A. coluzzii Ir25a*	This paper, Molecular Instruments	RNA in situ HCR probe set	See Appendix 2 'In situ probe sequences'

Appendix 2

In situ probe sequences

The following coding sequences (no introns or UTRs) from FlyBase were used by Molecular Instruments, Inc (Los Angeles, California) to produce custom probe sets:

Antenna

Ir76b (1911 bp; Probe set ID PRH997)

AUGGCCACUGGCAUCGAGCUGCUGGUGGCCGCCGCCCUCUGUGUCGCCUGUCCGCC
GCUGAACGAUUCCCCGCCGACGAACCUAAUCCAAAUGGGCGAGAAUGGCACUCUUU
CCCCGGUCACCGAGCUGCCCAUGGAUGUGGACGCAUCGGAAGCUGGAUUCGAUGCG
GAUGCCCCCGUGGAGACGCUGGAGACCAUUAACAGGAAGAAGCCGAAGCUGCGGGA
GAUGCUCGAUUGGAUCGGCGGCAAGCACCUGCGCAUCGCUACCCUGGAGGACUUUC
CGCUCAGCUACACCGAGGUCCUGGAGAACGGCACCCGUGUGGGGCACGGAGUCUCC
UUUCAGAUCAUCGACUUCCUCAAGAAGAAGUUCAACUUCACCUAUGAAGUGGUCGU
GCCCCAAGAUAACAUCAUCGGCUCGCCUAGCGACUUUGAUCGCAGUCUCAUCGAGA
UGGUAAACAGCAGUACGGUGGACUUGGCGGCGGCCUUCAUACCCUCGCUCUCUGAC
CAGCGCAGCUUCGUCUACUACUCCACAACGACGCUGGACGAGGGCGAAUGGAUAAU
GGUGAUGCAGCGUCCCCGCGAGUCGGCUAGUGGGUCCGGACUGCUUGCGCCCUUCG
AGUUCGGGGUGUGGAUCCUGAUCCUCGUCUCGCUGCUGGCCGUGGGGCCGAUCAUC
UACGCGCUGAUCAUCCUGCGAAAUCGGCUGACCGGCGACGGCCAGCAGACGCCCUA
CUCCCUGGGCCACUGCGCUUGGUUCGUCUACGGAGCGCUGAUGAAGCAGGGCAGCA
CCCUGUCGCCCAUUGCAGACUCGACGCGGCUGCUCUUUGCCACCUGGUGGAUUUUC
AUCACGAUACUGACGUCCUUCUACACGGCCAACUUGACCGCCUUCCUGACCCUUUC
CAAGUUCACGCUGCCGUACAACACGGUCAACGAUAUCCUCACGAAGAACAAGCACU
UUGUGUCCAUGCGGGGCGGUGGAGUGGAGUACGCCAUUCGAACGACCAAUGAAUCC
UUGUCCAUGCUAAACCGAAUGAUCCAGAACAACUACGCCGUAUUCUCGGACGAGAC
CAACGACACCUACAAUCUGCAGAACUACGUGGAAAAGAAUGGCUAUGUUUUUGUGA
GGGAUCGGCCGGCGAUAAACAUAAUGUUGUACAGGGACUACCUGUACCGCAAAACC
GUGAGCUUUAGCGACGAGAAGGUCCACUGUCCGUUUGCCAUGGCCAAGGAGCCGUU
CCUGAAGAAGAAGAGGACCUUUGCCUAUCCCAUCGGAUCGAAUUUGAGCCAAUUAU
UUGACCCGGAGCUGCUACACCUGGUGGAAUCUGGAAUCGUGAAGCACCUGUCUAAG
AGAAAUCUGCCCAGUGCCGAGAUCUGUCCGCAGGAUCUCGGCGGAACGGAGCGGCA
GCUGAGGAACGGCGACCUAAUGAUGACCUACUACAUCAUGCUUGCCGGUUUCGCCA
CCGCACUGGCCGUCUUCAGCACGGAGCUAAUGUUCCGGUACGUCAAUAGUCGCCAG
GAGGCGAAUAAGUGGGCGCGCCACGGAAUCGGACGAACGCCCAACGGCCAGUCGGU
GGCUCCAUCCCGGUGGCUCCGUGGCUGGAGGCGAUUGAACAGUGGACAUGGGCAGC
UCCUGGGCGCCUCCACCCACGGCCAAAAUGUCACUCCUCCGCCGCCGUACCAGAGC
AUCUUCAACGGCGGCAGUCACGGAGAUCCACUGAAUCGCUGGCGACGUCCCCUCGC
AAACGGAAACGCCCUUGGCAAUGGUGUCCUCCUGGGCGGCGAUUCUGAAGGUGGUG
UACGGCGCCUGAUCAACGGACGCGACUACAUGGUAUUCCGCAAUCCAAAUGGUCAA
AGCCAGCUCGUGCCGGUUAGAUCGCCCUCGGCGGCCCUCUUUCAAUACAGCUACAC
UGAGUAG

PALP

Ir40a (2203 bp; Probe set ID PRH239)

AUGCAUAAGUUUCUGGCAUUGGGCCUGCUGCCCUACCUUUUGGGAUUGCUAAACAG
CACAAGGCUGACUUUUAUUGGUAACGAUGAGUCAGACACUGCAAUAGCGCUCACCC
AAAUUGUAAGAGGCUUGCAACAAUCUUCUCUUGCCAUAUUGGCGCUACCAAGCCUC
GCUCUAUCUGAUGGAGUUUGCCAGAAAGAGCGCAACGUUUAUCUUGACGAUUUUCU
GCAGCGUCUUCAUCGCAGUAACUACAAGUCGGUGGUAUUCAGCCAGACGGAGCUCU
UUUUUCAACACAUUGAGGAAAACCUUCAAGGUGCAAACGAGUGCAUCAGCCUGAUU
UUGGACGAGCCCAACCAGCUGUUGAAUAGCCUCCACGAUCGACAUCUCGGACAUCG
CUUAAGCCUAUUUAUUUUCUAUUGGGGAGCACGCUGGCCACCCAGCUCCCGUGUAA
UUCGUUUUAGAGAGCCGCUUCGAGUGGUAGUCGUAACUCGUCCUCGCAAGAAGGCC
UUCCGCAUUUACUACAACCAGGCUAGACCCUGUAGCGACAGUCAGCUACAGUUGGU
UAAUUGGUACGACGGCGAUAACCUUGGUCUGCAACGAAUUCCCCUCCUCCCGACUG
CAUUAUCCGUGUACGCCAACUUUAAAGGUCGUACCUUUCGGGUGCCCGUAUUUCAU
UCUCCGCCGUGGUUUUGGGUAACGUAUUGCAAUAACAGCUUCGAAGAGGACGAGGA
GUUUAACAGCCUAGACAGCAUAGAGAAGAGAAAGGUUCGGGUCACUGGUGGCCGCG

AUCACCGCCUACUCAUGCUGCUAUCUAAGCAUAUGAACUUUCGGUUUAAGUAUAUC
GAAGCACCCGGUCGAACCCAGGGCUCAAUGAGGUCAGAAGAUGGCAAGGAUUCGAA
CGACAGUUUCACAGGGGGCAUUGGAUUGCUGCAAAGUGGACAAGCUGACUUUUUUU
UGGGAGAUGUCGGUCUAAGCUGGGAACGGCGGAAGGCCAUCGAGUUCUCUUUUUUC
ACACUGGCUGAUUCAGGAGCGUUUGCUACACACGCUCCCAGACGCCUUAAUGAGGC
CCUGGCGAUUAUGCGCCCGUUUAAGCAAGACAUCUGGCCCCAUCUAAUCCUUACGA
UAAUUUUCUCCGGCCCUAUUUUUUAUGGCAUUAUUGCCCUGCCUUAUAUUUGGCGU
CGACGAUGGGCGAACUCAGAUGUUGAACAUCUCGGAGAAUUAUAUAUCCAUAUGAC
GUACUUAAAAGAGAUAACCCCACGCUUAUUAAAGCUCAAACCCAGAACUGUGCUGU
CUGCCCACCAGAUGCCCCAUCAACUUUUUCAGAAGUGCAUAUGGUUCACUUUACGU
CUGUUUUUAAAACAAUAUGGCAUGCAAUGAACUACAUAACGGAUACCGAGCCAAGU
UUUUGACCAUAGUGUAUUGGAUAGCAGCGACCUAUGUUUUGGCCGAUGUAUAUUCA
GCUCAACUGACCAGCCAAUUUGCACGUCCAGCUCGCGAGCCACCAAUCAAUACUCU
UCAGCGCCUGCAAGCAGCGAUGAUUCAUGACGGUUACCGGCUAUAUGUGGAGAAGG
AAAGCAGUUCAUUGGAGAUGUUGGAGAAUGGGACAGAACUGUUUCGUCAGCUUUAU
GCUCUGAUGAGGCAGCAGGUGAUCAAUGACCCUCAAGGAUUUUUUAUUGACUCUGU
GGAAGCGGGAAUUAAACUAAUUGCAGAGGGCGGCGAGGACAAGGCAGUACUCGGAG
GGCGUGAAACACUGUUUUUCAACGUUCAGCAAUACGGAUCAAACAACUUUCAGCUC
AGUCAAAAACUUUACACUCGUUAUUCGGCUGUGGCUGUUCAAAUCGGAUGUCCCUU
UCUAGGUAGCCUCAAUAAUGUCUUGAUGCAGUUGUUUGAGAGCGGAAUCCUAGAUA
AGAUGACCGCUGCCGAAUACGCAAAGCAGUACCAGGAGGUAGAAGCCACGAGAAUA
UACAAGGGCAGCGUGCAGGCGAAAAACAGUGAGGCUUACAGUCGAACCGAAAGCUA
UGACAGCACGGUUAUCAGUCCGCUUAAUCUACGAAUGCUGCAGGGCGCUUUUAUCG
CUCUCGGAGUUGGUUCAUUGGCUGCAGGUGUAAUUUUGCUGUUAGAGAUAGUAUUU
AUAAAACUGGAUCAAGCGCGCGAUUGUGGAUGCUGUGCUCACGGCUGCAAUGGAUUAG
AUAUGACAGGAAAGUGUAA

Ir51a (1830 bp; Probe set ID PRD951) – sequence derived from Potter lab *wildtype* strain, which has no predicted premature stop codons.

AUGCAAGGAUUUCAAGAAGCCAAUGCACAGUUAACCACCAUGUACAACGUUCUGGUAUUG
UUCCUAUUGCUUUUCACUCGUGCCCAGAUGGAACCCCAUAGAAGAGGUCACAACAUGACU
UUGCUGAGAUCGGUGCUGACAGUCAUCCGCGGCAGGGAGAAUUGGAAAAAUACCCC
CAUCUUCUUAGGCGGACAUUGUAAUUCGGAUGACCUGAAUAACUUGAUGAGUUGGC
UUCAAAAUACGAUGGAAGUAACUUGUCAUACGGUGGAUACAUCUACUUCAGCCAAAAACG
AAAACGCUCUGGGUCACUUUAACAUAAAUGCGGAUAAUUCGCUUGGUUUGUUGUUUUGCC
AAAGCUCCCAUGAAUUGAUUUGGUUUAAUAUGGAUAAGAGACUUCGGCGAUUACGU
GGUAUUCGCCUUAUUGUGAUUCUAUCAGACAAACGAAGUUCAUCCAGCAAAGCUAUAAUG
AGCACGUUUAAGAGACUGUGGCACUUUCAGUUCCUCAGAGUUCUUGUUCUGCACAG
AGAUCAGAUUUAUUCGUAUACUCCUUAUCCAGUCAUUCGAUUCUUUAAGCUUGAUAGUGA
CGUCUAUCCGCUUUUCCCACCGAGUGCAAAAAAUUUCCAAGGCUAUGUGGUGUCUACCCC
AGUGGAAAACGACAUUCCGCGAGUGUUUUUCGUGAAGGACAAGAAAACCGGACGCA
AGCAGAUCAGAGGAUUUGGAUAUCGCACAUUUGUGGAGUACCUGCAUCGCUACAAU
GCCUCUUUACAUGUCAGUAAUUCUCAGCAGGAGCAUGCCAUCAACAGCAGCGUGAAUAUG
GGUCGGAUAAUUAAUCAGAUUGUGGAUGGCCAAUUAGAAAUCUCCCUGCAUCCGUA
UGUAGACGUUCCGGAAAAUAUGGGAGAUAACAGUUAUCCCCUUCUAAUAGCUAGCAAUUG
UCUUAUUGUUCCGGUCAGGAACGAGAUAUCUCGCUACAUGUAUCUACUAUUGCCUCUCAA
CCAAUCAAGCUGGAUACUACUGCUCGGUUCUGUAAUUUAUAUCAGCGGAGUGCUCUACUA
CAUUCAGCCUGGUCUGCUGCACCGCACCUGGGAUCAGCGGAUUGGCCUCAACAUCC
UAGAUAGCAUCAGCCGAAUAAUUAAUAUAUGCUCUCCCUCCAGGAUUUACAACCCAUCCC
UGAGGUAUUUUAUAGUUUCGGUGCACCUUAGUAUUCUGGGCUUUGUGGUGACCAAC
CUCUACAGCAUUAUGUUGGGCAGCUUCUUCACCACCUUGGUAGUGGGCGAGCAGGU
GGACAGCAUGCAGCAGCUCAUCCAGCAACAGCAAAAGGUACUUGUAAAAUAUUACGAAGU
CAGUACAUUCUUACGGCAUGUGGAACCAGAUUUGGUGGACGGAGUAGCGCAACUAU
UAGUGGGCGUGAAUGCCAGUGAGCAGGUGUCCGCUCUUCGGGAUUCAAUCGGAGC
UAUGCCUACCCCUUCACCCUGGAGAGAUGGGAGUUCUUCUCACUACAACAGCAAUACGCC
UUCAAGCCAAUCUUCAGAUUCUCAUCGGCAUGCCUGGGCUCCCCGAUUAUAGGCUAUCCC
AUGAAAAGUGACUGCCACCUGCAGUCGUCAUUGAACAUGUUCAUCAUGCGGAUCCA
GGCCGCAGGACUUCUGCGGCACUGGGUAGUAUCCGAUUUUAACGAUGCAAUGCGCG
CUGGCUAUGUUCGACUUCUGGAAAACUUCCUAGGAUUUCACUCGUUAGAUGUCGAUUCCU
UGCGCCUGGGGGUGGGCAGUACUCCUAUGUGGGUGGCUGCUAUCCACCUUGAUUUUUU
CUUUGCGAGCGCUGGCGCUUUUUACCACUAA

Ir60a (2151 bp; Probe set ID PRD952)

AUGUGGUGUAAUAAUCCGGGUCUCAUCAUCAUCAUCUUUCUGGGGGCAGAUUUUAAA
CCUGUGCCAGGGGAUAGUGAAUCUUUCGAAUGAGACGGCCAACACGGUCAUCUUCA
UGCUGCCCGAAAAGGACUUGGGUCCCGAUGUGUGGAAGGCUGGAGUGGGCUGCCUC
GAUAGCUUCGCCCAAAUCUUCUUCUUUCGCAACCCGAAGGAGCGCUUCACCAGAGC
CUAUAACUUGAUGCUGGGUGCACGCCUUUCAUCUGUCCAGUCCGGCGGAUCAGAUCC
AGGAAGGAUUCAGCAAACUGAUCAACGAAGCAGUCACGAAUCCAGGGCCGCCGGAC
AGGGAGGAACUCUUCCAAAUGCGCGUGGCCAGUGAUUACAACAUCACGAAUGGGAC
CGAAGACAAGGGAGAGCUGAUCCUAGCGGACAAUUAUGUGAUAGUGGUGGACUCGG
UGGAUCGAUUAAAAGAGCUAAUGAAGAAAAAAUUGUCGAAAUGCGAUCCUGGAAU
CCAGGAGCGCGUUUUCUGGUGCUCUUUCAUAAUGCGACUUGUCGGAAUCGACCGCU
UGGCGUAGCCUCCAAUAUUUUCAAGGACCUCAUGGAAAUGUUUUACGUGCACCGAG
UUGCUCUUCUCUAUGCCAACUCCACCAUGAACUACAAUCUGCUGGUCAAUGAUUAC
UACAGCAAUGUAAACUGCAGGAUUCUGAAUGUCCAGAGCGUGGGCCAGUGCCACGA
UGGCAAACUUUACCCCAAUAAUGCUGUCGUUAAGGCCUCCAUGCAGGACUACGUAU
CAGGAUUCAGUCCCAGGAACUGCACCUUUUUUGCCUGUUCCUCCAUCUCUGCUCCCC
UUUGUGGAGGCCGACUGUAUCCUGGGACUAGAGAUGAGGAUCCUGGGGUUCAUGAA
AAAUCGACUGAAAUUCGAUGUAAACCAAACCUGCAGCCUGGAGUCACGUGGUGAAA
UGGAUGGCCCAGCUAACUGGACUGGAUUACUGGGGGAAAGUCCAGAACAACGAGUGC
GACUUUGUCUUCGGCGGCUAUUAUCCGGACAACGAGGUGGCGGACCAUUUUUGGGG
AUCCGAUACCUAUCUGCAGGAUGCGCACACGUGGUACAUAAAAAUGGCCGACAGAA
GACCCGCCUGGCAGGCGUUGGUGGGUAUUUUCGAAGCCUACACCUGGAUUGGAUUC
AUCCUGAUUCUAAUAAUCAGCUGGCUGUUCUGGUUCACCCUGGUUAUGAUUCUUCC
GGAGCCGAAGUAUUACCAACAGUUGAGUCUUACGGCCAUUAAUGCCCUGGCCGUCA
CCAUAUCGAUAGCCGUCCAGGAACGACCCAUUUGCGAGACGACGAGGCGGUUCUUC
AUGGCCCUGACUUUGUAUGGCCUGAACGUGGUGGCUACAUACACGUCCAAGAUGAU
AGCCACCUUCCAGGAUCCCGGCUACCUUCACCAGCUGGACGAGCUGACGGAAGUGG
UGGCCGCGGGUAUUCCGUUUGGCGGCCACGAGGAGAGUCGCGACUGGUUCGAGAAU
GACGACGACAUGUGGAUCUUUAACGGAUACAACAUUUCGCCGGAGUUCAUUCCGCA
AUCGAAGAACCUGGAGGCGGUGAAGUGGGGCCAGCGGUGCAUCCUGAGCAACCGGA
UGUACACGAUGCAGAGUCCCCUGGCGGACGUCAUAUACGCCUUUCCCAACAACGUU
UUCAGCAGUCCGGUGCAGAUGAUCAUGAAGGCGGGAUUCCCCUUUCUCUUCGAGAU
GAACAGCAUCAUCCGCCUCAUGCGCGACGUGGGCAUUUUUCAGAAGAUCGACGCGG
ACUUUAGGUACAACAACACGUACCUCAACAGGAUCAACAAGAUGCGCCCCCAGUUC
CCGGAAACGGCUAUCGUCCUGACCACGGAGCACCUGAAGGGACCCUUCUUCAUCCU
GGUGGUGGGCAGCUGCUGGGCCGCCCUCACGUUCAUUGGCGAGCUAAUAAUCCACA
GAUGGCGAACCCAGCUGGUCAGCACGAGCGAGCAGCAGGACAGGAGGAGUGACAAG
AGGAGGAGGAGGAGGAGGAGGAGGAAGCCAGAAAAGGAUAACCGCUGGCAGCGACA
AGUUCAAGUGGCUCCAGUCGUUCGAUUUACGCCAGUCAAACGACGCAAAGUUUUCC
AGGGACAAACAAGUCAAAAGUAA

Ir62a (1821 bp; Probe set ID PRD953)

AUGUAUCUUCAGUUUUUGUUCGCGCUGUUUUUGUCGCGCUACCAAAUCGUGGCCAC
CGAAAACUUUGACCGCGCUUUCGAGCUGGCUCUGUUUCUGGACAGGAUCGGCCGCG
UGCAUCGCUUGCAUGCCAUCACUAUAGUGAACAGCCUGGGAUCUGUUGAUCCCAGC
UAUCUGGACGAUCUGCAUCGCGGCCUGAUGUGCAACAGCAGCAAUCACUUCUACAU
GCUGCCGCAGAUGACGGCCACGGACAAGGAUUCCUCGCACGUCCACUUCAGCAGCC
UGCAGGAUGAGGAGACCAUAUAUUUGGUCUUCGCCAGGGAUUCCAAGGAUGCGGUG
AUUUACUUGCAGGCCGAAAGAGCCAGAGGAAGGCGUUACACGAGGACUAUGUUCCU
GCUAAGAAAGCAGGAGUCGCAAAAGGACAUUAAAUACUUCUUUGAACUCCUGUGGA
AACUGCAGUUCCGGAGCGCUUUGGUAGUGGUGGCCGCCAGAAACUUCUACCAAAUG
GAUCCAUAUCCCACUGUUAGGGUGAUACGCAUGCGAAGAUUAUCCUCCUAUGAUCC
GCAUCAUGUUUUUCCGCCUGCAAAUCGAAAAAUUUCAGAGGCUACAGGAUGCGAU
UGCCCGUACAGCAGGAUGUGCCCAAUACUUUUUUGGUACAAGAAUCGCAGGACGAAG
GCCUGGGAACUGGCCGGAUUGGGCGGGAUCUUGAUCAAUCAACUGAUGAUGCACCU
GAACGUGACCAUGGAUUUGUUUAGAUUUGAAGUAAAUGGCUCUUCAUUGCUGAAUA
UGGCUGCGCUCACGGAUCUGAUUGUAAAGGGCAAGGUGGAGCUGAGUCCGCACUUG
UACGACACACUGCAAUCAAACACCAGUGUGGACUACUCAUAUCCCACGCAGGUGGC
ACCGCGCUGCUUCAUGAUCCCAUUGGACAAUGAAAUUUCGAGGAGCCUCUAUGUGU
UCCUGCCAUUUAGUUUAACCAUGUGGCUGUGCUUGCUGUUUGUUCUGCUCGUAGUG
CACUUCGUGUAUGUGCGCCGCCCUGAUUCCAGACGGACAUUUUUGGGGCCAUACUAGG

AGUGCCUGGGUGCUGGUCAAGUCAGAUAUGGCAACCGCAAGCCGGUCAGGCGCUUUA
GUACCUUUCUGAUCCUCUUCGGAAUAUUCAUUCUUGGGCAAACGUACAGCACCAAA
CUAACUUCAUCUCUGACCGUGACUCUGAUCCGAAGACCAGACAACAGCUUGGAGGA
GCUAUUCCUGCUGCCGUAUCGCAUUCUAGUGCUGCCCACGGAUGUGUACGCCAUCG
UUGAUUCCCUGGGUCAUGCCGAGCAGUUUAGCACAAAGUUUAGCUGCACGGAUGCC
GAGAACUUCAGCCAGAAGAGAAUCUCCAUGCAUCCGGAGUAUAUUUACCCCAUCAG
UACAAUUCGUUGGCGUUUCUUCGAUAUGCAGCAGCGCUUUCUGAGAAAGAAACGCU
UCUAUUUCUCCAAGAUUUGCCACGGCUCCUUUCCCUAUCAGUACCAGCUCAGGGUA
GACUCACAUCUCAAGGAUGCCCUCCAUCGAUUCCUGCUGCAUGUGCAGCAAGCCGG
GCUGCAUGAUCUUUGGCUGGAUACGUGCUAUCGCAAGGCCCAUCGCAUGGGCUAUC
UCAAGGAUUUCUCCCACACUGGCGGAGCUGGAGGAGAAACUGAGGCUCCGCCCACUG
GCGCUCAAUCUGCUGGUGCCCGCGUUCAGUCUGUUUCUGUGCGGAAUGUUGGGCAG
CGGAAUCGCCUUCCUGGUGGAGAUCCGUCACAGCUUCGGGUGCAGACAAAAGCCAC
CGUCCAUUAACCGCAACCCCGGGGAUUAA

Ir76a (3281 bp; Probe set ID PRH240)

AUGGAAAACUUGCUGGUAGAGUCAUAUUACUUUAGCACUGUGCUUAGUUUUUUUGC
UCAGCAGUUCUUCGCGGACUCGCAUGCCACUUGUAUUUUUUGGCACCCGGCGUUUG
AUUUUCGUCUGGAAACGGUUCAUCCAAUGCCAUUAAUAAUCAUGGACUGGCACAGA
UGGGCCAAUCGUUCCGAUCAAGAUGUUUAUGAUUACAAAAUAAAGGAGGAUGAGUU
CGAGGGGAAGGGAAUCCCCUACAACGAUUGGACUCUUAGACUGACUGUUGCCAUCG
AAAGGUCGCACUGUGAGCUAGUCAAAGAUAGUAUCACACUUAGAGUAGGUAUCCCG
CUGACAGUGAUGACAUGUGGCUCCAUCAAAACUCACUUGCAAGUGUUUAUCAUUCC
UGAACUUAUCUGUGAACUUUUUCCGAGUAUCCGGUGUCUUAAUGAAAUCGAGCGUU
AGCAAAAGCCGGUCUUUCCGAUCCGCUCCUGCAUCAGCCACAUUGUCCAAAAAUUG
AUUUACAUCCUCGAUAGGCAUCUUCCAAUGUUUUCCCAAUCUCAGAUGAUUUAGGU
UAUAGCAAUUUUGUACUAGCAACAUAAGUUGGCGACUUGGGUUUGCAGGUGAGUCA
AUGCAAUCCAGGGCCAGGCACUCGAGAUCUUUCAACUGGCCCAACUGGGACACCGA
UUGAGCUGGCCAGUUAUCACAGUCCAGAGCGUUGAGUUGCCUAAUCGCCAGGAUGU
GAUGCACUUGGUCACCUCUAACGCGGACGGAUAUGAGCUGUAGCUUUUGGAGGUUA
CUAACUCUUUUGGCCACCGACCUAUAAAAGUCGUUGUCCACUUCUGCUGUCCAACG
UGAGAUUAGGCGCAGGGAUCGGAGACCUUUAAAUUCACCCAACUCCGGGAAGCUCA
UAUCAAAGUUUUCGAGAGUAAGGUGAUCCAAGUUGGGAAACUUAUCUGCCAACAAC
GGGACCUGGUGAGAUCUCCUGCGAUCCGGUCCGAAAUUGAGAAGCAGUCGCUUCAG
GGAAGCCAUACUUUCAAACAUUUGUUGGAAGGAGGCGUUGCUGAGGUUUGGGUCGA
UUCCAUCCAAGUCCAAGGCCUCCAGUUUACUGAAGUGCCGCAAUUGAUCUAGCUGU
GCAGAUCUGGCAUCGAUCAGAGUGAGAUUGGUUAGACUGGGUAGCUCCAGGAGGAG
CUGCAUGAUGUGGCCCCUGUCCCCACUUUUCGGCGGCGACUCUGUAACGGCGUGCA
UAAAUAUGAUGACUGCCUGUCGCAGUUUGGGGCAGUGCCGUCCCAGGAGCCCCAGA
AAGGGGUAGGUAAACGGCUCAUCCCAGCUACCAUGGGGCACUUCGCACCUGGACAC
UUCGGAACCGCACAGCUGCAGCAGGAACUCCCAGUCCGGAAUGGUUUUCAGAAGCC
GCACAUUGAUUUUUUUGUGGCGCGUUCGCAAAAUGUCCGUCAGUACAACCUGGAAU
AGUGGAUGGGCCCGGCCCAGAUUUAGCUGGUCCUCCAGCACAUUUAUAUAUGAAAA
UAUCUGAUGGUAGCAGUCGUAGUUGAGAUCCAGGAAACCGGGUCCCCCACUCAUAC
UCUGCGGUCUUCCGACCAGGAAGGAGAAGGGGCAGCCUAAUCCCAGUUUGUCCAUA
CCUUCAUAGCAUUUCAGGAGCAGAUUCCCGAAUUCGCCAGAUAUUUUUAUCACGCC
AGCAUCUACUCCAUUUGGAGAUCUCUGCGAAAUCGUUUUAUGUUCGUUUACACUAA
AGAGUUUGAGGACAAAAAAGAUAGUUAUCUGUCCGGUUAUAUAUUCCAAGAUCAAC
CUAACAUCUUGGUAAUUACUUCACAAUACCUGAACUCAAGCACUUUUGAAAUUAAA
ACGAACCGAUUUGUCGGUCCGCGAAACUUUAACAAAAACCCGGAGCCUGUUGAGUU
UUUACAUACUCCAGCGUUUCGAUGCCAAGGGUACGAAAGCUACUUGGGAAACCCAGA
GUGCAAUGUCCAGCAAGAUGCGAAACCUCAAGGGACGCGAGGUAGUCAUAGGCAUC
UUCGACUACAAGCCUUUUAUGCUAUUGGAUUAUUUAUGUGAGUUAGGAAAAGCCAC
CAUUAUAUUAUGAUCGUUUUAUGAACACGACGGAUGUAACCAUUGAUGGAACAGAU
AUUCAACUAAUGCUCAUUUUCUGCGAGUUGUACAACUGCACCAUUCAGGUGGACAC
AUCUGAACCAUACGACUGGGGUGACAUCUACUUGAAUGCCUCGGGCUAUGGUCUGG
UUGGAAUGAUCCUCGAUAGACGAAACGAUUACGGAGUAGGGGGCAUGUAUUUGUGG
UACGAGGCGUACGAGUAUAUGGACAUGACUCAUUUUCUGGGACGAUCUGGAGUAAC
CUGUCUGGUGCCCGCUCCGAACCGUUUAAUCAGCUGGACGCUCCUGCUCCGACCAU
UCCAGUUUGUCCUCUGGGAUGUGCGUGAUGCUCUGCCUUCUGCUCGAGAGCUUAGCU
CUUGGUAUAAACCCGUCGCUGGGAACACUCGUCGGUUGCGGCAGGCAAUUCCUGGAU

CAGUAGUCUGCGCUUCGGUUGCAUCAGUACGCUGAAACUUUUCGUAAAUCAGAGCA
CCAAUUAUGUGACCAGCUCGUAUGCUCUAAGAACCGUCCUAGUGGCCAGCUACAUG
AUCGACAUUAUAUUGACCACUGUGUACAGUGGCGGUCUGGCGGCCAUCCUCACUUU
GCCCACUUUAGAGGAAGCGGCGGACUCUCGCCAACGUCUCUUCGACCAUAAGCUCA
UUUGGACGGGGACUUCACAGGCCUGGAUUACCACCAUUGACGAGCGAUCGGCCGAC
GCCAGUUCUUCUUGGUUUAAUGGAGCAUUACCGAGUUUACGAUGCCAAUUUAAUAU
CCGCCUUCUCGCACACGGAGCAAAUGGGAUUUGUCGUCGAGCGCCUUCAGUUUGGU
CAUUUGGGCAACACCGAGCUAAUAGAAAACGAUGCCCUAAAGCGGCUGAAACUUAU
GGUGGAUGAUAUUUACUUUGCAUUUACGGUGGCGUUUGUGCCGCGACUGUGGCCGC
ACUUAAAUGCCUACAACGACUUCAUUCUGGCUUGGCAUUCCUCGGGCUUUGACAAA
UUCUGGGAAUGGAAGAUCGCCGCCGAAUACAUGAAUGCGCACCGCCAAAAUCGCAU
CGUGGCAUCUGAGAAACGAACCUAGAUAUAGGACCUGUUAAACUUGGCAUUGAUA
AUUUUAUUGGCCUAAUCCUGCUUUGGGUGCUUCGGCAUGAUUUGUAGCCUUCUGACA
UUUCUCGGAGAACUCUGGAGGGGACAGGGGUAG

Ir93a (2607 bp; Probe set ID PRH241)

AUGAAUCCUGGCGAAAUGCGGCCUUCGGCUUGCCUUCUGCUCCUGGCUGGACUGCA
GCUCUCUAUCCUGGUACCCACUGAGGCCAAUGACUUUUCGUCCUUCCUGAGCGCCA
AUGCAUCGCUGGCCGUUGUGGUGGAUCACGAGUAUAUGACGGUUCAUGGCGAGAAU
AUAUUGGCUCAUUUCGAGAAAAUCCUGAGCGACGUAAUACGGGAGAAUCUAAGGAA
CGGUGGCAUAAACGUAAAAUAUUUUAGCUGGAAUGCAGUGCGAUUGAAGAAGGAUU
UUUUGGCUGCCAUAACUGUUACGGAUUGCGAGAAUACAUGGAACUUUUACAAGAAC
ACUCAGGAAACUUCAAUUCUACUGAUCGCCAUUACGGAUUCCGACUGUCCCAGGCU
GCCCCUAAAUAGAGCUCUAAUGGUACCCAUCGUUGAGAACGGCGAUGAAUUCCCCC
AACUUAUUCUGGAUGCCAAGGUCCAGCAGAUUCUAAAUUGGAAGACCGCCGUUGUU
UUUGUGGAUCAAACCAUAUUGGAGGAGAACGCACUUCUGGUAAAAUCGAUUGUGCA
CGAAAGUAUAACCAACCACAUCACCCCAAUCUCCCUGAUCCUUUACGAGAUCAACG
ACUCCCUGAGGGGGCCAACAGAAGCGAGUUGCUCUGCGCCAAGCUCUGUCUCAAUUC
GCUCCCAAAAAGCACGAGGAGAUGCGCCAGCAGUUCCUGGUCAUAUCUGCCUUUCA
CGAGGACAUCAUCGAAAUAGCCGAGACCCUGAACAUGUUUCACGUGGGCAAUCAGU
GGAUGAUUUUCGUGCUGGACAUGGUGGCUCGGGACUUCGAUGCCGGCACUGUGACC
AUAAACCUGGACGAGGGAGCCAACAUAGCCUUCGCCCUCAACGAAACGGAUCCCAA
CUGCCAGGACUCGCUAAACUGCACGAUCUCGGAAAUUAGUCUCGCUCUGGUCAACG
CUAUUUCCAAAAUUACCGUCGAGGAGGAGUCCAUAUAUGGUGAGAUCUCCGAUGAG
GAAUGGGAGGCCAUCCGCUUUACCAAGCAGGAAAAGCAGGCCGAGAUUCUGGAGUA
CAUGAAGGAAUUCCUGAAGACCAAUGCCAAGUGCUCCAGCUGCGCGAGAUGGCGCG
UGGAGACGGCCAUUACCUGGGGCAAAAGCCAGGAGAAUCGCAAGUUUCGCUCAACU
CCCCAACGCGACGCUAAGAACCGAAAUUUUGAGUUCAUCAACAUUGGCUAUUGGAC
ACCCGUGCUGGGAUUCGUCUGCCAGGAGCUCGCCUUUCCGCACAUCGAGCACCACU
UCCGCAACAUAACCAUGGACAUUCUGACCGUGCACAAUCCACCCUGGCAAAUCCUU
ACCAAGAACAGCAAUGGGGUCAUCGUGGAGCACAAGGGCAUUGUUAUGGAGAUCGU
CAAGGAGCUGAGUCGCGCCCUAAACUUCAGCUACUACCUUCACGAAGCCUCCGCAU
GGAAGGAAGAAGAUUCACUCAGCACAUCAGCGGGCGGAAAUGAAAGCGACGAGCUA
GUUGGUUCCAUGACCUUUCGUAUACCCUAUCGAGUGGUGGAGAUGGUGCAGGGCAA
UCAGUUUUUCAUCGCUGCCGUGGCAGCCACCGUUGAGGAUCCCGACCAAAAGCCCU
UCAAUUAUACCCAGCCCAUCAGUGUGCAGAAGUACUCCUUCAUCACCCGCAAGCCG
GAUGAGGUGUCCCGCAUUUACUUGUUCACGGCACCCUUCACCGUGGAGACUUGGUU
CUGCCUAAUGGGCAUCAUUCUGCUGACUGCUCCCACGCUGUACGCCAUUAAUCGCC
UAGCUCCUCUGAAGGAGAUGCGAAUCGUGGGCCUGUCCACAGUUAAGAGCUGUUUU
UGGUAUAUAUUCGGGGCUUUGUUACAACAGGGAGGCAUGUACUUGCCCACAGCAGA
CAGUGGGCGCCUAGUGGUCGGCUUUUGGUGGAUCGUGGUUAUCGUGCUGGUGACCA
CCUAUUGCGGCAACCUUGUGGCCUUCCUCACGUUCCCCAAAUUUCAACCGGGCGUG
GACUAUUUGAAUCAACUAGAGGACCACAAGGACAUUGUACAGUAUGGAUUGCGAAA
CGGCACCUUCUUCGAGCGGUACGUUCAGUCGACAACGCGGGAGGACUUCAAACACU
ACCUGGAACGGGCGAAAAUCUACGGCAGCGCCCAAGAGGAGGACAUCGAGGCGGUG
AAGCGUGGCGAGCGCAUCAACAUCGAUUGGCGGAUCAAUCUGCAGUUGAUUGUUCA
GCGGCACUUCGAGCGGGAGAAGGAGUGCCACUUUGCUUUGGGCAGGGAGAGCUUCG
UGGACGAGCAGAUUGCCAUGAUUGUGCCGGCCCAGAGUGCGUAUCUGCACCUGGUA
AACCGCCACAUCAAGAGCAUGUUCCGGAUGGGCUUCAUCGAGCGCUGGCACCAGAU
GAACUUACCCAGCGCGGGCAAGUGCAACGGGAAGAGCGCCCAGCGCCAGGUUACCA
ACCACAAGGUGAACAUGGACGACAUGCAAGGGUGCUUUCUGGUCCUGCUCUUGGGC

UUCACGUUGGCUCUUUUAAUAGUGUGCGGCGAGUUCUGGUAUCGUCGCUUUCGGGC
CAGUCGAAAACGGCGUCAGUUCACCAACUGA.

Orco (1461 bp; Probe set ID PRD954) – positive control

AUGACAACCUCGAUGCAGCCGAGCAAGUACACGGGCCUGGUCGCCGACCUGAUGCC
CAACAUCCGGGCGAUGAAGUACUCCGGCCUGUUCAUGCACAACUUCACGGGCGGCA
GUGCCUUCAUGAAGAAGGUGUACUCCUCCGUGCACCUGGUGUUCCUCCUCAUGCAG
UUCACCUUCAUCCUGGUCAACAUGGCCCUGAACGCCGAGGAGGUCAACGAGCUGUC
GGGCAACACGAUCACGACCCUCUUCUUCACCCACUGCAUCACGAAGUUUAUCUACC
UGGCUGUUAACCAGAAGAAUUUCUACAGAACAUUGAAUAUAUGGAACCAGGUGAAC
ACGCAUCCCUUGUUCGCCGAGUCGGAUGCUCGUUACCAUUCGAUCGCACUGGCGAA
GAUGAGGAAGCUGUUCUUUCUGGUGAUGCUGACCACAGUCGCCUCGGCCACCGCCU
GGACCACGAUCACCUUCUUUGGCGACAGCGUAAAAAUGGUGGUGGACCAUGAGACG
AACUCCAGCAUCCCGGUGGAGAUACCCCGGCUGCCGAUUAAGUCCUUCUACCCGUG
GAACGCCAGCCACGGCAUGUUCUACAUGAUCAGCUUUGCCUUUCAGAUCUACUACG
UGCUCUUCUCGAUGAUCCACUCCAAUCUAUGCGACGUGAUGUUCUGCUCUUGGCUG
AUAUUCGCCUGCGAGCAGCUGCAGCACUUGAAGGGCAUCAUGAAGCCGCUGAUGGA
GCUGUCCGCCUCGCUGGACACCUACAGGCCCAACUCGGCGGCCCUCUUCAGGUCCC
UGUCGGCCAACUCCAAGUCGGAGCUAAUUCAUAAUGAAGAAAAGGAUCCCGGCACC
GACAUGGACAUGUCGGGCAUCUACAGCUCGAAAGCGGAUUGGGGCGCUCAGUUUCG
AGCACCCUCGACACUGCAGUCCUUUGGCGGGAACGGGGGCGGAGGCAACGGGUUGG
UGAACGGCGCUAAUCCCAACGGGCUGACCAAAAAGCAGGAGAUGAUGGUGCGCAGU
GCCAUCAAGUACUGGGUCGAGCGGCACAAGCACGUGGUGCGACUGGUGGCUGCCAU
CGGCGAUACUUACGGAGCCGCCCUCCUCCUCCACAUGCUGACCUCGACCAUCAAGC
UGACCCUGCUGGCAUACCAGGCCACCAAAAUCAACGGAGUGAAUGUCUACGCCUUC
ACAGUCGUCGGAUACCUAGGAUACGCGCUGGCCCAGGUGUUCCACUUUUGCAUCUU
UGGCAAUCGUCUGAUUGAAGAGAGUUCAUCCGUCAUGGAGGCCGCCUACUCGUGCC
ACUGGUACGAUGGCUCCGAGGAGGCCAAGACCUUCGUCCAGAUCGUGUGCCAGCAG
UGCCAGAAGGCGAUGAGCAUAUCGGGAGCGAAAUUCUUCACCGUCUCCCUGGAUUU
GUUUGCUUCGGUUCUGGGUGCCGUCGUCACCUACUUUAUGGUGCUGGUGCAGCUCA
AGUAA.

Drosophila sechellia **experiments (using** *D. melanogaster* **sequence)**

Orco – see above

Ir25a (2396 bp; Probe set ID PRL623)

CAAACGCCCCAUCUGAUCCUGGACACCACCAAAUCGGGCAUAGCCUCGGAAACGGU
GAAGAGCUUCACCCAGGCUCUGGGUCUGCCCACCAUUAGUGCCUCCUAUGGCCAGC
AGGGCGACUUGAGGCAGUGGCGCGACUUGGAUGAGGCGAAGCAGAAGUAUUUGCUG
CAGGUGAUGCCGCCGGCGGAUAUUAUUCCCGAGGCCAUUCGAAGUAUAGUGAUUCA
CAUGAACAUCACGAAUGCUGCCAUUCUGUACGAUGAUUCCUUUGUCAUGGACCACA
AGUACAAGUCCCUGCUGCAGAAUAUACAAACCCGUCAUGUGAUCACCGCCAUAGCC
AAGGAUGGUAAGCGGGAGCGCGAGGAGCAAAUCGAAAAGCUGAGGAACUUGGACAU
CAAUAACUUCUUUAUUCUGGGCACCCUGCAAUCGAUCCGCAUGGUCCUGGAGUCGG
UGAAGCCAGCGUAUUUCGAGCGCAACUUCGCCUGGCACGCCAUCACUCAGAACGAA
GGAGAGAUUAGCAGUCAGCGGGACAAUGCGACCAUUAUGUUUAUGAAACCCAUGGC
GUAUACGCAAUAUCGAGAUCGCUUGGGAUUACUGCGAACCACUUACAAUCUGAACG
AGGAGCCGCAGUUGUCAUCCGCGUUUUACUUCGAUCUGGCACUUAGGAGUUUCCUU
ACCAUCAAAGAAAUGUUACAAUCGGGCGCCUGGCCAAAGGAUAUGGAGUAUCUGAA
UUGUGACGAUUUCCAAGGUGGCAACACACCCCAAAGGAACUUGGAUCUUCGAGAUU
ACUUCACCAAGAUUACCGAACCGACUUCGUAUGGAACCUUUGAUCUCGUCACGCAA
UCCACUCAGCCAUUCAAUGGGCAUAGCUUCAUGAAAUUCGAAAUGGAUAUAAAUGU
GCUGCAGAUUCGUGGUGGCAGUUCCGUGAACAGCAAGUCCAUUGGCAAAUGGAUAU
CGGGUCUGAACUCGGAGCUCAUCGUCAAAGACGAGGAGCAGAUGAAGAAUCUCACU
GCAGACACUGUUUAUCGAAUCUUUACUGUAGUGCAAGCUCCUUUCAUAAUGCGCGA
UGAAACGGCUCCGAAAGGAUACAAAGGAUACUGCAUUGAUCUGAUCAACGAGAUAG
CCGCAAUUGUCCACUUCGAUUACACCAUCCAGGAGGUGGAGGACGGCAAGUUUGGC
AACAUGGACGAGAAUGGGCAAUGGAAUGGCAUUGUGAAGAAGCUGAUGGACAAACA
GGCGGACAUUGGCCUUGGCAGCAUGUCGGUGAUGGCCGAACGGGAGAUAGUCAUUG
ACUUCACCGUUCCGUACUACGAUCUGGUCGGGAUUACGAUCAUGAUGCAGCGACCC
AGUUCGCCAAGCUCGCUGUUCAAGUUCCUUACCGUGCUGGAAACGAACGUGUGGCU

UUGCAUCCUGGCUGCCUACUUCUUUACCAGCUUUCUCAUGUGGAUCUUCGAUCGCU
GGAGUCCCUAUAGCUAUCAGAACAAUCGAGAGAAGUACAAGGACGACGAGGAGAAG
CGCGAGUUCAAUCUGAAGGAGUGCCUCUGGUUCUGCAUGACUUCAUUGACACCUCA
AGGCGGUGGCGAGGCUCCAAAGAAUCUGUCUGGCCGUUUAGUGGCCGCCACCUGGU
GGCUAUUCGGUUUUAUCAUUAUUGCUUCGUACACGGCCAAUUUGGCUGCCUUCUUG
ACCGUAUCACGUUUGGAUACGCCCGUUGAAAGCUUGGAUGACCUGGCGAAGCAGUA
CAAGAUCCUAUACGCUCCAUUGAAUGGCUCAUCUGCGAUGACAUAUUUCGAGCGUA
UGUCCAACAUAGAGCAGAUGUUUUACGAGAUUUGGAAGGAUCUGUCGCUGAACGAC
UCCCUGACCGCCGUGGAGCGCUCCAAGCUGGCUGUUUGGGAUUAUCCAGUGAGCGA
CAAGUAUACCAAGAUGUGGCAGGCCAUGCAGGAGGCGAAGCUACCGGCCACCCUCG
ACGAAGCGGUGGCCCGGGUUAGAAAUUCGACAGCUGCCACGGGUUUUGCCUUUCUG
GGCGAUGCCACCGAUAUACGCUACCUGCAGUUGACCAACUGUGAUUUGCAGGUGGU
GGGCGAGGAGUUCUCCCGGAAACCCUAUGCCAUAGCUGUUCAGCAGGGAUCGCAUC
UCAAGGAUCAGUUUAAUAAUGCAAUCCUGACCCUGCUCAACAAACGACAGCUGGAG
AAGCUCAAGGAGAAGUGGUGGAAGAACGACGAAGCUCUGGCCAAGUGCGAUAAGCC
GGAGGAUCAAUCGGAUGGCAUCUCGAUCCAGAACAUUGGCGGCGUCUUCAUUGUCA
UAUUCGUGGGCAUUGGAAUGGCCUGCAUCACGCUGGUCUUUGAGUACUGGUGGUAC
AGGUACCGCAAGAAUCCGCGGAUCAUCGAUGUGGCCGAAGCCAA.

The following genomic sequences from VectorBase were used by Molecular Instruments, Inc (Los Angeles, California) to produce custom probe sets targeting coding sequences:

Anopheles coluzzii experiments
Orco (10,821 bp; Probe set ID PRL382) – AGAP002560
CGTCGAGCGGAAAGGACGTATCAAGTCGATTCGTCTATCAGTGTCGGAACGATAGTGATA
GAAATCTACAGGCGCCAATCATAAACCGTTTACTGCTCGCGATAGGACACGCTTTGCTAA
CGTCTTGTGCATCGCGAAAACTAGTGATTGGAGTGTGGTTTTGTAGCTGTTTGTCGTTCT
GTGCTCCACGTTGACTCTGTGTGTGTGTGCGCTGAATTCAACAAGACTTTTCTGCAACAG
CATCATTTGCAAAGAATAACCGGCGCGACTTACGCGGTCTGACTTGCTGGTGCGCTGCTT
TGTACGGCAAACGGCTACACAAGCGAATCGAATTATTTTCCTATCACGCTGCGCTTACCA
GCGCCTGCTGGTAGGCAAAGAATGTGCAAAGTTTCATTTGGCTTGGTTCGTCTGCTTTGC
TGTGAACGTGTGCACGGTTGCATCGCTAAGGTTTCGGTGTGAGCCGAGAAGTTGCAGATC
GAAACCCCTTTGTGTGTGTGTGTGCCGTGGGAAGCATTGTGTTTAGTGAGAAGTGAAAAG
AAAAGTGCTGAAAAGTAAGTATTCGATGTAGCTTCAACCTTTACACTTGACAAGGCGGAG
ATCTCAACCATTTTTCTGGTTCGAACGTTAAGCGGAACATTTGATCCTTTCAAAACAGTG
TGACTGTGTGTGTGTGTATGTACAATCGCCCCCCCATGTATTCCAAATATTTGCTTCTCGCAAAT
CAGGTCACAAAGCTGTGCTCAATGTTGGCACAATCAAAGCTTTCCCCATTCGTCTGGGCC
AAGCCTAGCTCAATTGTTTGTACGAGAGATTTTACCGTTTGGCTCCAAGCATTTGCAATT
GTCCTTTCCTGTACGCTTGCCGCCGCTTCACTGCGCCCTTCTAAGTACACAGAGCACACA
CAGCTTAACTCTTCCCTGTAGCTGTACGGCTTGGTGTCTGTTACCTAAAAATCGATAAATCAAT
TAGTCTCTTGCCGACCACACCAAACGACCACTACAAACGAGCCCGACTCGACCCGTTCAC
TTCCCGTTCGCAGATGCAAGTCCAGCCGACCAAGTACGTCGGCCTCGTTGCCGACCTGAT
GCCGAACATTCGGCTGATGCAGGCCAGCGGTCACTTTCTGTTCCGCTACGTCACCGGCCC
GATACTGATCCGCAAGGTGTACTCCTGGTGGACGCTCGCCATGGTGCTGATCCAGTTCTT
CGCCATCCTCGGCAACCTGGCGACGAACGCGGACGACGTGAACGAGCTGACCGCCA
ACACGATCACGACCCTGTTCTTCACGCACTCGGTCACCAAGTTCATCTACTTTGCGGTCA
ACTCGGAGAACTTCTACCGGACGCTCGCCATCTGGAACCAGACCAACACGCACCCGCTGT
TTGCCGAATCGGACGCCCGGTACCATTCGATTGCGCTCGCCAAGATGCGGAAGCTGCTGG
TGCTGGTGATGGCCACCACCGTCCTGTCGGTTGTCGGTATGTGTGTATGTGTGTGGCCGT
TTGGGAAAGTGTCTTTGCGGCAGAACCCCAATCTACTGTTACGCTTGACTGGGTTTTTGT
TTTTTTCTCGGTGGAGGGACGGGATAAAATATCTGAAAGAATAATTGAGTCAACCCACAG
GGGGATGCAAGACATCGCAGGCAGAGAGTTTGGGTTTGATTTATCACCGCACACCGAATA
TCTTCACGGTTCATAAGCTTCACCGCGGTGAAAAGGGAACTCCCCATTTCCCTGTTTTCT
TTTTTTTCTTCCTCTCGATAAATTACTCATCGCTTTTCGTTTTTTTTTTTTTTGTTGTTGCTTCTTTCT
TCTTTCATCCCTACTAGCCTGGGTTACGATAACATTTTTCGGCGAGAGCGTCAAGACTGT
GCTCGATAAGGCAACCAACGAGACGTACACGGTGGATATACCCCGGCTGCCCATCAAGTC
CTGGTATCCGTGGAATGCAATGAGCGGACCGGCGTACATTTTCTCTTTCATCTACCAGGT
ACGTTGGCGGAATGTCCTGCGCGTCACAGTTGGCAGTCAGTGAGCGGCAACACGGC
GAAAAAATGGGACTAAAACCGGTCTTCACAGAGCCAACACATTCCTACAGCAATTGCATA
CCTTCGGGCGGTCGGGACTGGGCAATGCAGCTACAACATCCTCGCCTAAAGTTATGCAAT
TCGAGCGACAAATGTTGCCGTGTTAGGGCTTTTTGTGATAATAGTCGTTTTTTTTGTCCTCTCGC

TTATCAAACTCTATCAACGGAGGAAATCCATTTTCGCTACAATGCCTACAGCTCAAGTTT
CAAGGTCAATCGAGCGGGTGGGGATCAACTTTTTTATTCATTTTGCTAACGCCCCATCAA
CAAATTCTATGTTCTCAATGGCAAAGATTACTGCCCGCACCAATCGCCCAACGAAACGGC
AAAAGAAAAGCGACGATTATGAAGATGTCCAAACCATTGCCCGCCCGACGCTTTATCTGA
TGATTTGCGGGATGGCTTTTACTTGTCTGCTACTTTCAGGCACAAAAGGAAATGAAACCA
GCGCAGGCTCGTTTGCCGGCTTGCGGAGGTTCTTCAGGCACTGAGGCTGAGTACTTAAAT
CGAACGATTTTTACGATTCTGGATCCAGTTTTATGATGTGGCCTGCATTACAGTGGCAATTATA
CCCTGATGTTCATTTCATTGCATTTTGTAAGTTTGTGCTGGTAACGCCCGTAACGATTAATTCT
TTTCAAAGAGATTCTTTCAAAGAGATTCAAAATGTGTATAACAAATGCTAACGAATGGAC
CGTACTTGGAGGGTTGCGGAAAGTAACGTTTTAAAATATTCATCACAATCCTCTGCAAAC
TTGTGCTTAATTAATTGGTGCACAATAAGTTTAAACTGTGGCGGCAGATGTGTCGCTGTC
CGCTTCCTTCCTTCCCAGCAAGCTCGTGCGAAATAATTTATTCCATCATTTTAATACAGCCGTT
TGTGCATTTTAATTAGCAAAGCAATATAAAAAGCAGCTAACCATCCCCATTAAAACAAAG
TGCTTCCGGGCCCAATTGTTATGGCGGTGGAAGTAATGGTTTTACCAGTGGAAGTGTCCT
TTCCCATCGTGGGTACTTCGCGATATTCTTGTCTTATAACAAGTGCATACAGAAAAAAGG
AACAAATCCTCCTTGCTATGGTCTAAGGGCCAGCTTCGGTACCGCTTCCGCTTCGGGATG
TCATAAAGTTTGATGGGTGTTTTTAACATTACTTCCGCTCTTAACCACCTAATGGACTTTTCAT
GCTTGAGCTAAAGCTAAACCAGCCACCAGCGGTACGCACCGAGCCACGGTTGATTTCGGC
GGCGGCCTCATCCCCAGTTTTGCGCCACCAATATTGCCTTCATTAATCTGTACCCTCGGA
GCGTTAGGGCCCGCGGACGAGTCCTCGTTGTAATGCACCGCCATGCCACGGGACGGGATA
ATCCGTTGGGACGGCGCGAAAGCGACTATCGCGGACGGATTGGTTCGACCGTGCTACAAC
ACATTTTATGCTTCACAGATTTACTTCCTGCTGTTTTCGATGGTCCAGAGCAACCTCGCG
GATGTCATGTTCTGCTCCTGGTTGCTGCTAGCCTGCGAGCAGCTGCAACACTTGAAGGTA
GGTACGGTAGCAAACGTGGTTGTCTTTACATCCGCGTGCAGCATTATCCTTATCGACGTG
TAGTGTTAACGGTAAAAGAGGAAGCGATAAAAAAGCAACATTCTCTCACACCCTCGATCT
CTCTTTATTTTCTCTCTCTCTCTCTCTCTCTCTCTCTCTCTCTCTCTCTCTCTCTCTCTC
TCCATCTCCCTCGGGCAGGGTATTATGCGATCGTTGATGGAGCTTTCGGCCTCGCTGGAC
ACCTACCGGCCCAACTCTTCGCAACTGTTCCGAGCAATTTCAGCCGGTTCCAAATCGGAG
CTGATCATCAACGAAGGTATGTGAAACGTGTGCTCGTGGCAGACGGACTCAAAGAGAGCA
TAACACAATCCCCTGGTAGTTCATTTCAATGACCTTAACACTCGGCAAGCTAAGCGAGAC
AGTGGGGACAGTGAGAAAGAGAGAACAAGAAAAAAAACCATCATCCGTACGACATCATCG
CTACGTACCGGTATTTCAGGATGAGGAAATAAAACGCTAGGGGAATGAAAGTGCGACAGA
ATGATAAAACAATCCCCACCCAGGCCCCCAGCCTGGACGAACGGATGTAGTGTGCGAAGC
GAGCAAAAAAAGTCAAATAAATTGAAGTTTAAAAATAGATTTTCCCCGTCCATCCGTGGT
GGAGCGTAAAGCCCGGCGGACAACTTCGAGCACGGCGACCGTGCACAGTACTGTGC
CACAGTTGTAGGGACGGATAAGCTCCGTTCCTTTTTTATCCTTTTTTTTTGGAGATTTGTTTGC
GTTCGCATCGTTAGACGAGCTTAGTGCCGTGTTGCTCTAATTGCTATTTATTATAAAGCGCTTC
CAAATAGAAGATCGGTTCTCTCCATTTAATCTATCGCGCCTGTACGCCTGAAACTATGCA
CTGTGCTGTGAAACCGTCAAGCTCGAGCACGACGAATGGCCCACCGTACCACGCCCGTGG
TGCCCAAAGCGCAACGCGAATTGCATGTTAACAAACCTTTGCCTACCATCCAATCCGTGT
GAAATTGCCCGCTCTCTTTCTCTCTTTTGCGCTTTCGGTGTATCGAACGGTTTTGTCCCTTTTT
TTTACTTTGCTCTTGATCTCTTGCTGTGCTCACTTTCATCTCATGTTTTGCCTGACGGTGGTGG
GTTTTCGAAAAAGAGCGATTTCTTCTGCGTGTGTGTGTGGTTTTTTTAAATAACCGCTC
CAGGTCGTGTTGAACGCTGCAGGACCGATCGGAGCTAGTTTATTATCAGCTTTAGTGTTT
ATCCCACCCATGCCCCACATCACGTCTGTGGAGAGTGGGGGAAGCTTAAGTCCAATGTAA
TTTACCGTGTTTCTGTCGTTCGTCACCTTCTTCGTCGATGGAGATTGGTGCGGTTGGCAC
GATAAAAGCCCACTGCACGTTACGGACCGAGGGAAAGGTCTTTTTGTAGGCCTAGCAACG
GTCCTCATTCACCGCATGGGGGTGTAGCTCAGATGGTAGAGCGCTCGCTTAGCATGTGAG
AGGTACCGGGATCGATACCCGGCATCTCCAACCCACACAAAACGTTTTTTAAGAAGATTT
TTAGGGAAGATATTAACGCGGGTACACTGTGCTCCTCTAAGTTGGAAGAGTAGATGAGAT
GATGACAAGGGAGAAGGAACATGTGTACGTGTTTGATAGCAAACACACAAACAACAATAT
CATCTCTGATAATAATCTGATGTGTGATGTGTGTGTATTGTTGTTATGCTGCCTTTGCCATCTT
GTCCCTCTCTCTCCTGTTCAACTCCTAAAAGAATTGTTTGGAGTCCTCTCAGTTCCTCGT
AAAGATCCTTTCGAGATTCTTCTTTCCTTTTTATTATTTATTCCACGAGCCTCTGACATAAGTA
GCCTTCCGCTTATTTCCTTCTCCTTGCACTTGTCAGTTCCGTGTAGAGCGTCATTTTGAGGTTT
ACACATTTCCCACCGACGCCTGATTGTTACATTGTCATCTACATTGCTTTCCGTTTACCGTTCC
GCCCTTTTTTTTTAACGCTACCACAGAAAAGGATCCGGACGTTAAGGACTTTGATCTGAG
CGGCATCTACAGCTCGAAGGCGGACTGGGGCGCCCAGTTCCGTGCGCCGTCGACGC
TGCAAACGTTCGACGAGAATGGCAGGAACGGAAATCCGAACGGGCTTACCCGGAAG
CAGGAAATGATGGTGCGCAGCGCCATCAAGTACTGGGTCGAGCGGCACAAGCACGTTGTA

CGGTAGGTATGGTAATTTCTAAGGTGTGGTGTAAAGCCTCCAGGTTCCATGAAAAAGGGA
TACTTTACCACAGTAAGAGTTTGTTTTGCTGGACTTACATTCTTTGGAGCATTGTTTGGTGTTG
TGCTGAAACCGGTTGCAATATCGTTTTGCGAAGAAATTATGTGTAAAGCGTATTACAATCTCAT
TCCTCTGTTAATCTGTACCAATTGTGTCAGCCCCGACCGAAAGCAGGCCTAATTCGTACC
AGAAAAACCACAAGCTGTTTGTAAGCATCGATACGCCCGAAGCTTTCAATCCAGCCAAGG
CGCCACCTACTATTGACGTGACTTTTTGCACGTTCACACTCTCCCTCTCCCATTCTTTCTATAA
CCAATCGTCGCTCAGCCAGCATCGCCCGGAGTGAAGTTTTTATTTGAACGATATCACCCG
TATCGATTTTCCACTAAACATGCTTAAATCGTTTCACAAAGCTCCCCCAAAATCCCATTTCACC
AATCCACCAATTTGAAGTCCGTCGTCCTTTGTGTCCTTGTGTTTGTGTGTTTGTGTGAGC
TGGAGACATGGGGGAGTGAGTAACCGAACAACCTCTTGCCGCTGCTTCACGATATCGAAC
AGCACCAAGATAAGCATCCCTTTTTTCCCTAGCCGATGTCTCCGATATCTCGATTCCGCTT
CCAGCGAGGCAAAGAAAAAGGCGAACTGGCTGACCTCACCCGGGGCGAGGAAAAAG
CGTAGGGATTACGTCGAGCAGCACGAGTTGTGATTTCTTCTTCTTCTGGTTCCATAAATC
GCTGACGGTTTCCATTACCGCCTGCGGAGTGCACACACGTGAAGGGAAAGCGAAAACGTT
TAGATTCCAGCAGCAACGGCAGCACCAGAAGCAGCAGCAGCGCGGCAAATTGAATCATCC
TGACGCGATGAGTTGTCTGGGTTTTCGGGTCGGTGGCTTACAGCACCACACCATCTGCTG
CAGCTAATACAGCTGTAAATTTCGTTAGACATAGACTTGATTTTACAATATTACACACACACTT
ACACACAGCTATAGATTTGTCGCTTGGCGTATGGCTCTGTACGGCGTGCCGTACATGC
CGCGAGCCGTGTTGCTGCTGGTTGCGATACGGATCACGTCCGATTCGATTCAGCCTGCGT
GTTTTTGGTGAAGATCCTTATCGGTGACCCACTTTCAGTGTGTCGAGAGCGAGGGTCACT
ATGGCGCCTGTCAGTTGGAAAGCTAGGCTCGATTCAAAGGGCCATTGTGCCAGTGTTCTT
TTTAAGATAGCGATAAGCTTTTGATCGAAATAGTAAATCAAACATTGTTTCTTTTTTCCTATTC
CAAACTGTTGCCAACCTCATTATTACGTTTTTGCAGCGGGTGTATAGTAAATTGCATACTTTAA
GGCGTGATTTTCAAATGTAGCGTTCCGTATGCAGAAACGCCATGGATTATGCAATTTAAA
CAATGCTGCTTCCTTAACATTCAAATAACGGCTTATTAAGGAACTTTTTGTGCAATTTGTTTTT
AACAGCAAATAGTTAGCTCAGAACGATCACATTTAGTATCGCTTCAACAAAGAACTCTTT
TAAACACACAATTTGTAATGCCATTCCCTCGAGAAAGTTTCTTGTCAGTCCTCCTCTGCA
TCACAGCAACAACCAAACCTGCTCATGTTTCCTGCTCGTTTCCTAGCTGTTTTGAACGTT
ATTTCCGATTCCTGTGCTTGCCCGCTTTTCTTACAATCAACCACAATGGTTCAGATTTCGCTCT
TATTTTATTGACCCACTGCTTTCGTGCTGAAGCCCGTGGAAACAATGCGCCAAGCTCAGC
ATCCAGCCATGCATGTAAAATGAGCCACGCGACAGATTTTAGACATCGCTTTCGCTCTGC
ACCGGAGGTGGTTTTATTCTTGTTTCCGATTCCCACGTCCATTCGTCCTGGGTCCGTCCG
CCGGGCCCGAAACCGTAAGCCGTGCGGGGAATTACGCAATCGAAACGAGCCAGAAA
ATGAGCACGCCAAATGCAAAGAAAATCCCCTTTTGAGTGGTGCTCCTGCCACCACTCATC
TCCCCAACTGGTGGGTGAAAAACCTTGTGCGCCCCTTCTCTTTCCAGAAAAAAAACGCCT
CGCTCGCACAAAAACATGCTCGCCCGGTGAAGCTGCGTATGTCGCAGAAGCTCAAACCAA
CGCCGCCAGCAAGCATCAACAATTTCTATTCAAACACCCAACGCAGCGCCCAAACCGGGT
GCACTGTACTCAGTAGCGAAGATGCTCAGATTGTCCCGTGCGCTGCTTTCGATGCCCGTT
TCGGAGCGGGAAGCCATCGCTTGCCAACGTTGGCGATGTCTTTTAGCCGTGGATTTGAAT
TTTCTGAATATCACAGGCGGGCGCGGTTTGCCTGCAAGGTTGTTGCTTCCCACACGAGCA
TTGCTTTCCGTACCGCGGTGGGGCGAGTTTTCAACGCAACCTTCTACAAGCAACGCCACA
ACGCCTGGGAGCGATATTTAACAGAAACAAGAACATCCCGAACTTCAGCACATGCCGTGA
TTTGCCTGTTGGAAAAGCTTTTGTGAGCGTGTGAGTTGAACGAGCTCTATTTTCCCAGCG
ATGGGTGGCATTTGTGTGGCATGCTATCGTCAGCTTTTCTTGAATCTTTACCTCTCCATTCGCC
TCCATTAGTACACGCGTATGGAAAATGGGTGCAACGGATCAGAACGGATTTTCCGCGACA
GACTTAATAAAGGGAAAGCAACGCGTTTTTTGCATGTGTAGTGTTTATGAGCTTTATGCCGTTA
CTTTGCAATTAAAAATAGCAAAAAATAACAGTTTTTTTTTGTAAGCGGATTACAAAGAATGTAT
CAGAATATTACGTGAAACATTCATTTCATGCTGTTAACGCTCAAATAGAATAGTTTTGTAACAC
GGATTGCATACCTTGCCGGTATCGGTTACATTTTCGCCTAACAGTATGCAATCTGTTTAGCTTT
GTTGTTTAATGACTGCGTTGGTAGTACAATATTTATTTACACCGCGTAATTTATCTCACAAATT
GCAAAAAAATGTCAATCTGTATCGATTATTCACACAAATCAGATCCCGGAACCAGTGTAG
CCCAATGTGCTCTTTATTGAATTACCACGAACAAATCAACCTGATGCCCGGGTCCGTTGG
CAAACAGCTTGCGCCGAAGCCGCTCAGTGTTTCGTGCACTACCGTGCTGCCATTTTGCTG
CCCTCATCGAACAGATAAACAGAAGGGCAACTCTTGTGAGCATCGCAATGCCCGTCTGAA
GTTCCGTCGAAAATGGGCCTAAATTCAATTTGACGCATTTACCCGCGAACAATTGCGCGA
AGGCTGTCAAGTGTGTTCCACGAACTGCGACAACAAGCACACACACAAACACAAATGTTA
TCGTTTCGGCATGTTTCTCGGTACAAAGCGTGTGGCGCTATGTGGCATGCCGATTCCCAG
ACAGAGTGATCGATAGTAAATGTAGCCTATCCGGTAGCATTCAATTTCCTTTTCTATCCTCGCA
AACAAAGCCCATTCTGGGGAGGCGTGGTGAAGCTTTCAAAGGCATTGTGAAACAAATGTC
CTGGTTCGGAGGGATGCTGGGGAAAGCAAACACGGTGCCGCCATCGCTGCTACCGTCAAT

CGATCATGCATGATGTGATTAATATTTGTGTTATTCACCTGCGTATCTATGCGTCCGTCGTGTC
GTTCGATTTCCGGAGTCAAGGAAAAAGCGACTCCATTTGGGATTGGTTTTTGCAGCGAAA
AATCAAAACATTCGCACAAAACCGTCCTCCATTTCAAATGCCTACACTTGTCACTGTATATCTC
TCTTTCTCTCGTTTTGCCACGTTGCAGTCTCGTTTCAGCAATCGGAGATACGTACGGTCC
TGCCCTGCTGCTACACATGCTGACCTCCACCATCAAGCTGACGCTGCTCGCCTACCAGGC
AACGAAAATCGACGGTGTCAACGTGTACGGATTGACCGTAATCGGATATTTGTGCTACGC
GTTGGCTCAGGTTTTCCTGTTTTGCATCTTTGGCAATCGGCTCATCGAGGAGGTACGTGC
GCTCGGCGTGTTGCCGTGGGAAAGCATTCTCCCTGCCCCATATCGCTTCATTCTCCCAGA
TCACACATTTGCATCACAAAGCCAGCACACTTTTGCTTCGCCGCTGCCATCTCGGCTTCT
GAATGTTTTCACTCTCCCATACCTCTCCCGTGCAGAGCTCATCCGTGATGGAGGCGGCCT
ATTCCTGCCACTGGTACGACGGGTCCGAGGAGGCAAAAACCTTCGTCCAGATCGTTTGTC
AGCAGTGCCAGAAGGCGATGACTATTTCCGGAGCCAAGTTTTTCACCGTTTCGCTCGATC
TGTTTGCTTCGGTAAGTGTAGCCTGGTGGCTGGCACAGAACAGGCTGGCAAAACAGGGAC
TTTGGCTCTAGCCTGATGGGTGGTATATGTGTGTCTATTTTTTGCTACCATTCTCGCATCCCTT
CCTTTCCAGGTTCTTGGAGCCGTTGTCACCTACTTCATGGTGCTGGTGCAGCTGAAGTAA
ACAGCCGTGGCCCGGAAGGATGTGTTTTTTTTCGCTCGTTCGGTTGTTTGTTTGTGCACA
CTTTCTCTTGGACATTTTCTCTACTGCAAAGGTTTAACAAACAGCAACAACAAATAATCC
CAAGTTTTCTTTTACAGATCTTTGCAAAATGATTAGATTTTAATAGATTAACAGTGCTTGATTA
TCTGTCCTGTAGCAACCGGGGCTGAAGAACGTTGATTTGGTAAAAGTACAAAAGGGACGT
TGGAAATTGAAACAACAGAAGAGTGATATTTATGCAAAGCTCACCAAGGGAAATCTATGT
ATGTGTGATTTGCGCTCATCAAGCACTGTATGTGCCTTTCAACTAGTGCAGCAATAAAGA
GTACAAATGTTTCTTAG.

Ir25a (4005 bp; Probe set ID PRK149) – AGAP010272

CCGTCGCTTATAGACCGATTCCGCTATACTGTTCGGCTTGGGTATATGTGTGTATTACAAAAAT
ATCATGGATCCTAAGAACGGAAGGCGTTGGCTGGTTTTAATCCCTATTCAGCTTGCATCA
TATGCAATTATAGCGATCATGGGACAAACTACCCAAAATATTAATATATGTAAGCATTTTCATT
AATTAACTCCTTTTGCACTGGAAGTAGAGATTGTTGTGAACATTAGAAAAAGCTCAAATT
ATTTTAAAACGTAAATTTCACTTTATTACCAGTGTTTGTCAATGAGGTCGATAACAATTTGGCT
AATGTTGCTGTTGAAGTCGCACTGAACTATGTTAAAAAGAATCCTCAACTGGGGCTGTCC
GTTGATATGATGTACGTAGAAGGGAACCGCACCGACTCCAAGGATCTGCTACAAGCGCGT
AAGAACTATGAACACTTATGTCGTTGTTGTTATCTCTCTGGTGTTACTGCTTAAGGTTACAAAA
CGTACTATTTAATTGTGTGTGATTTTTACCTTTTCAATGTCTAATTTGGTAAATGAGAAAGTGT
GCTCGAAGTATGGCCAGTCTTTGAGCGAAAATCGACCGCCACACTTACTACTGGATACCA
CGCTGACTGGAGTATCATCGGAAACGGTGAAATCGTTCAGTCTGGCACTTGGCATACCAA
CCGTATCGGCTTCGTTTGGACAGGAAGGAGATTTACGCCAGTGGAGAGACTTGACGCCAA
CCAAACGCGGCTATTTGCTTCAGGTAAATCATTATGTCTTCTGCAGGGTGCGGTTGCAAT
GGTAGTTTTCAGTGCCTTGCTTAGGCTGCAATCAAAATCGTTATGAAATGAAGCCAGAAC
GTTATGATTCAACATTCTTTATCCATGAAGGTTATGCCCCCGGCTGATATGATTCCGCAAGTGA
TTCGATCTATCATCATTTACATGAACATAACGAATGCTGCAATTCTGTACGACAACACATTCGT
AATGGATCACAAATATAAAGCTTTACTACAAAATATACCCACGCGCCACGTCATCACCAC
CATTGCTGACGATCGCGATAGAGCCAGCCAGATTGAAAAGCTTCGCAATTTGGACATAAA
CAATTTCTTTATACTAGGTTCTTTAGCATCGATCAAGCAAGTATTGGGTAAGTGGGTTAGTAGT
TGTCGTCGGAGGTGCGCGTTTTAATTAACGCTATTCTTGTTTTGGTCACTTGTTTTCACAGAAT
CGGCTAAAAATGAGTATTTTGAACGTAACTTTGCCTGGCATGTAATAACGCAAGAGCAAA
AGGATCTAACGTGCAATGTTGAAAATGCCACTATCATGTTTCTTCGTCCGATGTCTGATAGTTC
AAGCAAAGATCGATTGGGCAGTATACGCACAACATACAATCTTAAGCAGGAGCCTCAAAT
TACCGGATTTTTCTACTTCGACCTGACACTGCGCGCGTTAATTGCAATTAAGTAATATATCAAG
CTTTATATGGTTGGCTAGCATTAGATGCTGAACTGAGTTGTTTTTTTAAATTATTTTCTTTCAT
TTGCTAGAAATATTTTGCAGTCCGGATCCTGGCCATCAAACATGAAATACATCACGTGTG
AGGATTACGACGGGACAAACACACCAAATCACACAATCGACCTTAAAACGGCTTTCATTG
AGGTGACCGAGCCAACCACTTTCGGACCGTTTGAAATACCAAAAGGCGGAAAAATGCAAT
TCAACGGTAACACTTACATGAAGTTTGATATGGACATTAACGCCGTTTCCATCCGTAGCG
GCGCATCCGTTAATACGCGCAGTCTCGGAACATGGGAAGCGAGCTTAAATGCACCGATAA
ATGTAGCAAATGAGGCGGAAATAAAAAATCTTACTGCCGATGTTGTTTATCGTGTCTATA
CGGTTGTGGTAAGTGCGAGTGGATAAGATAATATATTGTAAGCGACAACAATGTTAACAA
GCGTAAACCCCGTTTATTTCAGCAAGCGCCATTCATAATGCGAGACCCAACGGCACCAAA
GGGCTTCAAGGGATACTGCATCGATCTGCTCAACAAAATTGCCGAGATCGTCGAATTTGA
CTATGAAATACGCGAAGTGGAGGACGGAAAGTTTGGCAACATGAATGAAAACGGCGAGTG
GAATGGTATCGTACGGAAGCTGATCGACAAGCAAGCAGATATCGGACTCGGCTCGATGTC
TGTAATGGCCGAGCGGGAAACAGTTATAGACTTTACCGTCCCGTACTATGATCTAGTTGG

GATTAGTATTATGATGCAATTGCCAAGCACGCCGAGTTCGCTGTTTAAATTTTTAACCGTGCTG
GAAACGAATGTGTGGCTCTGCATTTTGGCTGCCTACTTCTTTACCAGCTTTCTGATGTGG
ATTTTTGACCGCTATAGTCCATACAGCTACCAGAATAATCGAGAGAAGTACAAGAACGAC
GACGAAAAACGGGAGTTCAATATTAAAGAATGTCTGTGGTTCTGCATGACATCGTTGACA
CCGCAAGGTGGCGGAGAAGCACCCAAAAATTTGTCCGGTCGCTTAGTCGCTGCCACATGG
TGGTTGTTTGGGTAAGTAGTAGCAGTATTGATAGAAGGAAAAATATGTTTCCATTGTGTG
CCGTTTCCACCCGCGTGGTTACACGGTAGGTGTAATTATCATTGCATTTCTATCATTATGTCAT
TATTCAACAGATTTATCATCATTGCCTCGTATACGGCTAATTTGGCAGCTTTCTTGACTGTATC
CCGACTAGACACGCCGGTTGAATCGCTGGATGATTTATCAAAGCAGTACAAAATTCTGTA
TGCTCCACTGAATGGATCATCGGCTATGACGTACTTCCAGCGAATGGCTGACATTGAAGC
TAAATTCTACGAGTAAGAAGTGCCATATACCGGCGCAAGTATCTAAGGATATGTTGCTTACTTA
TTTTACTACTTTCTGGCAAACGCAGGATTTGGAAGGAGATGTCGCTCAATGACTCTCTGA
CGGCGGTTGAGCGATCGAAGCTAGCTGTCTGGGACTATCCGGTCAGCGATAAATACACAA
AGATGTGGCAAGCCATGCTTGAGGCAGGTTTACCGAACAGTCTCGAAGAAGCCGTACAGC
GCATACGAAATTCGACATCTGCCTCTGGATTCGCATTTCTGGGCGACGCAACCGACATAC
GCTACCAAGTGTTGACAAATTGCGATTTACAGATGGTTGGCGAAGAGTTTTCTCGCAAAC
CGTACGCGATCGCCGTCCAGCAAGGATCACCGCTGAAGGATCAATTTAACAATGCGTACG
TATTAATTTCATTATTCCTTTTTGCGTTTTCTAACCTACACTTCTCTTCGCTGTTTAGTATACT
GATGCTACTGAACCGACGCGAGCTGGAAAAGTTGAAAGAACAATGGTGGAAGAATGATGA
CGTACAAAACAAGTGCGAAAAGCCAGATGACCAGTCGGATGGCATCTCGATACAAAACAT
CGGAGGCGTATTCATCGTAATATTTGTGGGGATAGGGATGGCGTGCATTACGTTATTGTT
TGAGTTTTGGTATTACAAGTATCGAAACAACTCCAAAGTGATCGATGTTGCCGAATCAAC
GGACCAGCAACACGGTGGAACAATAGTAAAAAATGTCCGTCCCGCTGGTAAGCTTATGAA
GCAAGATTCGTTAAAAGACTCAACAAAAGGTCACAATTATCAAAACCTCCGAACACGTAC
CTTGATGCCGAATTTGAGCAAGTTTCAACCTCGCTTCTAAAGTAATGCGTTTTTGACTGC
GCTTTGGAAGTACAACGAAAACATACTAATGCGTCGTGAGATTTACGAGCATTAGTACGA
CTACGGATAGTTATGAACTGTATTTTTTTAATTTTAACGTATGATATGAATTTAATGGGGATAT
ATATGTAACTATCTTTACCAATCTTATATAACGATTTGTGCATTTTGAGCAATTCTTTGAATTA
TGCAACAAAACGCTAAAAATTAAATGAAA.